Multi-physical Developments for Safety Related Investigations of Low Moderated Boiling Water Reactors

Zur Erlangung des akademischen Grades

Doktor der Ingenieurwissenschaften (Dr.-Ing.)

der Fakultät für Maschinenbau
Karlsruher Institut für Technologie (KIT)

genehmigte

Dissertation

von

Dipl.-Ing. Markus Thomas Schlenker

Hauptreferent: Prof. Dr.-Ing. habil. Robert Stieglitz
Karlsruhe Institut für Technologie

Korreferent: Prof. Dr.-Ing. Hans-Dieter Berger
Technische Universität Braunschweig
AREVA GmbH, Erlangen

Tag der mündlichen Prüfung: 19.12.2014

Für meine Eltern, Jörg und Birgit

Für Katharina

Für meine Familie

Preface

This dissertation was carried out during my activities as a Ph.D. candidate at the Institute for Neutron Physics and Reactor Technology (INR) at the Karlsruhe Institute of Technology (KIT) in close cooperation with AREVA GmbH.

I want to express my deep gratitude to Professor Dr. Robert Stieglitz and Dr. Victor Sánchez-Espinoza of INR/KIT for their guidance and encouragement during the three years of research. I am also very grateful to Professor Dr. Hans-Dieter Berger and Dr. Matthias Rost of AREVA GmbH for their support and useful comments which substantially contributed to this work. Special thanks go to Miriam Däubler and Dr. Uwe Imke of INR and to Gerhard Bender and Dr. Otmar Bender of AREVA GmbH for their technical support and many fruitful discussions. Without the experience of these people this thesis would not have been possible.

At this point, I want to acknowledge the financial support of AREVA GmbH and the Reactor Safety Research Program of the KIT for this work.

Last but not least, I would like to deeply thank my family for their unlimited support during all my life and Katharina Schanz for supporting and encouraging me during the last years, especially in difficult times.

Würzburg,
im Dezember 2014   Markus Thomas Schlenker

Abstract

Multi-physical Developments for Safety Related Investigations of Low Moderated Boiling Water Reactors

The main objective of this dissertation is the development and optimization of a low moderated boiling water reactor (BWR) core with improved fuel utilization to be incorporated in a Gen-II BWR nuclear power plant. The assessment of the new core design is done by comparing it with a full-MOX BWR core design (reference design) regarding neutron physical and thermal-hydraulic design and safety criteria (inherent reactivity coefficients, shutdown reactivity margin, power distribution, thermal limits) and different sustainability parameters (conversion ratio, fissile inventory ratio, fissile plutonium consumption, and discharge plutonium quality).

To meet these technical challenges, first of all design studies at fuel assembly (FA) level were performed to identify the optimal geometry parameters and initial fuel material composition of the low moderated FAs. Based on these investigations, the most promising FA design regarding the design criteria listed above was selected as starting point for the following design investigations at core level.

Because of the harder neutron spectrum in low moderated FA, validation of the computational solution approach used to carry out the design optimizations studies is crucial. For this purpose reference transport solutions were created to test especially the energy group structure of macroscopic cross-sections used by 3D core simulators. These investigations have confirmed that the current computational route applied to the analysis of Gen-II BWR core designs is also applicable to neutronic design studies of low moderated BWR FA and cores as those investigated here.

As next step, core design studies followed the FA design investigations to assess low moderated core designs regarding the safety and sustainability criteria mentioned above. In this context, four BWR cores consisting of low moderated fuel assemblies were extensively analyzed. For this, an iterative approach between the core-level and FA-level simulations was followed to find the low moderated BWR core design that best meets the fuel utilization and safety requirements.

This final core design consists of 784 fuel assemblies with 12x12 fuel rods with a height of 270 cm. The main characteristics of the core were compared to the one of the reference BWR core regarding the design and safety criteria demonstrating the feasibility of the new low moderated BWR core design. The void reactivity coefficient is clearly negative (< -30pcm / %Void) but lower than the one of in the reference core design (< -80pcm / %Void). The predicted cold shutdown margin is significantly improved from -1.5 % in the reference core to less than -4 % due to reduced reactivity swing between hot and cold core conditions and increased relative moderator displacement by the control rods in the low moderated core design. In comparison to the full-MOX BWR core, the same discharge burnup of 51 MWd/kgHM (heavy metal) can be achieved and the fissile plutonium consumption is reduced from 600 kg to 515 kg. In addition, the plutonium quality of fuel discharged from the low moderated core is with 56.6 % significantly higher than in the full-MOX core (47.3 %) making a second recycling feasible.

Finally, the thermal-hydraulic design limits were assessed with a sub-channel code. For this purpose, first the available critical heat flux correlations of the code were validated against BWR-relevant experimental data of the NUPEC BFBT tests knowing that the design of the reduced moderated FAs differs from the one of the Gen-II BWR FAs. The subsequent, thermal limit analysis regarding boiling transition and peak cladding surface and fuel centerline temperature for selected hot fuel assemblies of the developed low moderated core design has demonstrated that the proposed FA designs fulfill the safety limits for steady state conditions. These thermal-hydraulic investigations are primarily of academic character since the critical heat flux correlations applied to predict the critical power ratio are of limited applicability to the low moderated BWR fuel assemblies developed here.

Kurzfassung

Multi-physikalische Entwicklungsarbeiten für sicherheitsrelevante Untersuchungen niedrig moderierter Siedewasserreaktoren

Das Hauptziel der vorliegenden Dissertation ist die Auslegung und Optimierung eines niedrig moderierten Siedewasserreaktors (SWR) mit verbesserter Brennstoffausnutzung zur Nutzung in einem SWR Kernkraftwerk der Generation II. Die Bewertung des neuen Kerndesigns wird anhand des Vergleichs zu einem Voll-MOX SWR-Kerndesign durchgeführt. Hierbei werden neutronenphysikalische und thermo-hydraulische Design- und Sicherheitsparameter (inhärente Reaktivitätskoeffizienten, Abschaltsicherheit, Leistungsverteilung, thermische Limits) und verschiedener Nachhaltigkeitsparameter (Konversionsrate, Konservierungsfaktor, Spaltstoffverbrauch, Plutoniumqualität in entladenem Brennstoff) berücksichtigt.

Um die technischen Herausforderungen zu erfüllen, werden zuerst Designstudien auf Basis einzelner Brennelemente (BEs) durchgeführt um optimale Geometrieparameter und frische Brennstoffzusammensetzung für die niedrig moderierten BEs zu ermitteln. Die bei diesen Untersuchungen ermittelten BE-Designs werden als Startpunkt für die weiterführenden Studien auf Kernebene genutzt.

Wegen des härteren Neutronenspektrums in niedrig moderierten BEs ist die Validierung der für Designstudien genutzten Rechenprogramme unumgänglich. Aus diesem Grund wurden Referenzlösungen mit Transportrechnungen erstellt um insbesondere die Energiegruppenstruktur der makroskopischen Wirkungsquerschnitte zu testen, die von 3D-Kernsimulatoren genutzt werden. Diese Untersuchungen haben bestätigt, dass die aktuelle Rechenstrategie zur Auslegung von SWRs der zweiten Generation auch zur Untersuchung der niedrig moderierten BEs und Reaktorkerne genutzt werden können, die in dieser Arbeit entwickelt werden.

Im nächsten Schritt werden Kernauslegungsstudien durchgeführt um niedrig moderierte Kerndesigns mit den oben genannten Auslegungskriterien zu bewerten. Es wurden vier SWR-Kerne bestehend aus niedrig moderierten Brennelementen ausführlich untersucht. Hierbei wurde ein iterativer Ansatz zwischen Rechnungen auf Kernebene und BE-Ebene

genutzt um jenes Kerndesign zu finden, welches die geforderten Anforderungen an Brennstoffausnutzung und bestimmte Sicherheitsparameter am besten erfüllt.

Dieses Kerndesign besteht aus 784 Brennelementen mit 12x12 Brennstäben mit einer Höhe von 270 cm. Die Eigenschaften des Kerns wurden mit einem Voll-MOX SWR als Referenz verglichen, um dessen Eignung hinsichtlich Design- und Sicherheitsparameter zu zeigen. Der Void-Reaktivitätskoeffizient ist deutlich negativ (< -30 pcm / %Void) aber betraglich kleiner als im Referenzkern (< -80 pcm / %Void). Die berechnete kalte Abschaltsicherheit ist maßgeblich von -1.5 % zu unter -4 % verbessert. Dies ist im niedrig moderierten SWR zum einen durch die geringere Reaktivitätsbindung zwischen kaltem und heißem Reaktorzustand und zum anderen durch die stärkere relative Verdrängung von Moderator beim Einfahren der Steuerstäbe begründet. Im Vergleich zum Voll-MOX SWR-Kern kann der gleiche Entlade-abbrand von 51 MWd/kgHM (HM: Schwermetall) erreicht werden und der Verbrauch von Spaltstoff kann von 600 kg auf 515 kg verringert werden. Zusätzlich ist die Plutoniumqualität in aus dem niedrig moderierten SWR entladenen Brennstoff mit 56.6 % deutlich gegenüber dem Referenzkern verbessert (47.3 %), wodurch eine zweite Wiederaufbereitung erleichtert wird.

Im letzten Schritt wurden thermo-hydraulische Designkriterien mit einem Unterkanal-Code bewertet. Zu diesem Zweck wurden zuerst die für SWR-Bedingungen relevanten und verfügbaren Korrelationen zur Bestimmung der kritischen Heizflächenbelastung gegenüber experimentellen Daten des NUPEC BFBT Tests validiert. Dies wurde in dem Wissen durchgeführt, dass das Design niedrig moderierter BEs sich von dem Design der BEs für Gen-II SWR unterscheidet. Die anschließenden Untersuchungen der Sicherheit gegen Austrocknen der Heizfläche und der maximalen Hüllrohr- und Brennstabtemperaturen für ausgewählte heiße BEs der entwickelten niedrig moderierten Kerne hat gezeigt, dass die vorgeschlagenen BE-Designs Sicherheitslimits im stationären Betrieb einhalten. Diese thermo-hydraulischen Untersuchungen sind hauptsächlich akademischer Natur, da die verfügbaren Korrelationen zur Bestimmung der kritischen Heizflächenbelastung nur begrenzt für die Untersuchung der hier entwickelten niedrig moderierter SWR Brennelemente anwendbar sind.

Table of content

Nomenclature

Symbol	Definition	Units
B_n	Discharge burnup in core with n batches	[MWd/kgHM]
β	Delayed neutron fraction	[-]
$Calc_i$	Calculated power form factor for the determination of e_i	[-]
CHFR	Critical heat flux ratio	[-]
CPR	Critical power ratio	[-]
CR	Conversion ratio	[-]
D	Diameter of fuel rod	[m]
DC	Doppler reactivity coefficient	[pcm/K]
e_i	Error in local power form factor	[%]
f_{rad}	Radial power form factor	[-]
f_{ax}	Axial power form factor	[-]
ITC	Isothermal temperature reactivity coefficient	[pcm/K]
k_{inf}	Infinite neutron multiplication factor	[-]
k_{eff}	Effective neutron multiplication factor	[-]
k_{target}	Real unbiased k_{eff} of a reactor core used in design calculations	[-]
LHGR	Linear heat generation rate	[W/cm]
MFR	Moderator to fuel volume ratio (independent of moderator density)	[-]
P	Pitch between the centers of neighboring fuel rods	[m]
P_{NL}	Non-Leakage factor	[-]
PC	Power reactivity coefficient	[pcm/MW]
Pu_{fiss}	Fissile plutonium content in fuel	[wt%]

Pu_{tot}	Total plutonium content in fuel	[wt%]
Pu_{qual}	Ratio of Pu_{fiss} to Pu_{tot}	[-]
q''	Surface heat flux	[W/m²]
q''_{crit}	Critical surface heat flux	[W/m²]
Ref_i	Reference power form factor for the determination of e_i and PWE	[-]
ρ	Reactivity	[pcm], [$]
T_{fuel}	Fuel centerline temperature	[K]
T_{clad}	Cladding surface temperature	[K]
VC	Void fraction reactivity coefficient	[pcm/%Void]

List of Acronyms and Abbreviations

A10	ATRIUM^{TM} 10XM fuel assembly
ABWR	Advanced Boiling Water Reactor
ADF	Assembly Discontinuity Factor
ANEM	Advanced Nodal Expansion Method
ANM	Analytical Nodal Method
BBWR	Breeding BWR
BOC	Begin Of Cycle
BOL	Begin Of Life
BPR	Burnable Poison Rod
BTE	Boltzmann Transport Equation
BWR	Boiling Water Reactor
CE	Continuous Energy
CHF	Critical Heat Fflux
CHFR	Critical Heat Flux Ratio
CPR	Critical Power Ratio
CR	Conversion Ratio, Control Rod
CSDM	Cold ShutDown Margin
CSP	Core Support Plate
CZP	Cold Zero Power
DC	Doppler reactivity Coefficient
DNB	Departure from Nucleate Boiling
efpd	equivalent full power days
efph	equivalent full power hours
EOC	End Of Cycle
ESC	Extended Step Characteristics
EWE	Error-Weighted Error
FA	Fuel Assembly
FBR	Fast Breeder Reactor
FIR	Fissile Inventory Ratio
FLWR	Innovative Water Reactor for Flexible fuel cycle
FMFD	Fine Mesh Finite Differences
FP	Fission Product
HCBWR	High Conversion BWR
HCLWR	High Conversion LWR
HCPWR	High Conversion PWR
HFP	Hot Full Power

HYBRID	combined ANM/NEM solution kernel in PARCS
HZP	Hot Zero Power
ITC	Isothermal Temperature Coefficient of reactivity
LHGR	Linear Heat Generation Rate
LTP	Lower Tie Plate
LWR	Light Water Reactor
MC	Monte Carlo
MCHFR	Minimal Critical Heat Flux Ratio
MCPR	Minimum Critical Power Ratio
MFR	Moderator to Fuel volume Ratio (independent of moderator density)
MG	Multi-Group
MOC	Method Of Characteristics
MOX	Mixed plutonium and uranium OXide
NEM	Nodal Expansion Method
NP	Neutron Physics
NPP	Nuclear Power Plant
NTE	Neutron Transport Equation
PCI	Pellet-Cladding Interaction
PGBR	Plutonium Generation BWR
P_N	Spherical harmonics method
Pu_{fiss}	Fissile Plutonium
Pu_{qual}	Plutonium Quality (fissile fraction in plutonium)
Pu_{tot}	Total Plutonium
PWE	Power-Weighted Error
PWR	Pressurized Water Reactor
RBWR	Resource-renewable BWR
RMWR	Reduced-Moderation Water Reactor
RPV	Reactor Pressure Vessel
S_N	Discrete ordinates method
TH	Thermal-Hydraulics
UOX	Uranium OXide
UTP	Upper Tie Plate
VC	coolant Void reactivity Coefficient
wt%	weight-%

1   Introduction

1.1   Motivation

The rapid growth of the world's population and the technological development in emerging nations is linked to an increasing demand for primary energy. Taking into account the energy consumption of the last 40 years shown in Fig. 1.1 indicates the continuation of this trend. In addition, climate change calls for drastic reductions in the worldwide carbon footprint. Since the majority of greenhouse gas emissions results from fossil fuel use in e.g. electricity generation and transportation, the future development has to be to replace more and more fossil fuel with carbon-free energy carriers. To achieve this goal, all available energy conversion systems with low CO_2-emissions must be considered. Current options are wind, hydro, solar, and especially nuclear power which has a life-cycle carbon footprint comparable to the renewable alternatives [1], [2], [3]. Sustainability of nuclear reactors as well as improved use of the natural resources is in this perspective a crucial factor to deal with.
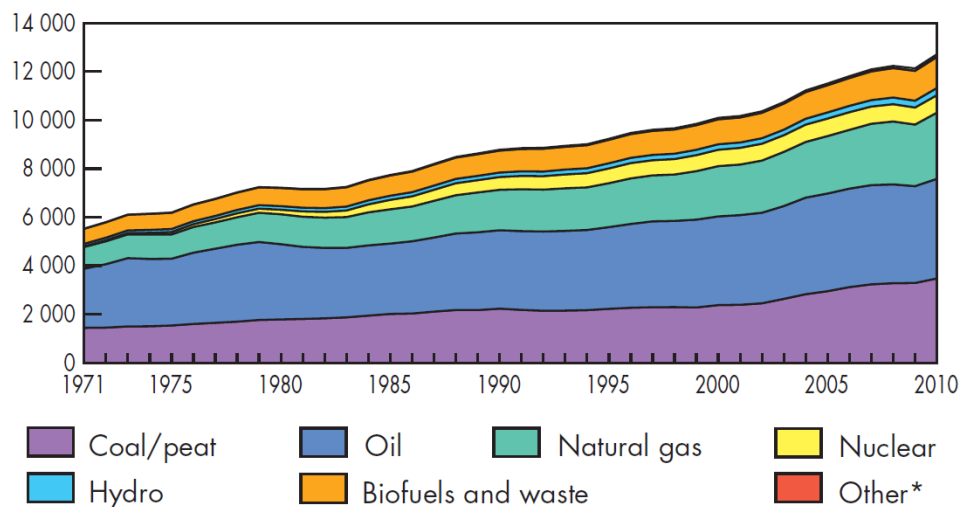
Fig. 1.1: World primary energy supply from 1971 to 2010 by fuel in Mtoe[1] [4].

In the once-through fuel cycle most commonly used in Generation II[2] light water reactors (LWRs), only about 1 % of the energy contained in the initial natural uranium can be used. In fast breeder reactors (FBRs), on the other hand, the resource utilization is around 60 % and

---

[1] Mtoe = million tonnes of oil equivalent

[2] The typical classification of reactor systems considers Gen-I as early prototype and power reactors as build up to the 1960s, Gen-II reactors as especially designed for commercial power generation, which represent the major fraction of currently operating nuclear power reactors and Gen-III and Gen-III+ reactors as reactors with improved evolutionary design (e.g. decreased core damage frequency or passive safety systems) [99].

only limited by losses in the processing steps as illustrated in Fig. 1.2. Unfortunately, FBR are not yet competitive for commercial energy production and, therefore, it is of special interest to improve the fuel utilization in the current conventional light water reactors. Although the energy turn-around has been decided in Germany, the prospects of nuclear energy remains good in Europe and worldwide as can be observed in recently established technology platforms like NUGENIA [6] and SNETP [7] [8].
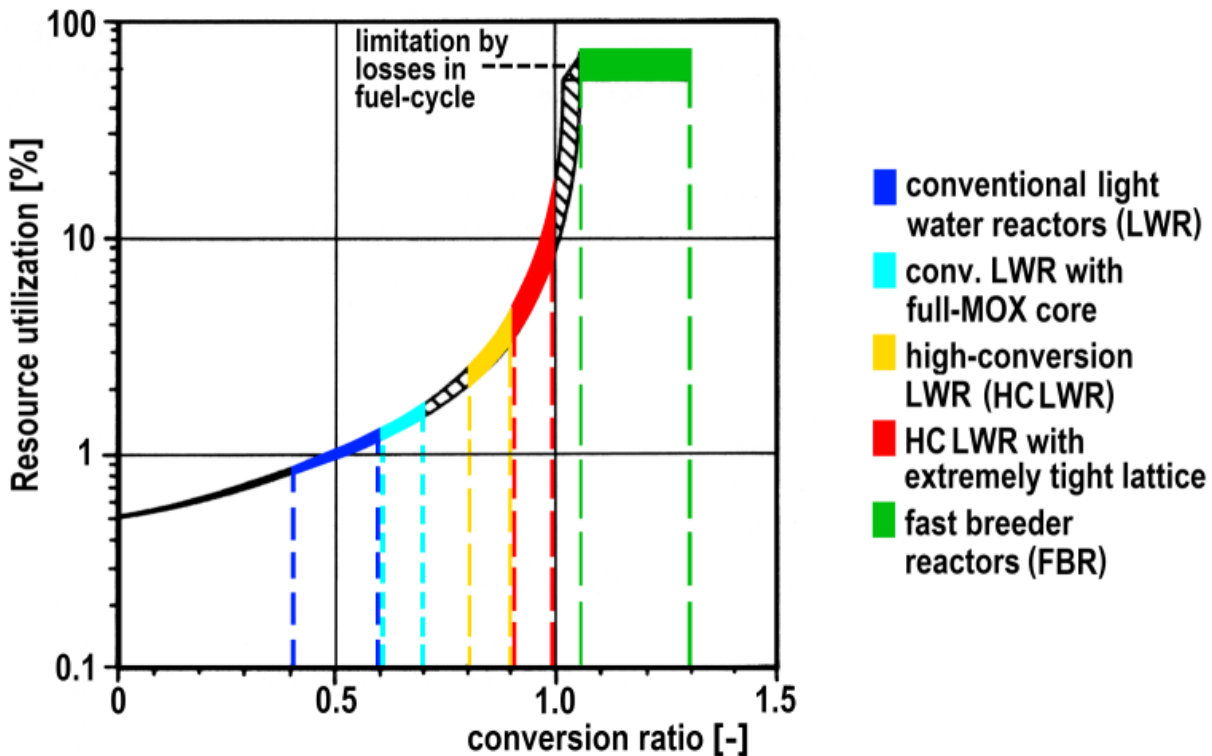
Fig. 1.2: Conversion ratio dependent resource utilization of different nuclear reactor systems (adapted from [5]). The resource utilization is in this context the actually generated fission energy relative to the theoretically available fission energy in natural uranium.

The transition from uranium oxide (UOX) loaded LWR to Gen-IV fast spectrum reactors is envisioned in six steps [9], [10]. Steps 1 to 3 consider core-loadings with mixed plutonium and uranium oxide (MOX) fuel assemblies (FAs) varying from 0 % to 100 % MOX loading. These developments lead to a transition from a once-through to a multi-recycle fuel cycle. In the next steps, the fuel rod lattice is supposed to become tighter compared to the one of a Gen-II LWR leading to a decrease of the neutron moderation and hardening of the neutron spectrum. Under these conditions, an increased amount of Pu is generated during operation due to the enhanced neutron capture in ^{238}U, which is directly used for fission and can be recovered subsequently by recycling. While in step 4 still square fuel rod lattices are used, from step 5 on hexagonal fuel rod lattices are considered. The final step of this evolutionary concept is the further reduction of the fuel rod distances to improve the fuel utilization.

Modern LWR core loadings include MOX fractions up to 50 % [11] and recent studies have shown that even core loadings with 100 % MOX FA in Gen-II boiling water reactors (BWRs) are realizable [12], [13]. In the present studies, low moderated, square lattice BWR core designs representing step 4 will be developed based on the work described in [12] and will be extensively investigated taking into account fuel utilization and safety considerations. A fundamental constraint to be considered in this dissertation is the requirement that the new low moderated BWR core to be developed must easily replace the current core of the Generation II BWR-Type 72 (reference plant) without additional needs for major plant modifications.

1.2 Description of the reference Generation-II BWR

The German BWR type 72 was selected as the reference nuclear power plant (NPP) here, meaning that the dimensions and thermal hydraulic core conditions of this reactor will define the global boundary conditions for all the analysis performed. The reference BWR is one of the remaining twin reactors KRB units B and C located at the Gundremmingen site in Bavaria It belongs to the Siemens KWU BWR construction line 72 with a rated thermal power output of 3840 MW_{th}. The plant design is well proven and continues to be one of the latest BWR series worldwide. In Fig. 1.3 the operational principal of the KRB NPP is shown [14], [15].
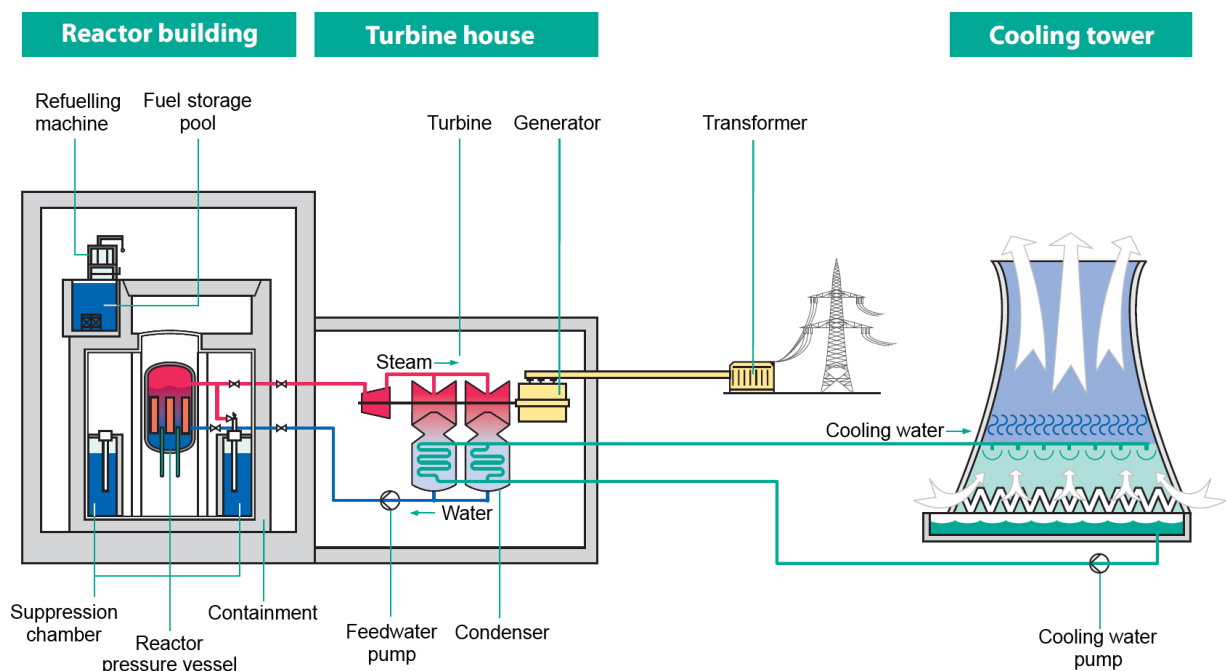
Fig. 1.3: Operational principal of Gundremmingen nuclear power plant [16]

The steam generation system of a BWR consists of reactor pressure vessel (RPV) including the reactor core, recirculation pumps and other internals, steam lines, turbine, condenser, feedwater lines, feedwater pump, and feedwater heaters which are arranged in the primary loop. In a BWR, in contrary to a pressurized water reactor (PWR), only the RPV with short parts of the steam and feedwater lines are encapsulated together with pressure suppression chambers and heat removal systems by a very compact containment forming the outermost of multiple barriers preventing release of fission products (FPs) to the environment. The first barrier is the fuel matrix of the cylindrical fuel pellets holding back especially solid FPs. These pellets are stacked in closed tubes, the so-called cladding, which form the second barrier. They are most suitable to withstand external and internal pressure from coolant and fission gas. A fission gas plenum in the upper part of the fuel rod filled with helium limits the pressure build up due to fission gas release and a hold-down spring is used to keep the pellet stack in place. The RPV and the feedwater and steam lines are forming the next barrier preventing direct leakage of materials released from potentially failed fuel rods. In case of a feedwater or steam line break outside of the containment, valves located directly before and behind the containment wall are closed to avoid release of any core inventory, especially coolant, fuel, and fission products, out of the containment. Keeping these barriers intact is the primary goal of reactor safety.

The approximately 4 m long fuel rods are arranged in a defined square lattice in 784 separate fuel assemblies (FA). These are again arranged in a square lattice forming an approximate cylinder which is surrounded by the core barrel. The distance between neighboring fuel rod centers within a FA is called fuel rod pitch or just pitch and is fixed by spacer grids which are axially distributed along the length in intervals of about 0.5 m. In the ATRIUM^{TM} fuel assemblies, an internal water channel improves neutron moderation especially in the upper part of the core and forms a skeleton to increase the FA stiffness. To obtain a defined individual coolant flow in each fuel assembly and to obtain a separate bypass flow path for moderation improvement and control rod (CR) blade cooling, each FA is surrounded by a fuel channel box over the whole height. The 193 control rods in the reactor core are designed as long cross-shaped blades inserted into the core from the bottom. Boron carbide is used as strong thermal neutron absorber to control the reactivity during operation and to shutdown the reactor. Each CR-cross is located between four fuel assemblies composing together a control cell as illustrated in Fig. 1.4. The general thermal hydraulic and geometrical data of the reference plant is summarized in Tab. 1.1.
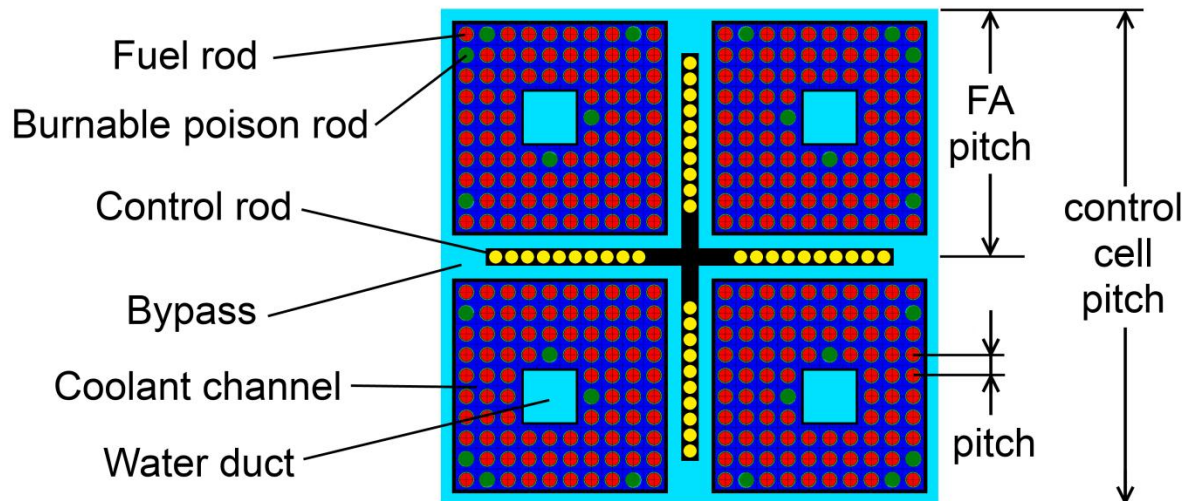
Fig. 1.4: Radial cut through a BWR fuel assembly control cell consisting of four FA of type ATRIUM10 and one central control rod cross (Figure generated with SCALE6.1).

Tab. 1.1: Reference plant core data [16], [17], [18].

Core data		
Rated thermal reactor power	3840	MW_{th}
Gross electric output	1344	MW_{el}
Average power density	57	kW/l
Reactor pressure vessel inner diameter	6620	mm
Average core diameter	4818	mm
Core outlet pressure	70.8	bar
Rated core mass flow	14300	kg/s
Rated steam mass flow at RPV outlet	2077	kg/s
Saturated steam temperature core outlet	559.15	K
Final feed water temperature	488.15	K
Fuel assembly data		
Number of fuel elements	784	
Total length	4470	mm
Active fuel height	3710	mm
FA pitch (distance from FA center to FA center)	152.5	mm
Inner fuel channel width (ATRIUM^{TM} 10XM)	134	mm
Control rod data		
Number of control rods	193	
Control lift from the bottom of the reactor core	3660	mm
Control cell pitch (distance between 2 control rods)	305	mm
Absorber material	Boron and Hafnium	

1.3   State of the art for high conversion light water reactors

High conversion light water reactors (HCLWRs), also referred to as low moderation or tight lattice light water reactors, combine features of LWR and fast reactors. The investigations of HCLWRs started already in the eighties after a proposal of Edlund devoted to plutonium recycling [19]. Hereafter, a short non-exhaustive summary of the most important concepts and their features will be given.

1.3.1   High conversion pressurized water reactor (HCPWR)

At the beginning of HCLWR research, mostly pressurized water reactors were considered as underlying LWR concept. Several high conversion PWR (HCPWR) designs and explanation of important corresponding neutron physics aspects are summarized e.g. in [20].

In the frame of a German-Swiss cooperation, several hexagonal lattice HCPWR concepts have been investigated extensively in [10], [21], [22] and [23]. The final design is characterized by a moderator to fuel volume ratio (MFR) of 1.2 and a core height of 3 m. In this so-called advanced PWR, the maximum conversion ratio achieved during the whole reactor cycle is 0.78 at end of cycle (EOC). The plutonium quality of the fresh fuel degrades from 67 % to approximately 63 % at discharge with an exposure of 53.7 MWd/kgHM [22]. Concepts with lower MFR of around 0.5 were also investigated, but their technical feasibility could not be demonstrated.

Another HCPWR concept consists of a so-called pancake core design with blanket layers surrounding a driving seed layer. The core has a low height of 1.1 m to increase the neutron leakage and, thus, to improve the void reactivity coefficient. The corresponding core power is around 1000 MW$_{th}$. Different hexagonal lattices with MFR ranging from 0.5 to 1.3 and different blanket materials have been investigated. High fissile plutonium (Pu$_{fiss}$) enrichment of above 10 weight-% (wt%) is needed in most designs but very high conversion ratios of 0.8 to almost 1.0 can be achieved with discharge burnup between 30 and 50 MWd/kgHM [24].

More recently the concept of a HCPWR was reconsidered for current PWR with MOX fuel and individual square or hexagonal fertile blanket assemblies in the core [25] or with thorium fuel and fertile blanket regions in each square fuel assembly [26].

1.3.2   High conversion boiling water reactor (HCBWR)

One of the first design studies for high conversion BWR (HCBWR) is documented in [27] for a German BWR type 69 of Siemens/KWU with a power of 770 MW$_{el}$ which is retrofitted

with a tight lattice BWR-FA. Quadratic and hexagonal lattices were investigated on lattice level and a conversion ratio of 0.8 was predicted for a quadratic FA with 7x7 rod lattice with rod clearance of 1.4 mm and low Pu_{fiss} enrichment of 4 wt%.

Another concept, called the Plutonium Generation BWR (PGBR) [28], [29], is characterized by a very tight hexagonal lattice with a fuel rod coolant gap of 1.5 mm and below. Control rods clusters, which are located in guide tubes within the fuel assemblies, are used instead of control rod crosses between the fuel assembly channels as in Gen-II BWR. This allows increasing the size of the fuel channel across the bypass gap until neighboring channels almost have contact which leads to a very low MFR of around 0.5 with a conversion ratio of almost unity.

Based on the concept for the ABWR-II [30] another HCBWR was proposed in Japan in the nineties [31], [32]. The square FA cross-section is doubled and combined with an adapted control rod lattice with control rod followers. Both the enlarged FA and the control rod followers reduce the amount of bypass moderator. The fuel rods are arranged in a hexagonal lattice to reduce the MFR to around 0.5 and, thereby a conversion ratio of approximately 0.9 is obtained. A low void reactivity coefficient can be achieved with the arrangement of UOX fuel pins in the MOX FA periphery to create an island-type fuel assembly [33].

A similar but yet different approach is the Breeding BWR (BBWR) [34], [35]. In this case, the square bundle size is increased to cover not two but four FA positions and in the square fuel assembly the fuel pins are arranged in a hexagonal lattice. The conventional control rod lattice is used but followers are added at the top to remove moderator when they are withdrawn. Remaining water paths in the bypass are significantly reduced with water removal structures attached to the channel box. To achieve an adequate void reactivity coefficient, the upper half of one third of the 1.6 m high FA is replaced with neutron streaming channels to increase the leakage. By these measures the MFR can be reduced below 0.5, so that breeding is feasible.

A further concept deals with the innovative water reactor for flexible fuel cycle (FLWR) [36] which is a multipurpose reactor for a smooth two step transition from current reactor generation to a LWR capable of breeding. While step one is a high conversion type reactor with a conversion ratio around 0.85, step two is a reduced-moderation water reactor (RMWR) with a conversion ratio larger than unity. The core for step one is 1.5 m high and it consists of a hexagonal lattice and axially homogeneous MOX FA with 9 wt% Pu_{fiss} content. To achieve breeding conditions and a negative void coefficient, the core height is further reduced to

below 1.3 m. An axial blanket-seed-blanket-seed-blanket configuration is adopted (called double-flat or parfait core design) with a high fissile plutonium content of 18 wt% in the seed layers. The most recent RMWR concept is called resource-renewable BWR (RBWR). The core designs with MOX fuel are considered in Japan [37] [38] and in the US [39] and core designs with thorium fuel in the US [40] and UK [41].

A spin-off of the RBWR concept with square lattice was investigated in [42] using thorium fuel for a single FA with similar axial seed-blanket parfait design. The core height amounts 2.3 m and the FA pitch is 142 mm. Radially, a homogeneous 10x10 fuel pin lattice with extremely tight rod to rod gap of only 0.49 mm is adopted. The very narrow FA gap at the FA side without control rod is only 1.39 mm wide. The investigations have shown that breeding is possible with this configuration but the technical feasibility and the safety parameters have not been assessed.

1.4   Main thesis objectives and solution approach

The main objectives of the present doctoral thesis are the neutronic development of a reduced moderation core based on square lattice fuel assemblies for a Gen-II BWR nuclear power plant the evaluation of the key steady state safety features, and the demonstration of the advantages of such a core in terms of improved fuel utilization without deterioration of the safety margins compared to a conventional Generation II core design. These technical goals require an iterative optimization of the core design. Thereby the below listed aspects partially conflicting each other are analyzed:

- **Fuel utilization:** Increasing the conversion ratio requires harder neutron spectrum by means of tighter fuel rod lattice.
- **Economics:** Adequate fuel exposure and cycle energy production in a harder spectrum demands increased fissile plutonium enrichment in the fuel matrix, which in turn yields higher fuel costs.
- **Neutronic safety:** Neutronic core design criteria are limiting the plutonium content.
- **Thermal-hydraulic safety:** A tighter fuel rod lattice leads to elevated core pressure losses and reduced heat transfer capability.

To achieve these goals, the following approach is applied here:

- General design studies on fuel assembly level with high geometrical resolution and fine energy discretization are performed with lattice physics codes to elaborate an optimized fuel assembly configuration (number of pins, geometrical dimensions, fuel

material composition, enrichment of the fuel rods within the fuel assembly) matching the above mentioned requirements on a low moderated BWR core.

- Systematic investigations of the neutron energy discretization for the generation of few-group condensed and homogenized cross-sections to be used by the 3D core simulators are conducted. For common LWR analysis, the material constants used in 3D reactor core simulators are generated with lattice physics codes in form of a 2 energy group structure. The increasing importance of the epi-thermal neutrons in low moderated designs, however, requires identifying the minimum number of energy groups for adequate representation of the fine-group flux spectrum. In this context, the deterministic lattice codes used here are systematically evaluated and validated by means of reference transport solutions.

- Next, homogenized and condensed cross-sections are generated with a deterministic lattice code for the fuel assembly types used in the core design.

- Then, a neutronic analysis of the core design is performed with a 3D nodal core simulator aiming at designing an equilibrium cycle. Here, important inherent safety features of the core are assessed and compared to each other such as reactivity coefficients, shutdown and excess reactivity for cold zero power (CZP), hot zero power (HZP) or hot full power (HFP) conditions as well as radial and axial power profiles. In case the core designs are not matching the technical constraints, the fuel assembly design and core design have to be iteratively optimized.

- Finally, the thermal limit assessment of the full core has to be done. However, for the tight square fuel lattices applied here, there are no appropriate heat transfer correlations for boiling transition prediction available in open literature. Therefore, the thermal-hydraulic analysis conducted here by means of a sub-channel code is of preliminary nature.

1.5   Main boundary conditions

The requirement that the fuel assembly and core design to be developed must fit in the reactor pressure vessel of the reference plant and that the new fuel assemblies can be easily fabricated by current technologies from material, enrichment and mechanical point of view, limits considerably the degree of innovations and pushes for an evolutionary approach. Regarding the plant, the upper limiting operation parameters like core mass flow rate and core pressure loss shall not be exceeded to avoid changes like replacing the coolant pumps or reinforcing core internals. The core lattice and the control rods shall be used as they are and, therefore, it is mandatory to maintain the control cell pitch and fuel assembly channel

geometry to ensure safe insertion of control rods and avoid a re-design of shutdown systems. The limiting rod to rod gap was arbitrarily pre-defined as 1.4 mm.

1.6   Structure of thesis

This doctoral thesis is organized in 8 chapters. Following this introduction, the fundamentals of reactor analysis relevant for this thesis are summarized in chapter 2 and the applied computational tools are briefly introduced in chapter 3. In chapter 4, fuel assembly level design studies for low moderated fuel assemblies are presented, in which geometrical and material parameters and the appropriateness of the lattice physics codes for high coolant void content in selected low moderated fuel assemblies are investigated. Afterwards, the energy structure of few group cross-sections generated with the lattice code SCALE / TRITON and used by the core simulator PARCS is validated in comparison to reference transport solutions in chapter 5. The full-core design studies for low moderated BWR cores, which are done iteratively between CASMO-4 and MICROBURN-B2, are presented in chapter 6. There, first the development steps leading to four different core designs are described and then the safety features and fuel utilization for all core designs are assessed in comparison to a reference full-MOX BWR core design. The thermal-hydraulic investigation of selected hot fuel assemblies of the four core designs are conducted in chapter 7. Finally, the major results are summarized.

2 Fundamentals of reactor analysis

2.1 Multi-physics and multi-scale approach

In the early times of nuclear engineering neutron physics (NP), thermal-hydraulics (TH), mechanics, chemistry and other involved topics were computed only separately. The ongoing trend is to directly couple different disciplines with increasing level of detail. Especially for reactor analysis, the coupling of NP and TH is very important due to the strong feedback of coolant and fuel thermal-hydraulic properties on the neutron behavior (cross-sections). Current state of the art is the coupling of these two fields of physics on the level of fuel assemblies for full-core calculations. Recent research efforts focus also on high-fidelity simulations at fuel pin resolution and by means of higher order methods for both NP and TH (see e.g. [43], [44], [45], [46]). However, their enormous computational effort still makes them unfeasible for production calculations. The incorporation of further tools to describe the mechanical fuel rod behavior and chemical reactions into the coupled codes even increases this effort and its complexity. For the analysis of LWR, the two last-mentioned capabilities are usually required in investigations of certain accident scenarios such as rod drop or loss-of-coolant accidents. Selected important issues of both NP and TH are discussed in more detail in chapters 2.2 and 2.3.

2.2 Neutron physics

The design of nuclear reactor cores requires detailed knowledge of present neutron physical processes such as the interaction of the neutrons with fuel, coolant and structural materials in the core. Generally speaking, NP describes the generation, distribution and motion of neutrons in a reactor and their interactions with matter. The common approach is to use the *Neutron Transport Equation* (NTE) to represent the appearing phenomena and to solve it mathematically with different simplifications depending on the intended application (reactor type, geometrical resolution etc.). The NTE is a simplified linear form of the *Boltzmann Transport Equation* (BTE) used originally to describe particle transport in gases. Its non-linearity can be avoided by neglecting interactions of neutrons with themselves. This simplification is appropriate because the neutron density in a power reactor is approximately 10^{14} orders of magnitude smaller than that of the nuclei in the surrounding matter (order of

10^{28} per m³). Therefore, neutron-neutron interactions are negligible compared to neutron-nucleus interactions. In the NTE, the neutrons are dependent on position, direction, energy (equivalent to speed) and time. In a homogeneous system, the nuclei are assumed to be isotropic in space and in thermal equilibrium with their surroundings and their characteristic physical properties are dependent on temperature and other factors (e.g. excitation). Possible interactions between neutrons and matter include capture, fission and scattering reactions that are described by an interaction probability called "cross-section" measured in barn (1 barn = 10^{-24} cm²). The reason, why today the NTE is solved only in simplified form (deterministic methods) or with statistical methods (Monte Carlo methods) is the great complexity resulting on the one hand from the very heterogeneous composition of a nuclear reactor systems and on the other hand from the strong energy dependence of the cross-section of many materials. Because an elaborate discussion of all aspects of reactor physics would exceed this review, only the most relevant aspects in this context are discussed. Further information may be found in e.g. [47], [48], [49], [50], [51] and [52].

2.2.1   General reactor physics solution approach

The geometrical heterogeneity of a reactor and the strong energy dependence of important cross-sections make it impracticable to compute the neutron flux distribution within the core directly. The relatively short mean free path of neutrons in thermal reactors additionally forbids the direct homogenization of local regions like fuel pin cells, because local effects could not be considered correctly. Currently, the common approach for LWR analysis is to use high geometrical detail and resolution in energy only in small and localized, but representative regions. Both are decreased with increasing problem size.

In the first step, cross-sections for homogeneous infinite dilute materials with high energy resolution (ideally point-wise nuclear data) are used in 1D or 2D fuel pin cell calculations to obtain an energy and spatially self-shielded neutron fine flux spectrum. This is then used to weight the problem independent multi-group cross-sections (usually not more than a few hundred energy groups) and to obtain problem dependent multi-group cross-sections for the subsequent processing. The second step is the infinite lattice calculation, in which these cross-sections are most commonly used in a 2D-model for one or a small group of fuel assemblies with reflective outer boundary conditions to obtain the corresponding neutron flux distribution. Afterwards, a correction with the fundamental mode approximation is utilized to account for leakages appearing in a real geometry and affecting the neutron spectrum before the multi-group cross-sections are collapsed into a user-defined few-group structure (two

groups for common LWR and up to several 10 groups for fast reactor applications). Subsequently all materials are homogenized to finally obtain the FA averaged group constants to be utilized in a 3D core simulator. In order to cover the whole thermal-hydraulic parameter space of a nuclear reactor, this step is repeated for various combinations of material properties (temperatures, densities), the so-called branches, which are then combined e.g. in multi-dimensional look-up tables or certain fitting functions. Fuel depletion is performed for a small selection of these branches (e.g. three history branches for the active coolant void contents of 0 %, 40 % and 80 % and for each void history one history with control rod withdrawn and one with control rod inserted) to capture burnup effects during operation. The full set of branches has to be computed for each burnup step and each history state. Finally, these generated tables or fits are employed in 3D core simulators to optimize fuel management and core design and perform e.g. core follow calculations. In Fig. 2.1 the described process is illustrated.
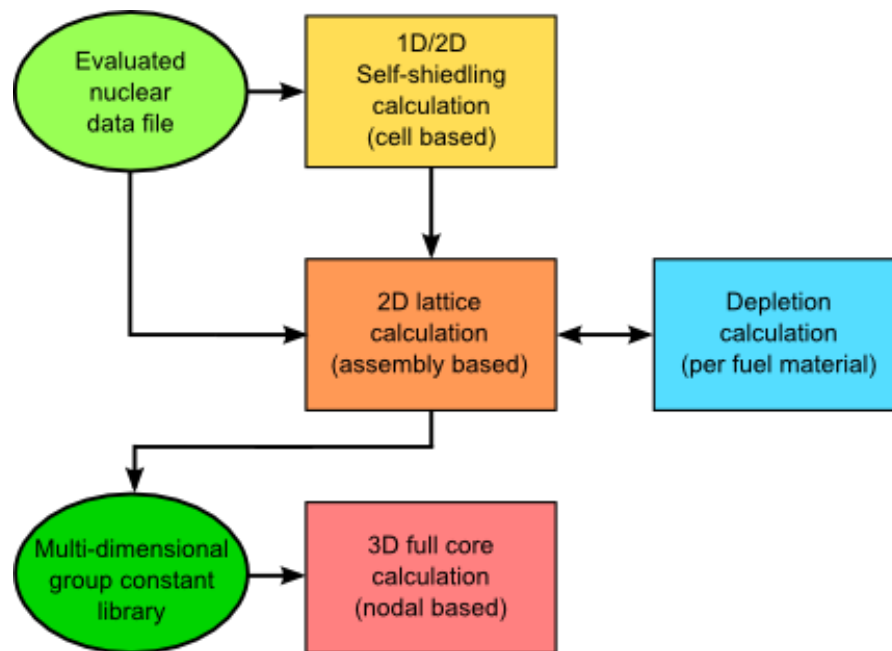
Fig. 2.1: General global computational scheme for deterministic reactor physics calculations

Depending on the application and the degree of detail, different simplifications and mathematical solution methods of the neutron transport equation are used. In the self-shielding and lattice physics calculations the collision probability method, the spherical harmonics method (P_N), the discrete ordinates method (S_N), and the method of characteristics (MOC) are widely used. For core calculations nodal methods based on the diffusion approximation or simplified spherical harmonics equations are mostly applied. To correct deficiencies in nodal methods for an accurate prediction of flux gradients between fuel assemblies or at the interface to the reflector, correction factors as the so-called assembly

discontinuity factors (ADFs) have to be applied. The ADF is the ratio of heterogeneous to homogeneous flux at an assembly surface. They can be determined from the lattice physics calculation in subsequent post processing. ADFs are then applied in core calculations for a consistent coupling of neighboring nodes. Depending on the heterogeneity of the core, this can improve but sometimes also deteriorate the solution (e.g. large spectral mismatch between neighboring fuel assemblies in MOX/UOX mixed cores). The effect of the correction on the superimposed errors originating from spatial discretization, spatial homogenization, group condensation and transport effects dictates how the solution is affected. Very beneficial cancellation of these errors for low order methods is often observed and the correction of single sources of errors is, thus, not necessarily improving the results [53], [54].

2.2.2   Nuclear data

To describe a nuclear reactor system, nuclear data for each individual material obtained from measurements are required. The corresponding experiments are challenging, due to the strong energy dependence of the different neutron-material interactions, covering several orders of magnitude in the energy range e.g. from 10^{-5} to 10^7 eV. Before nuclear data can be used in transport calculations, selected data have to be collected, evaluated and then stored in so-called "evaluated nuclear data libraries" (e.g. the general purpose libraries ENDF, JEFF, JENDL, BROND, or CENDL) to be used in reactor physics calculations. New measurements frequently call for re-evaluation of these files and new versions of evaluated libraries are released every few years. Of course, measurements are always accompanied by uncertainties, which are stored in corresponding covariance files. Currently, sensitivity and uncertainty analyses quantifying the influence of the measurement errors on the results of transport calculations are getting more attention in the nuclear engineering community. Such investigations can aid interpreting results and highlight potential for improvement.

2.2.3   Neutron multiplication and criticality

Important parameters characterizing the core state are the neutron multiplication factor and the reactivity. The criticality of any infinite nuclear reactor is quantified with the infinite neutron multiplication factor k_{inf} which is defined as

$$k_{inf} = \frac{\text{neutron generation}}{\text{neutron consumption}} \ . \tag{2.1}$$

For a real finite reactor the leakage of neutrons has to be taken into account with the non-leakage probability P_{NL} to get the effective neutron multiplication factor:

$$k_{eff} = k_{inf}P_{NL} \,. \tag{2.2}$$

A reactor state is called sub-critical, critical or super-critical if k is smaller, equal to or larger than unity, respectively. The reactivity ρ, defined in the following equation, is another common way to describe the reactor state:

$$\rho = \frac{k_{eff} - 1}{k_{eff}} \,. \tag{2.3}$$

It is stated most commonly in measures of pcm (1 pcm = 10^{-5}) or relative to the delayed neutron fraction β in units of $. The second method is especially important since it allows comparing the kinetics of different reactor types or reactors loaded with different fuel types since β is mainly determined by the material composition. Reactivity smaller than, equal to or larger than zero indicates a sub-critical, critical or super-critical reactor state, respectively. In addition, it is now possible to differ between delayed and prompt critical states for values below or above $\rho = \beta$ respectively. The reactor power will decrease in a sub-critical and will increase in a super-critical reactor. For k_{eff} of unity, the reactor can be operated with constant power in steady state. While the neutron flux converges to a finite limit for a delayed super-critical reactivity jump, prompt super-criticality has to be avoided because the neutron flux would increase exponentially. This means that a real reactor would not be controllable without the delayed neutrons having an average lifetime of several seconds compared to the lifetime of prompt fission neutrons of 10^{-7} s in fast reactors and between 10^{-3} s and 10^{-5} s in thermal reactors depending on the moderator.

Due to the uncertainties in nuclear data and computational methods, the critical eigenvalue may differ from unity when computing critical reactor states. This bias can depend on reactor type (e.g. BWR or PWR), material composition of the core, cycle burnup, fuel type, and current reactor state such as e.g. cold zero power (CZP), hot zero power (HZP) or hot full power (HFP). In PWR core calculations the bias is usually assumed to originate from the uncertainty in the boron concentration which is then adjusted to obtain an eigenvalue close to unity during the whole cycle. For BWR, on the other hand, this is not possible because no boron is used for reactivity control. Instead experience from core follow calculations of previous cycles is used to estimate an appropriate correlation of a target value for k_{eff} (k_{target}) versus cycle exposure to adjust the prediction of following cycles accordingly (cp. e.g. [55], [56], [57]).

2.2.4   Conversion ratio

For the optimal design of a low moderated BWR core, the fuel utilization is an important parameter to assess the design proposals. It can be quantified with the conversion ratio (CR) describing the ratio of fissile material production to the fissile material consumption during operation. If its value exceeds unity it is referred to as breeding ratio. The CR is defined as follows:

$$CR = \frac{\text{capture reaction rate in fertile material}}{\text{absorption reaction rate in fissile material}}. \tag{2.4}$$

An increase of CR can be achieved i.a. by reducing the moderator to fuel ratio (MFR) or the fuel radius. The first hardens the neutron spectrum by reducing the moderation, which increases neutron capture in the epi-thermal energy range (1 eV to 100 keV) especially in the fertile ^{238}U, which in turn results in increased production of ^{239}Pu. The second decreases the self-shielding effects in the fuel due to an increased surface to volume ratio. A very strong impact on CR is also induced by the fuel enrichment, which is easy to see in equation (2.4): less fissile material results in less consumption of that material. If not otherwise mentioned, fertile materials include ^{238}U and ^{240}Pu and fissile materials include ^{235}U, ^{239}Pu and ^{241}Pu.

2.2.5   Fissile inventory ratio

The conversion ratio varies strongly during a cycle and depends on many parameters. Hence it seems unfeasible to determine the absolute fissile material demand of a reactor from it. In addition it is an instantaneous parameter and can only be determined if the current individual isotopic reaction rates are available. Nodal reactor simulators usually use only FA homogenized material constants making it challenging to determine CR in a full-core calculation. Some nodal codes (e.g. MICROBURN-B2) consider a selection of important nuclides with microscopic cross-sections and yield nuclide concentrations in each depletion step. This allows to determine of the net consumption of fissile material during a cycle in the whole core or in a single FA and to compute the fissile inventory ratio (FIR), which is defined as follows:

$$FIR = \frac{\text{current fissile inventory}}{\text{initial fissile inventory}}. \tag{2.5}$$

2.2.6   Reactivity coefficients

Reactivity coefficients describe the feedback of a nuclear reactor core on a thermal-hydraulic parameter or material composition change. They characterize the kinetic behavior

and the inherent safety of the nuclear reactor core and can be used e.g. as input for a reactor point kinetic model. For a stable and safe reactor operation, the reactivity coefficients have to be negative, but should not be too large to avoid instabilities. Important reactivity coefficients are i.a. the reactivity coefficient of fuel temperature, moderator temperature and density, void fraction, core power and boron concentration. A detailed discussion of each reactivity coefficient can be found in various textbooks e.g. in [49]. Here only a brief overview of selected reactivity coefficients of relevance is given.

Fuel temperature reactivity coefficient

The fuel temperature reactivity coefficient, also called Doppler reactivity coefficient (DC), describes the reactivity change caused by the variation of the fuel temperature in a nuclear reactor core. An increase of the fuel temperature leads to stronger thermal movement of the nuclei and broadening of the resonances in the cross-sections (Doppler effect). The DC is crucial to limit the power increase caused by a prompt super-critical reactivity insertion and must always be negative. Main contributors to a negative DC are especially the capture resonances in fertile fuel materials like ^{238}U or ^{240}Pu. The DC is usually in the range of −1 to −4 pcm/K for LWR and becomes more negative for decreasing fuel temperature due to the inverse proportionality to the square root of the fuel temperature. In general the DC is very sensitive to the fuel composition. It tends to be more positive in harder neutron spectrum and can become more negative with exposure e.g. due to the buildup of ^{240}Pu.

Coolant void reactivity coefficient

The coolant void coefficient of reactivity (VC) is very important in BWR since any change of the void fraction in the core will significantly impact the neutron moderation due to the change of the coolant density. Since the neutron spectrum in low moderated cores is harder (higher average energy of incident neutrons) and the plutonium content in the core is increased compared to a Gen-II BWR core, the reactivity change caused by a coolant density change in the core is less negative. Two major mechanisms cause this effect [20]:

1) The number of neutrons per fission (η) caused by thermal neutrons is similar for ^{239}Pu and for ^{235}U. However, for increasing incident neutron energy, η becomes larger for ^{239}Pu than for ^{235}U, which is shown in Fig. 2.2. Consequently, a shift of the neutron spectrum from mainly thermal to more epi-thermal energies has a minor effect for ^{235}U, but a stronger effect for ^{239}Pu.

2) Fast fissions of ^{238}U happen only for incident neutron energies above 1.3 MeV. Therefore, the fraction of fast fissions increases for a harder neutron spectrum.

Since the VC is sensitive to the way it is determined and its significance in global perspective is limited, it has to be used with care. The moderator temperature reactivity coefficient at HFP with constant moderator density is negligible compared to the void fraction reactivity because the coolant has saturation temperature in almost the entire core.
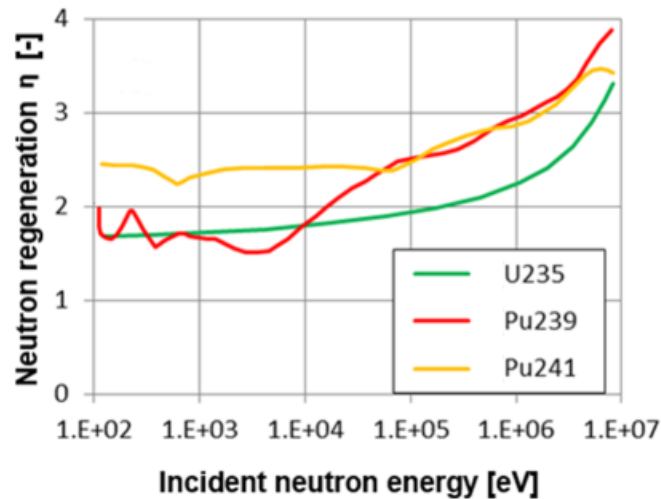
Fig. 2.2: Neutron regeneration η for different fissile isotopes as a function of incident neutron energy (figure generated with [58])

Isothermal temperature coefficient

The isothermal temperature coefficient (ITC) is especially important during the start-up of a reactor to keep the reactor controllable between cold zero power (20 °C) and hot zero power conditions (285 °C). It is determined assuming a slow heat-up which allows the reactor to attain a uniform temperature distribution within the fuel, the structures and the coolant. Positive values for the ITC are allowed for low temperatures as long as it becomes negative with sufficient safety margin to the operating temperature. The most important factors influencing the ITC are the moderator to fuel mass ratio in the FA and the neutron leakage rate into neutron absorbers and out of the core [59].

2.2.7   Long term reactor behavior and cycle analysis

Beside the instantaneous reaction rate balance, also the long term behavior of the reactor has to be modeled appropriately to obtain a best-estimate prediction of the cycle dependent fuel composition. For this purpose, not only the behavior of heavy isotopes during exposure but also the influence of important fission products and artificial neutron poisons has to be

considered. For general reactor application, it is sufficient to consider about 100 actinides and fission products and to add significant problem specific materials. To estimate the reactivity change over a cycle of a high burnup core appropriately, it is recommended to take into account up to about 400 nuclides [60]. In lattice physics calculations the sometimes complex decay chains of the various materials are modeled with a system of differential equations based on the Bateman equation.

Especially the strong neutron poisons ^{135}Xe and ^{149}Sm are important, which build up after reactor start-up depending on the power level in time intervals of days and weeks, respectively. After a reactor shutdown, xenon builds up further because the dominating removal process of neutron capture is stopped but the decay of the remaining precursors still continues. The remaining xenon completely decays once the precursors have vanished. These processes take some hours or days depending on the steady state power level before shutdown. Samarium, on the other hand, further builds up after shutdown from a continuing decay of its precursor promethium, but is stable by itself and removed during steady state operation only by neutron capture. Therefore, the samarium concentrations will converge to a limit above the steady state level. Once the reactor is started again, samarium concentrations will return to a steady state value depending on the core power level. The short time dependence of xenon and samarium concentrations in the fuel justifies the explicit treatment of these fission products even in core calculations with microscopic cross-sections.

The depletion calculation in core simulators is mostly done simply by using the nodal power and the heavy metal density to find the local fuel exposure. The generally used unit of exposure is the specific power generated per heavy metal mass: MWd/kgHM. Another common measure is the exposure in terms of equivalent full power days (efpd) or equivalent full power hours (efph) representing the generated power during a certain amount of time of operation at rated core power. The total generated energy, measured e.g. in units of TWh, can be used to compare cores of different size and rated power to each other.

To estimate the achievable multi-batch fuel assembly burnup from lattice calculations with core average thermal-hydraulic conditions, the linear reactivity model [61] can be employed. This model assumes a linear reactivity behavior versus exposure. Based on it, the discharge burnup of a core with n batches (B_n) can be extrapolated from a single batch discharge burnup (B_1) with the following equation:

$$B_n = B_1 \left(\frac{2n}{n+1} \right).$$

(2.6)

To account for leakage effects in the finite core, the B_1 burnup should be determined from the lattice physics calculation for k_{eff} reaching e.g. 1.025 instead of unity. Although this methodology is only a rough approximation, it is appropriate to compare different FA designs.

2.3 Thermal-hydraulics

Thermal-hydraulic analysis of nuclear reactor systems is important for reactor safety. In the thermal analysis, one uses the power distribution from neutron physics analysis to determine the temperature distribution in fuel, fuel rod gas gap, cladding and coolant, while the hydraulic analysis is used to determine the state of the coolant, flow pattern (important to predict heat transfer from cladding to coolant) and pressure losses. The underlying theory of reactor TH is well summarized e.g. in [62] or [63] and important aspects for this work are summarized in the following paragraphs.

2.3.1 Thermal analysis

Thermal analysis in the fuel is particularly challenging, because on the one hand the thermal properties (thermal conductivity, specific heat capacity) of the fuel changes strongly with temperature and the temperature difference in the fuel can range over more than 1000 K and on the other hand the fuel is highly affected by the irradiation, which changes material porosity, composition and stoichiometry (burnup, sintering, cracking, fission gas release). Limiting in the fuel material is especially the melting temperature which is around 3100 K and 2600 K for un-irradiated UO_2 and PuO_2, respectively. The melting point decreases by approximately 0.5 K per 1 MWd/kgHM burnup [64]. Usually a conservative upper design limit of e.g. 2850 K for UO_2 is set at the fuel rod centerline to account for uncertainties, which must not be reached.

The fuel rod gap in fresh fuel closes when the fuel is heated up during operation and finally stays closed after some fuel swelling (fission gas build up) and cracking of the fuel pellets. But even after the gap is closed it still bears the largest thermal resistance between fuel and coolant because the contact between pellet and cladding is never perfect. The effective fuel rod gap heat transfer coefficient can range between a few thousand and more than ten thousand W/m²K. It depends on the fabrication of cladding and fuel (quality of contact), the burnup (composition of gap gas depends on fission products), and the temperature.

In a thin Zircaloy cladding, linear temperature drop can be assumed due to the high thermal conductivity of the metals. To assure cladding integrity (first technological barrier to hold back fission products), design limits such as the temperature for heavy exothermal Zircaloy-water oxidation reaction at 1200 °C (heats up the cladding further and generates hydrogen) and the melting point of Zircaloy (e.g. 1850 °C for Zircaloy-2) are defined.

The heat transfer from the fuel rod surface to the coolant is strongly dependent on the flow regime within the coolant channels. Its determination depends on how the hydraulic analysis is performed. For production calculations, usually empirical correlations are utilized as function of i.a. geometry, pressure, coolant void content, and mass flux.

2.3.2   Hydraulic analysis

In most hydraulic calculations used for reactor core or system calculations, only averaged quantities describing the fluid motion and properties are used. The alternative is the direct numerical simulation (DNS) of all quantities, which is not feasible for production calculations because of the large required computational resources. The common approach is to calculate mass, momentum and energy transport as a coupled system of equations. Several unknowns appear in these equations because of the averaging of the fluid properties, which necessitates closure laws for their determination. Depending on the problem type and solution scale multiple spatial directions are described with a full set of equations (e.g. 3D CFD) or only one direction is sufficient (e.g. 1D system codes). In sub-channel codes for example, with primarily axial flow, lateral momentum transfer is additionally computed between connected channels with a coupling equation (often called 1.5D approach).

While single-phase flow can be modeled with one set of mass, momentum and energy equations (one field), two-phase flow is much more challenging. Several approaches exist, which are usually more or less appropriate for certain flow regimes due to different effects depending e.g. on coolant mass flux and void content, but also on the geometry. The simplest method uses one field to describe a homogeneous mixture of vapor and liquid and is appropriate for high mass flux. More sophisticated is the use of two fields with separate mass, momentum and energy equations for vapor and liquid. This approach is adequate to describe high void and low mass flux two-phase flow. An often used trade-off to save computational capacity is a model with one field for the mixture and one additional mass balance equation for the vapor phase. This approach gives good results for flow with low void and low mass flux. In some codes such as CATHARE 3 [65] and F-COBRA-TF [66] more fields are added

to model e.g. entrainment of droplets in the vapor. However, the larger the system of equations becomes, the more constitutive relations are required. The latter are derived mainly from experimental investigations. Unfortunately, not all mass, momentum and heat transfer phenomena at the wall and at the interface between different fields are experimentally accessible as required by the closure models.

Turbulence effects are usually not directly described in thermal-hydraulic system codes and sub-channel codes, but they are included e.g. via Reynolds-dependent friction loss terms. In more detailed simulation methods such as CFD, turbulences can be explicitly modeled with an algebraic turbulence model or a transport model for the turbulent kinetic energy with one or two differential equations (K-ε, K-w) [67]. Some of these turbulence models are strongly dependent on flow conditions and not applicable to model every system.

2.3.3 Boiling transition prediction

Boiling transition must be avoided in all operation states to ensure safe reactor operation and preserve sufficient safety margins to the above mentioned temperature limits for cladding and fuel. Therefore, the actual surface heat flux q'' [W/m²] has to be maintained below the critical heat flux (CHF) q''_{crit} marking the appearance of boiling crisis, which is dependent on the two-phase flow regime and leads to a sudden rise in the cladding surface temperature due to reduced heat removal capability of the steam. The first kind of boiling crisis, common for PWR, is the departure from nucleate boiling (DNB), where the high heat flux leads to the formation of an insulating vapor film on the fuel rod surface. The second kind of boiling crisis is the dryout of liquid film on the fuel rod surface, which appears usually at high steam quality (mass fraction of steam in steam-water-mixture) flow conditions and is, thus, especially important for BWR analysis. Appearance of dryout CHF condition depends on many parameters including coolant mass flux, steam quality, system pressure, geometry, boiling length (distance to the onset of bulk boiling), spacer type and surface condition. Unlike the local phenomenon of DNB, dryout depends strongly on the flow history upstream of the location where it appears. The first approach to determine boiling transition in BWR was the use of conservative lower limit lines (e.g. Hench-Levy) to obtain the critical heat flux ratio (CHFR) in a fuel assembly defined as:

$$\text{CHFR} = \frac{q''_{crit}}{q''}. \qquad (2.7)$$

To account for uncertainties and transients usually a safety margin was applied for the minimal critical heat flux ratio (MCHFR) in a FA (e.g. MCHFR = 1.9 for BWR transients). Unfortunately, this local design criterion does not capture integral axial effects which are gaining importance with increasing steam quality. It is, therefore, replaced with the integral minimum critical power ratio (MCPR) design limit, where the critical power ratio (CPR) is defined as the ratio of the critical bundle power at which local dryout appears somewhere in the FA and the actual operating power. The advantage of this figure of merit is its comprehensiveness. For example for a MCPR of 1.3, which is recommended in [68] for BWR steady state operation, one can directly derive a margin for power increase of 30 % until dryout appears, which is not the case for MCHFR = 1.3.

Due to the wide range of uncertainties in the numerical tools, the nuclear industry performs experimental investigations for new FA designs to derive the appropriate correlations that can be later on implemented in the numerical codes to perform safety evaluations.

2.4   Experience with mixed-oxide fuels

The knowledge of the neutron-physical and thermo-physical properties of the mixed plutonium and uranium oxide (MOX) fuels is required to predict of their behavior inside the core. MOX fuel is already in use since the 1970s and its properties have been investigated intensively for different reactor types (e.g. for BWR in [69]). Key aspects of MOX fuel technologies are discussed e.g. in [11]. There, the direct disposal of burned fuel raised serious non-proliferation concerns for centuries or even millennia. One alternative suggested in [11] is the reduction of the plutonium stockpiles by MOX recycling in addition to the introduction of advanced reactor designs with 100 % MOX cores, like advanced BWRs (ABWRs) or high conversion LWR. In current German BWRs of Gen-II, the share of MOX fuel assemblies in the core is limited to $30 - 50$ % [70] but recent studies have shown that 100 % MOX loading in a Gen-II BWR can be feasible [12].

Modern LWR MOX fuel can contain contents of more than 4 wt% (weight-%) fissile plutonium (Pu_{fiss}) corresponding to a total plutonium content (Pu_{tot}) of more than 6 wt% depending on the plutonium quality ($Pu_{qual} = Pu_{fiss} / Pu_{tot}$). The enrichment of plutonium in MOX fuel is only limited by the selected fabrication process to $40 - 50$ % (e.g. solubility in nitric acid). However, benchmark studies suggest keeping the assembly average Pu_{tot} content below 13 wt% to avoid a positive void reactivity coefficient [70]. In addition, the increase of

heat loads and radiation due to an increased Pu-enrichment of MOX is challenging for the reprocessing plants. This is also the case if multi-recycling of LWR MOX fuel is considered due to the continuous reduction of the plutonium quality and the increasing fraction of minor actinides in the used fuel [71].

Due to strong thermal resonances in ^{240}Pu and ^{242}Pu, the spectrum is hardened compared to uranium fuel in the same fuel lattice [70]. The smaller fraction of delayed neutrons emitted by fission products also cause reduced time constants in reactor kinetics and require careful analysis of relevant reactivity insertion transients. The use of MOX fuel in BWR does not necessarily require changes of the control systems because of the large water gaps between the fuel assemblies assuring a sufficiently large thermal neutron flux. Hence, the control assembly worth remains almost unchanged (cp. [70] p.350ff).

2.5 Fuel assembly and core design

The design of a fuel assembly mainly consists of maximizing the reactivity while minimizing the enrichment, enrichment levels and local power peaking. In practice, an acceptable trade-off between the different optimization goals has to be found. Current BWR usually contain heterogeneous core loadings with different fuel assembly types and different rod numbers as well as internal water structures (rods or channels) depending on the vendor. The individual enrichment of the fuel rods within a BWR FA is adjusted in such a way that the pin power distribution is as uniform as possible (e.g. peak pin power factor in fresh fuel below 1.3). Thus, the enrichment has to be reduced in fuel rods next to the bypass and internal water structures due to the improved moderation. To compensate the high reactivity at begin of cycle (BOC), burnable poison rods (BPRs) containing gadolinia (Gd_2O_3) are included in BWR FA. They can vary in number and gadolinia enrichment. The use of BPRs minimizes the need for control rod insertion during the operation cycle leading to a higher shutdown margin. A higher number of BPR in a FA induces stronger reactivity suppression while the amount of absorber per BPR affects mainly the time until the absorber is entirely burned. Usually the FA design is such that the absorber effect in fresh fuel wears off within the first cycle. Due to the self-shielding, Gd in the fuel pin center burns very slowly which causes a small reactivity penalty during the whole fuel residence time in the core.

Modern reload strategies in BWR often take advantage of quarter- or half-core symmetry and a low leakage loading, for which old FA are placed at the core periphery to reduce leakage of neutrons from the core and in this way also protect the RPV from neutron induced

embrittlement. Fresh FA are mostly grouped together with older ones having less reactivity in a control cell (group of 4 FA surrounding one CR cross) to reduce radial power peaking. The main limiting design criteria for Gen-II BWR are the reactivity coefficients, the dryout limit and the shutdown margin. Optimization of a core loading targets of course at a small reload fraction with low enrichment to reduce costs at simultaneously acceptable safety parameters [72].

3   Selected simulation tools

3.1   Lattice physics codes

The studies on lattice physics level and the few group cross-section generation for reactor core simulators are performed by means of CASMO–4 [73] and SCALE6.1 / TRITON [60]. Both codes are using transport theory as described in section 2.2.1 to determine the flux distribution in two–dimensional fuel assembly models. Selected features of the codes, discussed in detail in the manuals referenced above, are summarized below.

3.1.1   CASMO-4

In CASMO-4, nuclear data are available for 108 nuclides in a microscopic cross-section library in 70 ("L-library") or 40 energy groups. The neutron energies cover the relevant energy range for nuclear reactor analysis up to 10 MeV. It is based mainly on data from the ENDF/B-4 library. Effective resonance cross-sections are prepared for each individual fuel pin. Micro and macro group calculations are used to simplify the problem geometry and the energy group structure to significantly reduce the computational effort without sacrificing too much detail. The final transport calculation to obtain the heterogeneous flux in the infinite FA lattice is done with the method of characteristics (MOC) normally in 7 energy groups. Subsequently, a fundamental mode calculation is used to account for leakage effects as they appear due to the finite dimensions of a nuclear reactor. The depletion of fuel and absorber materials is performed with a predictor-corrector approach.

3.1.2   SCALE6.1 / TRITON

The SCALE6.1 / TRITON lattice physics control sequence in the SCALE6.1 code package (referred to as TRITON here) couples different independent tools. They form a computational route to generate macroscopic few-group material constants from individual microscopic cross-sections per nuclide provided by the ENDF/B-VII library in 238 energy groups covering neutron energies of up to 20 MeV. Resonance self-shielding calculations are done with CENTRM inside and BONAMI outside the resolved resonance region for each separate pin. To obtain the heterogeneous flux in the FA, the NEWT discrete ordinates transport solver is used to solve the transport equation with the extended step characteristics (ESC) approach which is more flexible but significantly slower as e.g. MOC algorithms [74].

The neutron spectrum used for collapsing of multi-group cross-sections to requested few-group structure is corrected using the B1-equations to account for neutron leakage. The depletion of fuel and absorber materials is performed with ORIGEN-S utilizing a similar but different predictor-corrector approach as in CASMO–4. Depending on the modeling needs, different amounts of nuclides can be taken into account in depletion calculations, ranging from using only the 15 most important actinides for scoping studies, to using up to 388 nuclides including actinides, fission products and other important nuclides for high burnup applications. In standard calculations 94 different nuclides are considered, which usually renders satisfying results for the common exposure range.

3.2   The Monte-Carlo code KENO-VI

KENO-VI is a Monte Carlo (MC) criticality program within the SCALE6.1 platform [60]. Definition of generalized geometry models is possible similar to NEWT. It can be used to compute e.g. the neutron multiplication factor and various energy- and region-dependent reaction rate densities in nuclear systems. Both continuous energy (CE) and multi-group (MG) cross-section libraries are available for calculations. If the multi-group mode is used, resonance preprocessing calculations for representative unit cells have to be done with e.g. CENTRM, as within TRITON.

KENO-VI is well validated (see e.g. [75]) and is performing well for systems with different fuel materials like uranium or plutonium in different forms and also with different structural or moderator materials. A known issue reported in [75] is the unsatisfying $S(\alpha,\beta)$ treatment in continuous-energy mode, which leads to a systematic under-prediction of the neutron multiplication factor especially for systems containing plutonium compared to experiments and KENO in the multi-group mode. This effect is even increasing when the moderation is reduced. Although the deviation is less than 1 % and hence still in the range of the cross-section uncertainties, this is an identified area for possible improvements which are supposed to be included in the upcoming program package version SCALE6.2.

Here, KENO-VI is especially applied to verify results obtained by TRITON and PARCS in connection with material constants generated with TRITON. As explained in [76] KENO-VI in multi-group mode can be used to verify the spatial and angular discretization and the scattering order applied in a NEWT model, while KENO-VI in continuous-energy mode versus KENO-VI in multi-group mode tests if the multi-group approximation is valid for the investigated case.

3.3 Reactor core simulators

3.3.1 MICROBURN-B2

The nodal core simulator MICROBURN–B2 [77] is optimized for steady state BWR core design and solves the two group neutron diffusion equations with the advanced nodal expansion method (ANEM) using an analytical reflector model to avoid explicit reflector treatment and to reduce the runtime. In connection with the CASMO–4 lattice code and the cross-section interface MICRO-B2 a state of the art BWR core design methodology is formed. Material constants generated with CASMO-4 comprise coolant density histories for 0, 40, and 80 % void content and control rod histories for each void content. Various branches are included to allow for cross-section look-up and interpolation from CZP up to HZP peak power conditions. The code performs explicit microscopic depletion of the common reactor poisons xenon, samarium, and gadolinium and 11 additional heavy metal nuclides which makes the evaluation of the full-core fuel utilization feasible. The xenon and samarium concentrations can be investigated with time-dependent decay calculations. State of the art pin power reconstruction capabilities are used to determine local power and exposure distributions. To account for the strong thermal-hydraulic feedback effects in BWR, an internal steady state BWR thermal-hydraulics model is included which separately considers each individual active fuel channel, water rod or channel and the bypass. Together with 3D pin power distributions and bundle dependent correlations, the TH-module is also able to predict CPR. Starting from a reference state, automatic algorithms are included to subsequently determine e.g. stuck-rod cold shutdown margins and important reactivity coefficients.

Measurements in BWR plants with a wide spectrum of operation and loading strategies have been used for the validation of the core simulator and the depletion predictor-corrector methodology. Fuel design validation basis includes square pitch lattices up to 13x13 pins with UO_2 and MOX fuel with exposure ranging up to 72 MWd/kgHM. Material validation covers ^{235}U enrichment up to 5.0 wt%, Pu_{fiss} contents of up to 5.5 wt% and Gd concentrations in UO_2 fuel up to 10 wt%. Various GE, KWU, and ABB core designs with different number of FA, core height ($3.5 - 4.0\,m$), types of control elements, and FA designs have been used for validation as well.

3.3.2 PARCS

The PARCS 3D reactor kinetics core simulator [78], [79] can solve steady state and time-dependent problems with the neutron diffusion equations or low order transport equations

(SP$_3$) in multi-group energy structure in orthogonal and hexagonal geometries. Available discretization schemes include fine mesh finite differences (FMFD), the analytical nodal method (ANM), and the nodal expansion method (NEM). Since the NEM method is more robust and the ANM method is more accurate, an implemented HYBRID solution kernel (NEM for "near-critical" nodes and ANM otherwise) combines the advantages of both. Outer core boundary conditions can be defined by means of albedos or by explicit modelling of the reflector in conjunction with vacuum boundary conditions (zero incoming neutron current). The interface GenPMAXS [80] can be used to extract cross-section information from various lattice codes (e.g. CASMO, TRITON, HELIOS [81], SERPENT [82]) and transfer it to multi-dimensional tables in the PMAXS format native to PARCS. The history and branch structure can be selected arbitrarily which allows a high flexibility and finer structures. On the other hand, larger number of data points increases the computation time required by the lattice code for cross-section generation. Node wise cross-sections are obtained from the PMAXS files by means of look-up in the tables and interpolation. Fuel depletion is done by power for the whole core with a predictor-corrector algorithm. Just recently also multi-cycle capabilities have been added to PARCS which enables its use for the determination of equilibrium cycles. Microscopic cross-sections for xenon and samarium can be used to compute their time-dependent concentration evolution. Similar as in MICROBURN-B2, 3D pin power distributions can be subsequently calculated with the pin power reconstruction method.

To predict feedback conditions more accurately, internal TH solvers can be employed for steady state core design analysis and an external coupling with one of the system codes TRACE [83] or RELAP5 [84] can be used for transient analysis. The lately implemented PATHS [85] thermal-hydraulic solver for BWR core analysis employs a four equation drift flux model and adequately reproduces TRACE results with significant runtime improvement. Unfortunately, the bypass is not considered in any of the thermal-hydraulic models. Thus, no local coolant properties are available and core averaged values have to be used for cross-section look-up instead. This is especially disadvantageous for analysis of BWR, which have very different coolant properties in bottom, radial and top reflector.

More potential for improvement of PARCS for BWR analysis is identified in a validation report in comparison to measurements [86]. While the calculated core eigenvalues for several different measured core states are adequate, the local power distributions predicted by PARCS strongly differ from TIP (traversing incore probe) measurement values especially for regions near inserted control elements and at the core periphery.

3.4   The sub-channel code SUBCHANFLOW

3.4.1   Methodology

SUBCHANFLOW is a sub-channel flow simulation code based on the legacy COBRA (Coolant Boiling in Rod Arrays) code family [87]. Important changes include mainly updating the code-structure to a state of the art and portable FORTRAN 95 computational tool. An iteration based fully implicit solver is employed to solve both steady state and transient problems. The fluid dynamic mixture model is used, which is composed of three equations for the conservation of mass, momentum and energy in flow direction (counter current flow like quenching cannot be computed due to the solution methodology) and one additional equation for the lateral momentum exchange. Various empirical correlations to describe friction losses and two-phase flow phenomena to close the system of equations are provided and summarized in Tab. 3.1.

Tab. 3.1: Available empirical correlations implemented in SUBCHANFLOW [87]

Subcooled void	Levy, Saha-Zuber, Unal, Bowring, no sub-cooled void model
Boiling void	no vapor slip, Armand slip model, Smith slip ratio model, Chexal-Lellouche model
Two-phase friction	homogeneous friction model, Armand friction model, Lockhart-Martinelli model
Turbulent friction	Blasius, Rehme wire wrap, Rehme grid spacer, Churchill
Heat transfer	Dittus-Boelter, Gnielinski, Subbotin for liquid metals
Critical heat flux (CHF)	Modified Barnett – Babcock-Wilcox, Biasi, OKB, W-3, Levitan, EPRI with shape function
CHF shape factor	no power profile correction, COBRA4I shape correction, Tong shape correction, W3 shape correction, Smolin shape correction
Fuel rod gap model	simplified model, TRANSURANUS-Model, benchmark VVER1000 cold gap

Thermo-physical correlations and tables are available for water (IAPWS-97 steam tables), liquid metals (sodium, lead) and gases (helium, air). However, two-phase flow models are only implemented for water and sodium. The heat transfer in the fuel rods is described by means of a finite volume method. Fuel material properties for UO_2 and MOX (UO_2PuO_2) are implemented based on formulations from the TRACE code [83]. Zircaloy and stainless steel (316 SS) are available cladding materials. Various benchmarks have been used for code validation [88], [89], [90], [91], [92], [93] and the code is used in various coupled NP / TH code systems [43], [45], [46].

3.4.2   Limitations

Up to today, two-phase flow phenomena are only theoretically describable in form of a general universal model. Different approaches try to model the various phenomena in increasing detail (e.g. separate sets of equations for the different fields steam, continuous liquid and entrained liquid, resulting in 9 equations) to avoid the use of empirical correlations. However, the route to a more accurate description yields an increasing number of unknowns, which themselves require closure laws or assumptions to be determined. Thus, the uncertainty in many two-phase flow simulations is naturally larger than in single phase flows.

Boiling transition phenomena like dryout are even more difficult to predict precisely. The implemented empirical correlations to determine the CHF have been obtained from measurements in single channels, round ducts or generalized fuel bundles. Geometry and TH-conditions have usually been chosen to cover the common LWR parameter range. Although the flow conditions in low moderated FA are similar, the tight lattice geometry is not covered by most CHF-correlations and an extrapolation is not recommended. Boiling transition is also strongly dependent on the local flow regime, which is affected by spacers. They are often only modeled as flow path obstruction causing local pressure loss and are not included in the generalized empirical CHF correlations. Therefore, in the industry separate correlations are usually obtained for each individual FA-design from full-scale bundle experiments.

4 Design studies for a low moderated BWR FA

Scoping studies for low moderated BWR FA are summarized in this chapter. They include investigation of different geometries and fuel compositions, but also the analysis of the influence of the solution method. The main results presented in this chapter are summarized from [94] and [95]. The major goal of these studies is to identify designs with superior fuel utilization and exclude potentially unsafe designs. Additionally model options of TRITON (angular discretization, mesh size, influence of user-defined Dancoff factors) are analyzed aiming to validate the deterministic methodology, which is the pre-requisite for reliable core level calculations.

4.1 Analysis Methodology

The design investigations are conducted with the lattice code TRITON, which utilizes the NEWT transport solver, and cross-sections in 238 energy groups based on the general purpose library ENDF/B-VII. In NEWT, the recommended options [76] for spatial discretization (4x4 cells per pin cell), angular discretization (S_6), and scattering order are applied (P_2 in water and P_1 in all other materials). More detailed options give only slightly improved results but unreasonably increase the runtime. Additionally, selected cases are compared with CASMO-4 calculations employing the available 70 group library. Verification of the NEWT results for one selected low moderated FA for different active coolant channel void content is performed with the Monte Carlo code KENO-VI both in multi-group (MG) mode with cross-sections in 238 energy group structure and in continuous energy (CE) mode (cross-sections for both cases based on the evaluated nuclear data file ENDF/B-VII). The parametric design studies are performed as infinite lattice assembly calculations. Subsequently a buckling correction of the flux spectrum is applied before the cross-sections are collapsed to a 2 group structure and all materials in the FA are homogenized.

The conversion ratio is determined from the 2 group material constants per nuclide which can easily be done from the CASMO-4 output where FA homogenized cross-sections are supplied for individual nuclides. Obtaining the CR from the NEWT output is significantly more effort because the cross-sections per nuclide are given only before the homogenization of the whole fuel assembly and, thus, the homogenization per nuclide has to be done

manually. The conversion ratio is computed according to equation (2.4) considering the fertile nuclides ^{238}U, ^{238}Pu, and ^{240}Pu and the fissile nuclides ^{235}U, ^{239}Pu, and ^{241}Pu.

While CASMO-4 automatically applies individual local Dancoff factors for each fuel pin to consider lattice heterogeneities (e.g. water rods or the bypass channel in a BWR FA) in resonance calculations, in TRITON the user has to determine them from separate calculations (e.g. with the KENO-VI based tool MCDancoff, which is included in the SCALE code package, or from corresponding CASMO-4 calculations) and supply them manually depending on the TH conditions and geometry to the resonance calculation tool CENTRM. This is most important for calculations of fuel assembly with heterogeneous moderation like BWR FA with voided active coolant and un-voided bypass moderator. As an example, for a void content of 80 % in a typical BWR lattice, studies have demonstrated an over-prediction of the infinite multiplication factor k_{inf} by 800-1100 pcm, if the default infinite lattice Dancoff factors are used [76]. Investigations have shown that it is sufficient here to use 3 averaged groups of Dancoff factors per low moderated FA design and TH state. The reason is the small number of rod types (only 4 enrichment levels, no absorber rods, no part-length fuel rods) the removal of internal water structures and the uniform enrichment distribution. They correspond to the groups of corner rods with 3 neighbors, peripheral rods with 5 neighbors and center rods with 8 neighbors.

Reactivity coefficients on lattice level are simply determined as the change in the multiplication factor between two cases divided by the change in the corresponding parameter.

The linear reactivity model described in section 2.2.7 is used to get an estimate on the achievable multi-batch discharge burnup from the one-batch burnup. The one-batch burnup is determined from the lattice calculations for k_{inf} dropping below 1.025, which accounts for leakage in full-core calculations. The value of 2.5 % leakage is determined from preliminary full-core calculations with the core simulator PARCS for the core design HC10-1 presented in chapter 6. With a six batch reloading scheme, an approximate multi-batch to one-batch ratio of 1.71 can be achieved. Because of the restrictions of the available cladding materials, a total residence time of the FAs in the core of 6 one-year cycles is considered as upper limit for the current studies. This corresponds to a discharge exposure of about 2000 equivalent full power days (efpd), taking into account refueling time.

4.2   Definition of investigated cases

The lower part of the ATRIUM[TM] 10XM [18] MOX fuel assembly design (referred to as A10 below) depicted in Fig. 4.1 is chosen as starting point for parametric studies of geometry parameters and as reference case. It has no empty fuel rod positions like the upper part caused by the 12 part-length rods which are fixed at the lower FA tie plate but are only half of the length of the other fuel rods. In lower fuel lattice with an average Pu_{fiss} enrichment of 4.43 wt%, 79 main fuel pins with 5 different Pu_{fiss} enrichment levels are used according to Tab. 4.1 to obtain a flat power profile, where the fuel colors light red, green, blue, yellow and pink in Fig. 4.1 correspond to the MOX fuel rod types 1, 2, 3, 4, and 5, respectively. Additionally, 6 UOX pins with low 0.5 wt% ^{235}U enrichment are used to reduce power peaks in the FA corners (dark red). Near the FA corners, 6 absorber pins with the same 0.5 wt% enriched UOX fuel matrix as in the UOX pins and 2.5 wt% Gd_2O_3 content (recognizable in Fig. 4.1 by multiple rings in the fuel pin) are introduced to control BOC excess reactivity.

The general core layout is adopted from the reference plant described in chapter 1.2, which dictates control rod geometry, FA pitch and maximum core height. To maintain compatibility with the reactor vessel and internals like control rods, the fuel channel box design (outer dimension, geometry of corners, etc.) used for the A10 is used for all investigated cases. The global design parameters for the reference core are shown in Tab. 1.1.
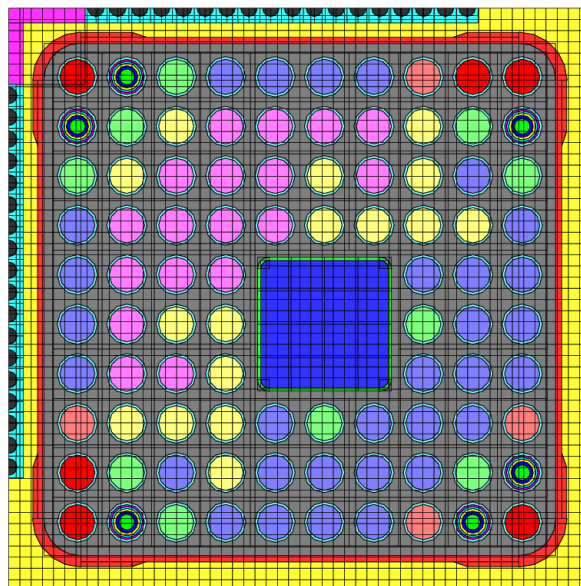
Fig. 4.1: Cross-section of a quarter core unit cell (15.25 cm * 15.25 cm) with reference fuel assembly ATRIUM[TM] 10XM. Each color represents a separate material. The 6 multi-ringed fuel rods near the corners contain the burnable absorber gadolinia (Gd2O3). The control rod cross is shown in the upper left corner of the unit cell.

Tab. 4.1: Individual enrichment of fissile and total plutonium (Pu-vector 1), ^{235}U, and Gd$_2$O$_3$ in different fuel rod types in wt%. Fuel rod type colors refer to colors used in Fig. 4.1.

Case	Ref			
	Pu$_{fiss}$	Pu$_{tot}$	^{235}U	Gd$_2$O$_3$
UOX rod type 1	0.0	0.0	0.5	0.0
Gd rod type 1 (6 multi-ringed rods near the corners)	0.0	0.0	0.5	2.5
MOX rod type 1	2.80	4.30	0.239	0.0
MOX rod type 2	3.50	5.38	0.237	0.0
MOX rod type 3	4.20	6.45	0.234	0.0
MOX rod type 4	6.15	9.45	0.226	0.0
MOX rod type 5	7.10	10.91	0.223	0.0
Bundle average	4.43	6.76	0.266	0.0

The first measure to decrease the MFR in the A10 pin lattice are to replace the internal water channel, occupying the space of 3x3 fuel pins, and all part-length rods with full-length fuel rods. Secondly, the fuel rod diameter can be increased and/or the fuel rod pitch can be decreased. In later design phases, proposals on how to regain the structural support need to be done which is provided by the internal water channel in the A10. One possibility would be the use of steel claddings in the corner rods of the fuel assembly. This will unfortunately have a negative effect on the neutronic performance of the FA design, but is inevitable from mechanical point of view. The axial fuel composition is assumed to be homogeneous in this study, although the effects of heterogeneous enrichment distribution could be addressed in a future analysis to improve the fuel utilization further.

For depletion calculations, the power density is obtained from a nominal core power of 4000 MW$_{th}$ used in [12] and the basic assumption of a constant height of the low moderated FA of 3.71 m. This results in a constant volumetric but lower heavy metal mass specific power density, since the reduction of the MFR is achieved by an increased fuel volume per unit length in the FA. In Fig. 4.2, the unit cells of a low moderated FA with a 10x10 and a 12x12 fuel rod lattice and the distribution of four enrichment levels corresponding to the fuel pellet color is presented. While, the resonance treatment in TRITON is done once per fuel enrichment major Dancoff factor group (see above), each pin is treated individually in depletion calculations. The impact of simplification of resonance treatment on the results is small [76] and is accepted in favor of the large computational time savings.
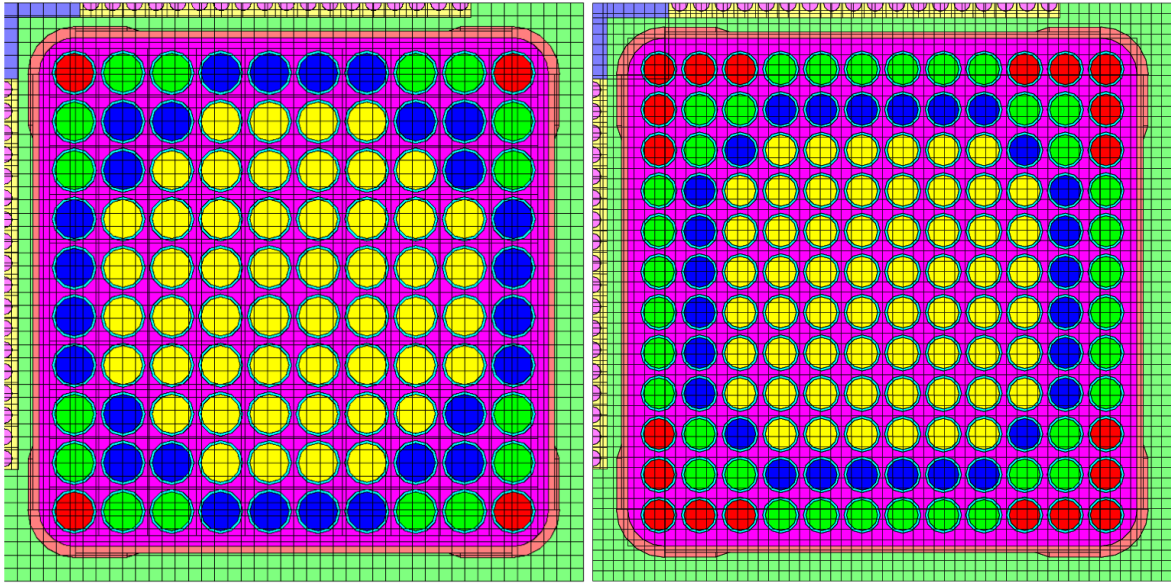
Fig. 4.2: Cross-section of quarter core unit cell (15.25 cm * 15.25 cm) with low moderated 10x10 fuel assembly (left) and low moderated 12x12 pin fuel assembly (right). Each color represents a separate material. The control rod cross is shown in the upper left corner of the unit cell.

The impact of the fuel rod diameter, the fuel rod pitch, the lattice dimension (meaning the number of fuel rods in one dimension), the enrichment and the fuel composition on the conversion ratio, the multiplication factor, and on reactivity coefficients is investigated in a parametric study to optimize the fuel utilization, while maintaining inherent safety parameters. The inner width of the FA channel and the distance of the peripheral fuel rods to the fuel channel wall are defined to be fixed parameters in this study. This reduces the degrees of freedom for parameterization and results in a direct coupling of lattice pitch, fuel rod diameter and lattice dimension. If the fuel rod size is adjusted, the cladding thickness and the fuel pellet size are adjusted to scale. A lower limit for the rod to rod distance of 1.4 mm is arbitrarily chosen for this study to allow for sufficient cooling capability. The feasibility of this assumption is further discussed in chapter 7. Only 7 selected representative cases of the various investigated cases are presented here and the corresponding parameterization is shown in Tab. 4.2. Evaluation of additional cases shows that results for FA designs with lattice dimensions 9x9, 11x11, 13x13 can be interpolated or extrapolated from cases 2 and 4. Also the influence of the enrichment on all designs can be approximated very well from comparison of the cases 2 and 3 or 6 and 7, which has been verified by separate calculations with average bundle enrichment up to 7 wt% fissile plutonium content. The used MOX fuel for these studies contains uranium oxide from tails with an ^{235}U content of 0.25 wt%. The influence of different plutonium vectors with different plutonium quality ($Pu_{qual} = Pu_{fiss} / Pu_{tot}$) is also investigated. These vector are adopted from [12] and are shown in Tab. 4.3.

Tab. 4.2: Overview of the design parameter matrix selected for the study

Case		1	2	3	4	5	6	7	Ref
Lattice dimension	-	10x10	10x10	10x10	12x12	10x10	10x10	10x10	10x10-9
Pitch	mm	12.90	12.84	12.84	10.70	12.84	12.84	12.84	-
Fuel rod radius	mm	5.45	5.72	5.72	4.65	5.72	5.72	5.72	5.14
Cladding thickness	mm	0.66	0.69	0.69	0.56	0.69	0.69	0.69	0.62
Fuel pellet radius	mm	4.70	4.94	4.94	4.01	4.94	4.94	4.94	4.52
Rod to rod gap	mm	2.00	1.40	1.40	1.40	1.40	1.40	1.40	-
Moderator to fuel volume ratio (MFR)	-	1.84	1.55	1.55	1.70	1.55	1.55	1.55	2.57
Fuel volume per unit length	cm³/cm	69.50	76.70	76.70	72.80	76.70	76.70	76.70	58.40
Average enrichment	wt%	5	5	6	5	5	5	6	4.43
Pu-vector	-	1	1	1	1	2	3	3	1

Tab. 4.3: Plutonium compositions in different MOX fuel (values in wt%) [12]

Pu-vector	^{238}Pu	^{239}Pu	^{240}Pu	^{241}Pu	^{242}Pu	Pu_{qual}
1	2	56.5	26.1	8.6	6.8	65.1
2	4	48	31	7	10	55
3	4	38	33	12	13	50

To flatten the pin power profile in the lattice, four different levels of enrichment, with reduced Pu_{fiss} content at the sides and corners of the FA, are used in the low moderated FA designs. In Fig. 4.2, the distribution of the applied four different enrichment levels can be identified with the different pellet color for the included 10x10 and 12x12 FA designs. The individual pin type Pu_{fiss} enrichments are summarized in Tab. 4.4 for each case, where the fuel colors red, green, blue, and red in Fig. 4.2 belong to the pin types 1, 2, 3, and 4, respectively. In Tab. 4.5, the corresponding total plutonium contents per pin and for the whole FA are given. It is not unusual to have even more than four different enrichment levels in BWR fuel assemblies (cp. reference FA), but for this study this number of levels is found to be sufficient to obtain reasonably flat power profile with pin power factors below 1.3 (maximal fuel pin power relative to average fuel pin power). Notice the high total plutonium content of 11 wt% to 18 wt% in the rod type 4 for all cases. This renders fabrication of the individual rods of this type challenging due to the generated heat and the radiation. Current MOX fabrication facilities are likely not able to handle plutonium of this composition. This is a crucial limiting factor, which has to be addressed in more detail in later stages of the assessment of the underlying reactor design. At this point, this appears not to be a criterion for exclusion in the view of a fabrication limit of 40 wt% Pu_{tot} in MOX and a reactivity limit of 13 wt% Pu_{fiss} in the whole bundle, as prescribed in literature (see chapter 2.4).

Tab. 4.4: Fissile plutonium enrichment distribution in low moderated FA in wt%

Case	1	2	3	4	5	6	7
Pu-vector	1	1	1	1	2	3	3
Rod type 1	1.10	1.10	1.20	1.00	1.10	1.10	1.20
Rod type 2	1.75	1.75	2.00	2.10	1.75	1.75	2.00
Rod type 3	2.95	2.95	3.40	4.60	2.95	2.95	3.40
Rod type 4	7.40	7.40	9.00	8.25	7.40	7.40	9.00
Bundle average	5.00	5.00	6.00	5.00	5.00	5.00	6.00

Tab. 4.5: Total plutonium content distribution in low moderated FA in wt%

Case	1	2	3	4	5	6	7
Pu-vector	1	1	1	1	2	3	3
Rod type 1	1.69	1.69	1.84	1.54	2.00	2.20	2.40
Rod type 2	2.69	2.69	3.07	3.23	3.18	3.50	4.00
Rod type 3	4.53	4.53	5.22	7.07	5.36	5.90	6.80
Rod type 4	11.37	11.37	13.82	12.67	13.45	14.80	18.00
Bundle average	7.68	7.68	9.22	7.68	9.09	10.00	12.00

The begin of life (BOL) reactivity in modern BWR FAs is too high to be compensated by control rods only. Burnable poison rods (BPR) with e.g. gadolinia are introduced additionally for excess reactivity compensation. In low moderated FA designs, however, no absorber rods are necessary, because the BOL reactivity needed to achieve cycle lengths comparable to a conventional FA design is much lower. The reason for this effect is a reduced reactivity attenuation caused by the increased conversion ratio.

The fuel temperature in each pin is set to 800 K for all cases and the fuel is smeared over the fission gas gap, resulting in a smeared fuel density of 9.94 g/cm³. Material compositions for structures are identical in all cases and taken from the SCALE material library.

In depletion calculations, an average coolant void content in the fuel channel of 40 % is assumed, while the moderator of the bypass stays un-voided. To obtain reactivity coefficients of the fuel lattice, various branches are defined at each burnup point, to cover the thermal-hydraulic parameter range of interest.

4.3   Results of parametric studies

To estimate and compare the cycle average conversion ratio from lattice calculations, the achievable discharge exposure has to be approximated for each case first. In Fig. 4.3 and

Fig. 4.4, the infinite multiplication factor k_{inf} is presented versus the exposure expressed in equivalent full power days (efpd) for all studied cases.

The cases 1, 2 and 4 have the same average enrichment and fuel composition, but a different geometry and MFR. Their k_{inf} results are close to each other, but the slope is steeper for higher MFRs. Slightly longer cycle lengths can be estimated for cases 1 and 2 than for case 4 if the same enrichment is used. Interpolation from case 2 and 3 with the enrichment levels of 5 wt% and 6 wt%, respectively, suggests an increased enrichment of 5.3 wt% Pufiss for the presented 12x12 FA for comparable cycle lengths. A much longer cycle length can be expected for case 3 because of the higher enrichment.
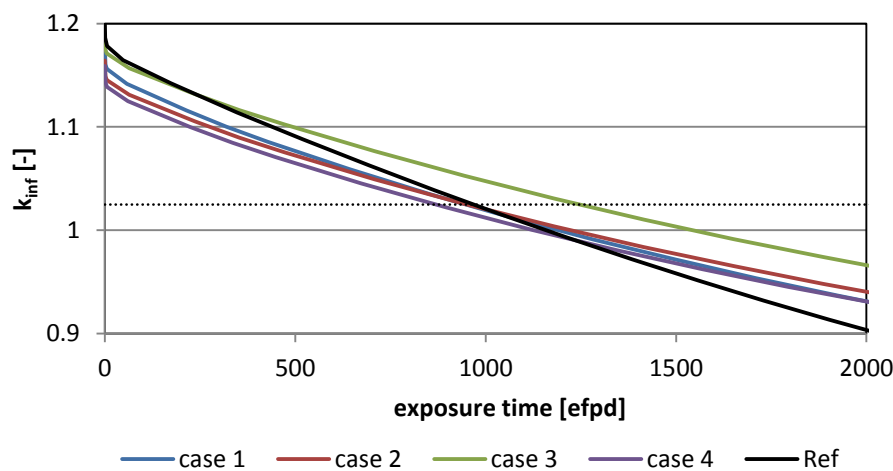
Fig. 4.3: Infinite multiplication factor in FA designs 1 to 4 as function of the exposure time
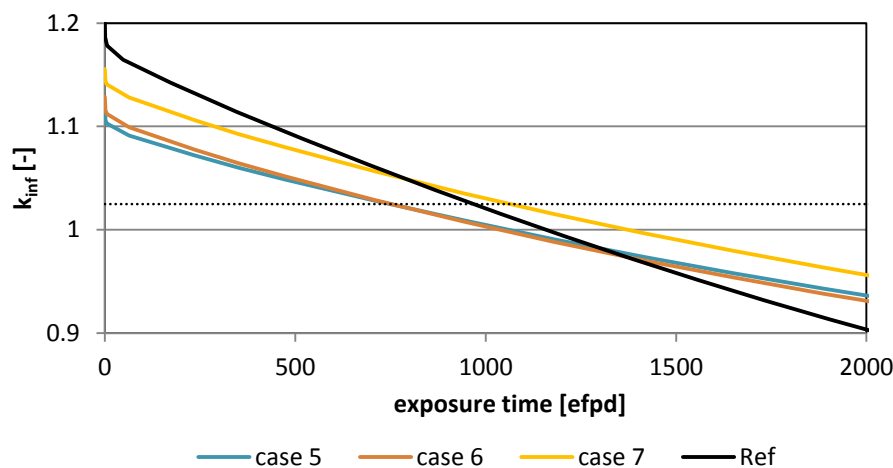
Fig. 4.4: Infinite multiplication factor in FA designs 5 to 7 as function of the exposure time

The use of lower plutonium quality in the fuel reveals causing a strong penalty on the reactivity, resulting in low discharge exposure for the same average enrichment. Interpolation from cases 6 and 7 suggests an enrichment of 5.7 wt% Pufiss for case 5 and 6 if similar cycle lengths shall be achieved as for the reference case.

In Tab. 4.6, the estimated discharge exposures and cycle lengths for the different presented cases are shown. Different mass specific burnup can be achieved even if the estimated cycle length is comparable, as e.g. for case 1 and 2, due to the differing power density. The achievable mass specific burnup is lower than preferable for all investigated cases because of the decreased power density. To overcome this, a reduction of the core height, while maintaining the total core power, would be a possible solution. However, FA designs with higher number of fuel rods as in conventional FA, like the here presented 12x12 design from case 4, would be essential for such an approach, to keep the linear heat generation rates below postulated safety margins. If the above suggested enrichment adjustments are applied to the cases 4, 5 and 6 via interpolation from cases 2, 3, 6 and 7, one may obtain comparable cycle lengths as for case 1 and 2, which is presented in Tab. 4.7.

Tab. 4.6: Achievable exposure in studied cases

Case	1	2	3	4	5	6	7	Ref
Discharge, efpd	1620	1629	2126	1491	1294	1294	1817	1654
Cycle, efpd	270	271	354	249	216	216	303	276
Discharge, MWd/kgHM	38.0	34.6	45.2	33.3	27.1	27.3	38.7	47.9

Tab. 4.7: Estimated achievable exposure in adjusted cases

Case (Pufiss)	4* (5.3 wt%)	5* (5.6 wt%)	6* (5.6 wt%)
Discharge, efpd	1641	1593	1593
Cycle, efpd	273	265	265
Discharge, MWd/kgHM	36	33	34

The reader should be reminded at this point that the results for the reference case are not representing a real ATRIUM[TM] 10XM fuel assembly, which has a more complex design with part-length rods. The results presented here are obtained for the lattice of the lower FA-part having no empty rod positions. Also the applied TH conditions are only an approximation of the core average conditions. This approach is sufficient as point of reference to quantify the influence of certain changes in the fuel assembly design but final quantitative conclusions demand full-core calculations actually considering leakage and also multi batch core loading.

The effect of the different geometry and material parameters on the conversion ratio (CR) are depicted in Fig. 4.5 for the different presented cases.
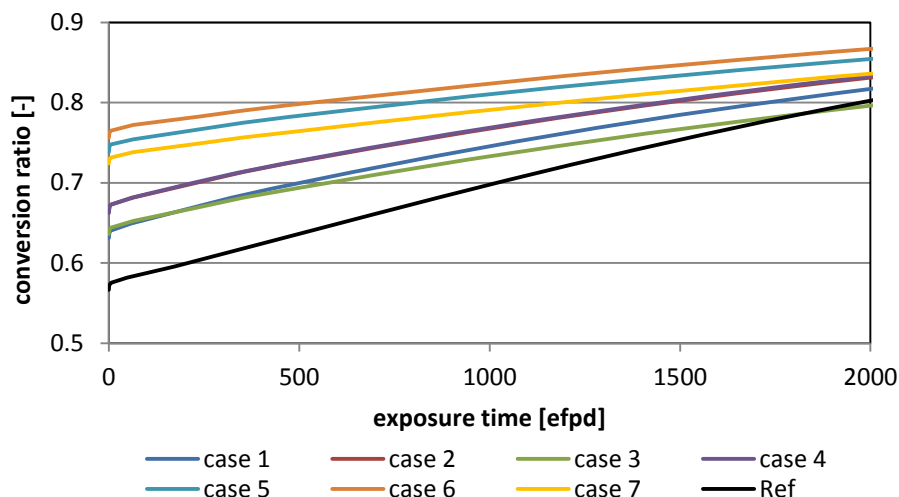
Fig. 4.5: Conversion ratio in FA designs 1 to 7 as function of the exposure time

For all cases, the CR increases significantly with exposure, because of the decreasing content of fissile nuclides. This trend is most pronounced for the reference case for which the fewest fissile nuclides are generated during operation. If plutonium vectors 2 or 3 are used, this trend is slightly damped. The relevant differences between cases shall be highlighted in the following paragraphs, to better understand their individual effect on CR. Case 1 and 2 have a 10x10 lattice and share a similar pitch, but the rods in case 1 have a smaller diameter, resulting in a larger MFR and a larger distance between the rod surfaces. In combination, this leads to a smaller CR for case 1, although the achievable cycle length is the same. Comparison of the cases 2 and 3 for the same exposure reveals a quite high penalty on CR of approximately 0.03 caused by increasing the enrichment by 1 wt% Pu_{fiss}. Case 2 (10x10 lattice) and case 4 (12x12 lattice) exhibit an identical dependence of CR on the exposure, although the MFR is larger and the pitch and rod sizes are smaller in case 4. Taking into account an increased enrichment for case 4 of 5.3 wt% to obtain the same cycle length as suggested above, case 2 seems superior to case 4 with a 1 wt% higher CR. A comparison of case 2 to the cases 5, 6 and 7 shows a rewarding effect of lower plutonium quality, with the highest CR for the lowest quality. Adjusting the average enrichment of cases 5 and 6 to 5.6 wt% to achieve comparable cycle lengths as for case 2 (see above) causes a penalty on CR. Nevertheless, the CR seems still superior to that obtained for case 2.

To compare the cycle average conversion ratio for the different cases from Fig. 4.5, the CR for the half of the estimated discharge exposure obtained above is used and listed in Tab. 4.8. This is only a rough approximation assuming linear dependence of the CR on the exposure but it is sufficient for this early study. The cycle average CR is higher for case 2 than for case 4 because the cycle length is slightly longer. Adjustment of the enrichment of case 4 reduces

the cycle average CR even a little bit more as can be seen in Tab. 4.9. For the cases 5 and 6, which have significantly higher CR than all cases, but low cycle lengths, the enrichment adjustment still keeps their CR superior to the comparable cases.

Tab. 4.8: Cycle average conversion ratio in studied cases

Case	1	2	3	4	5	6	7	Ref
CR	0.729	0.753	0.737	0.748	0.792	0.806	0.786	0.677

Tab. 4.9: Estimated cycle average conversion ratio in adjusted cases

Case	4* (5.3 wt%)	5* (5.6 wt%)	6* (5.6 wt%)
CR	0.744	0.780	0.794

One especially rewarding effect in a lower moderated lattice is the better discharge plutonium quality compared to that of a conventional FA. This is important if multiple recycling of MOX fuel shall be conducted to keep the total plutonium inventory in a later generation MOX fuel as low as possible and, therefore, obtain better void reactivity coefficient. The plutonium quality versus the exposure time is illustrated in Fig. 4.6.
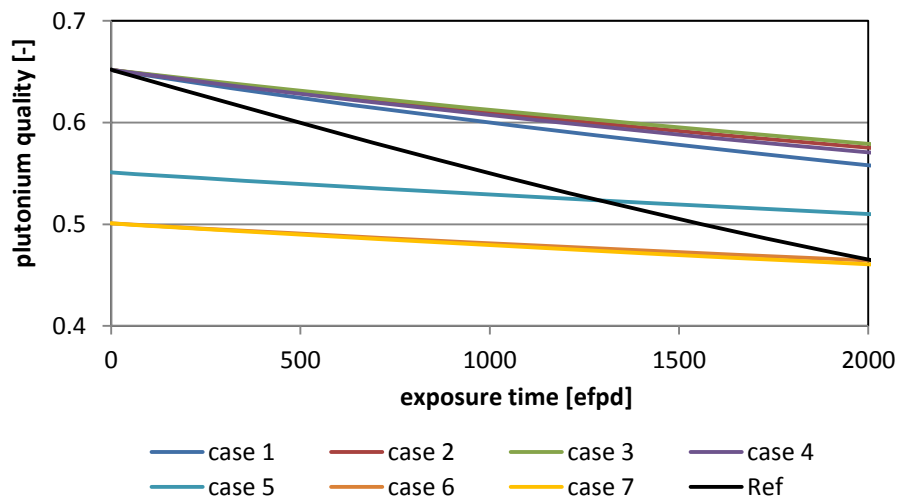
Fig. 4.6: Plutonium quality in different FA designs as function of the exposure time

Especially for the cases 1 to 4 with high initial Pu_{qual}, the plutonium quality decreases only half as much or less as for the conventional FA. In Tab. 4.10, the discharge plutonium quality is shown for the presented cases obtained for the cycle lengths given in Tab. 4.6. A comparison of case 3 to case 1 shows that due to the lower moderation and higher CR in case 3 the plutonium quality at discharge is comparable even if the burnup is significantly increased. Judging from comparison of cases 2 and 3 or 6 and 7, increasing the enrichment has negligible effect on the plutonium quality. Comparison of the discharge plutonium quality

obtained for cases 4, 5 and 6 to the respective cases 4*, 5* and 6* with increased enrichment reveals only small differences below 0.01.

Tab. 4.10: Discharge Pu-Quality

Case	1	2	3	4	5	6	7	Ref
Discharge Pu-quality.	0.573	0.587	0.575	0.589	0.525	0.478	0.464	0.493

The void reactivity coefficient (VC) has been verified to be linear between two considered void branches of 40 % and 60 % void content in the fuel channel for selected representative cases by computing intermediate steps. For this study, the VC is determined for the investigated cases from the k_{inf} change between these two void states. In Fig. 4.7, the VC is shown for different cases as function of the exposure time.
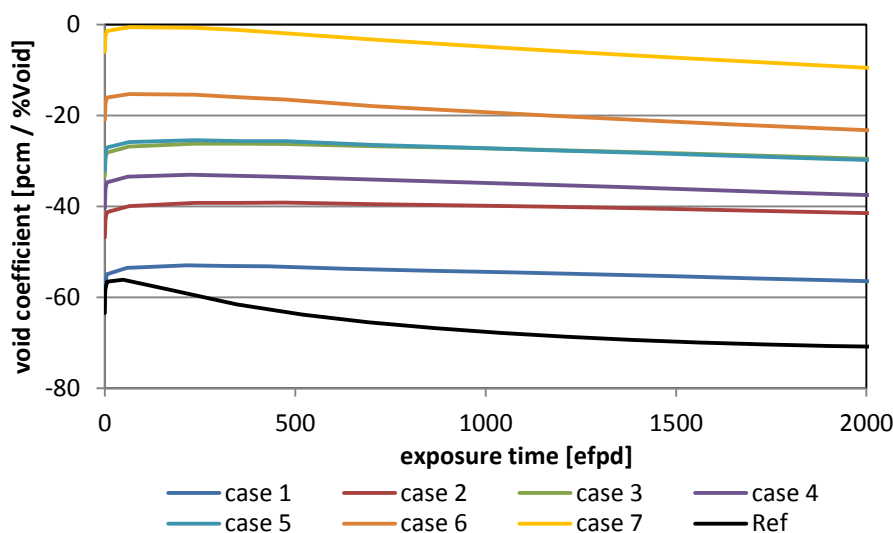
Fig. 4.7: Void reactivity coefficient for different FA designs as function of the exposure time

The computed VC is negative during the entire exposure range in each case. However, it has a small absolute value for cases with high enrichment and low plutonium qualities. Case 4* has a VC of about 5 pcm / %Void higher than case 4 and cases 5* and 6* have VCs, which are approximately 10 pcm / %Void higher as cases 5 and 6, respectively. The VC in a full A10 FA is usually lower as presented here, because the upper part of the FA is better moderated, due to part-length rods, which increases the neutron leakage. As additional reference one can refer to the VC in a conventional BWR FA with uranium fuel which is in the range of −100 pcm / %Void. These results have been verified with full-core calculations (see chapter 6.4.2).

To assess the influence of the fuel temperature on the multiplication factor, branches have been calculated for the fuel temperatures 800 K and 1200 K. Assuming the fuel temperature

coefficient to be a linear gradient between these two temperatures yields a similar behavior in all cases. As shown in Fig. 4.8, the Doppler coefficient at BOL is nearly -3 pcm / K in each case and its absolute value decreases in a similar way with increasing burnup.
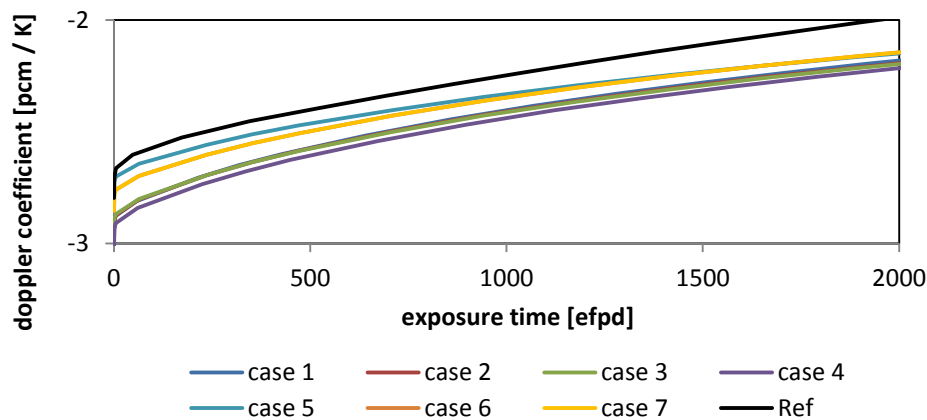
Fig. 4.8: Fuel temperature coefficient for different FA designs as function of the exposure time

4.4   Validation of NEWT with KENO-VI

The case 2 lattice is modeled with different active coolant void contents for a method validation study by means of the deterministic transport solver NEWT compared to the generally more accurate MC solver KENO-VI [96]. The results of this study are denoted in Fig. 4.9 for the NEWT calculation and for calculations with KENO in a multi-group mode (MG-KENO) as well as in continuous energy mode (CE-KENO).
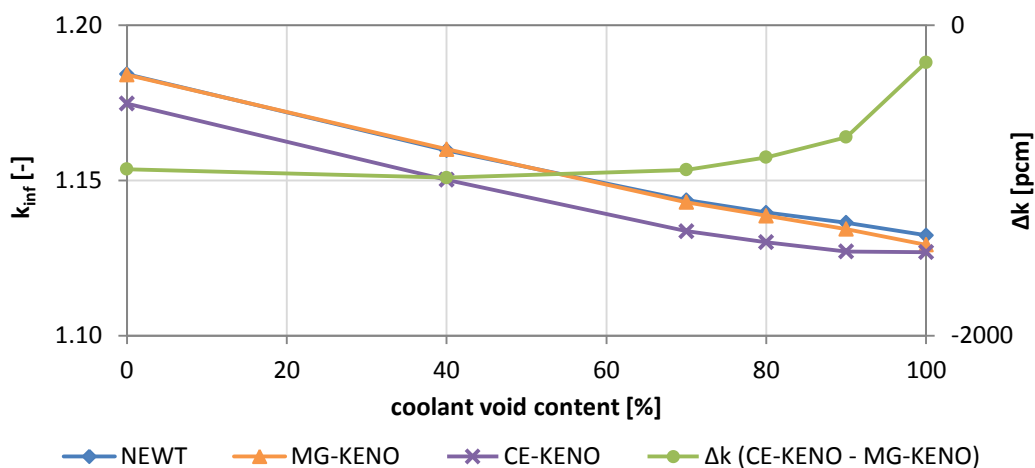
Fig. 4.9: Infinite multiplication factor for different solution methods and difference between CE-KENO and MG-KENO as a function of the coolant void content

User-defined individual Dancoff factors in 3 averaged groups as described in chapter 4.1, which have been determined with the MCDancoff code of SCALE, are applied to the CENTRM calculations of the individual unit cells preceding each NEWT and MG-KENO

calculation. Cross-sections of the ENDF/B-VII evaluation are used in both KENO calculations.

For MG-KENO, the library with 238 groups also used in the NEWT calculations is selected. To obtain a reasonably low standard deviation in the infinite lattice multiplication factor in the KENO calculations (below 20 pcm), 8000 neutrons per generation and 2000 generations with 200 skipped generations are used.

By comparing the results from NEWT and MG-KENO, it can be concluded that the grid structure and quadrature used in NEWT almost coincide throughout the entire coolant void range. For the highest investigated void content a small deviation can be observed. The comparison of MG-KENO with CE-KENO reveals a difference in the multiplication factor for the entire void range of about 1 %, except for very high void contents, for which the difference is decreasing. Since the k_{inf} trend at high void contents for NEWT with default DFs shown in Fig. 4.10 resembles that of CE-KENO better than with individual user-defined Dancoff factors, leads likely to the conclusion that DFs are predicted wrong by MCDancoff for high void contents.
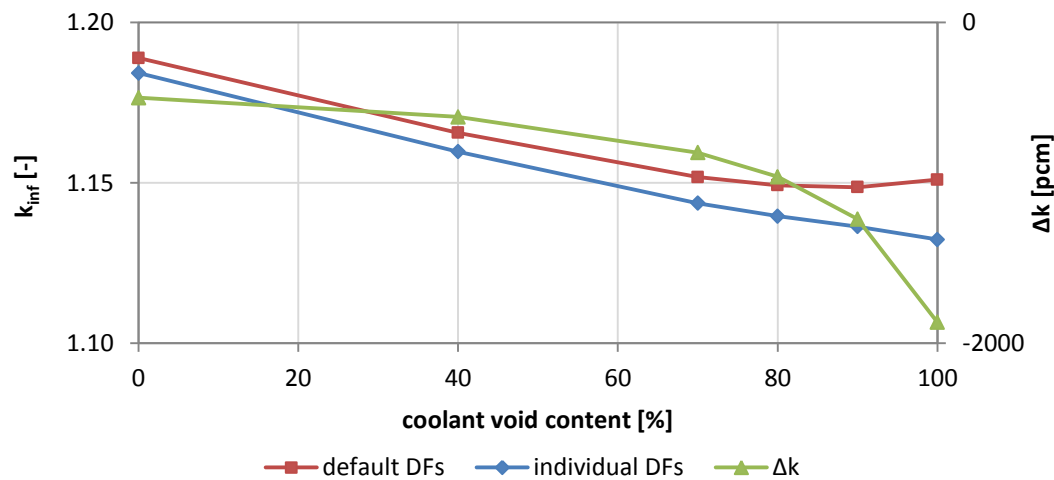
Fig. 4.10: Infinite multiplication factor for NEWT calculation with different Dancoff factor definitions as function of void content

This should be investigated locally for the individual pins to develop strategies to overcome this deficit. For fuel cycle studies this is of minor importance, because the developed reactor designs are not operated at void contents exceeding 80 %, but for transient safety studies with high voided core states this observed deviation demands improvements.

As indicated in chapter 3.2, investigations [75] for different critical thermal MOX benchmark experiments have shown that CE-KENO in comparison to MG KENO is consistently providing lower values of the multiplication factor of up to almost 600 pcm in the

worst case. This effect has been found to be stronger for configurations with lower moderation, which suggests an even stronger influence for the here investigated low moderated FAs. It is pointed out in [75] that the difference originates mainly from the $S(\alpha,\beta)$ data processing in CE-KENO. Improvements are said to be applied in the upcoming program version SCALE6.2. To get a better feeling of the found differences between MG-KENO and CE-KENO in the current investigations, one can refer to the documented uncertainty in the multiplication factor due to cross-section uncertainties for the investigated MOX benchmarks in [75], which is shown to be in the order of 1 % for all cases.

Taking into account these findings and additionally the simplifications applied to the here performed investigations of low moderated FA (e.g. grouping of Dancoff factors, spatial and angular discretization), the results obtained with NEWT can be considered reasonable and consistent. Hence, the methodology is supported to be valid at least up to average coolant void contents of 80 %. An accurate prediction of the void reactivity coefficient is, therefore, possible in this void range. For higher void contents, the difference in the obtained results indicates that no reliable prediction of the void reactivity coefficient in this thermal-hydraulic parameter domain can be expected. These findings should be confirmed in the future by calculations with the improved KENO versions in SCALE6.2

4.5   Comparison of NEWT to CASMO-4

Comparison calculations for selected low moderated BWR FA, have been done with CASMO-4. The purpose is to verify if the findings determined in the studies above can be extrapolated to CASMO-4, which is used for material constant generation for the core design studies. Results of one case of the code to code comparison for the 10x10 low moderated FA denoted above with case 2 are depicted in Fig. 4.11. The multiplication factor versus exposure time is predicted almost equally by both codes. NEWT predicts slightly higher reactivity in the fresh fuel. However, the difference between the results decreases almost linearly with increasing burnup, vanishes at approximately 15 MWd/kgHM and changes sign for higher exposure. The nonconformity originates i.a. from discrepancies in the methodology, the original cross-section library and the selected nuclides for depletion. A non-exhaustive enumeration of the differences between the codes is given in Tab. 4.11. Nevertheless, the agreement between CASMO-4 and NEWT is satisfying. Similar deviations between methods and libraries were also found e.g. in an international code to code comparison for a MOX fuel assembly [69].
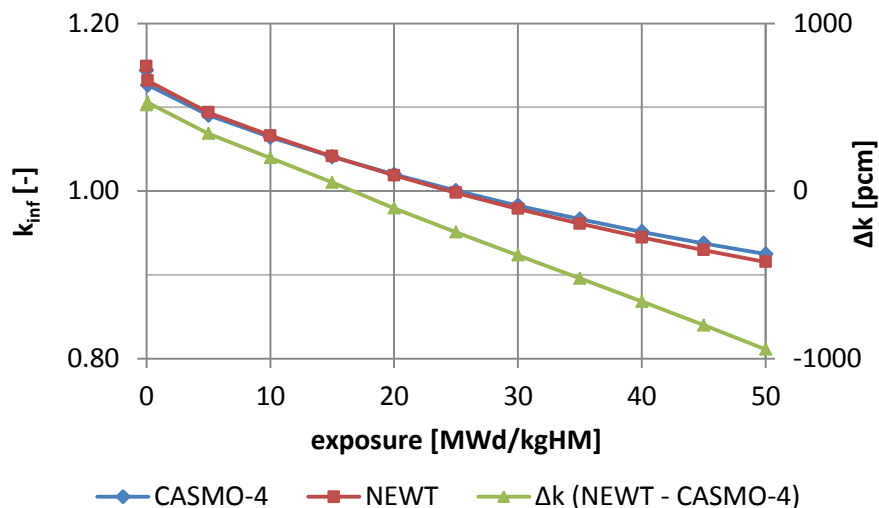
Fig. 4.11: Comparison of infinite multiplication factor for FA design of case 2 with different lattice physics codes as a function of the exposure

Tab. 4.11: Significant differences between CASMO-4 and NEWT

	CASMO-4	NEWT
Transport method	MOC	ESC
Neutron data origin	ENDF/B-IV	ENDF/B-VII
Basic neutron data energy structure for resonance calculation	70 groups ("L-library")	Pointwise
Neutron data energy structure for 2D-transport calculation	7 groups	238 groups
Depletion Materials	108	94
Cut off for up-scattering	4 eV	3 eV

4.6   Summary and implications for core design studies

Three selected geometries have been investigated with the same average enrichment, namely cases 1, 2, and 4. Case 1 is a 10x10 fuel rod lattice with 2 mm rod to rod gap resulting in a moderator to fuel ratio (MFR) of 1.84. In case 2, the MFR is reduced to 1.55 by using thicker fuel rods and putting them closer together (1.4 mm rod to rod gap). Case 4 utilizes a 12x12 fuel rod lattice with thinner rods and the same rod to rod of 1.4 mm as for case 2 (MFR = 1.7). While cases 1, 2 and 4 utilize 5 wt% average bundle enrichment, case 4* has increased enrichment of 5.3 % to obtain cycle length comparable to that in cases 1 and 2.

Comparison of cases 1, 2, and 4* yields the following results:

- The cycle average conversion ratio seems to depend mainly on the MFR and can be increased from 0.677 in the ATRIUM^{TM} 10XM lattice without empty rod positions to 0.729, 0.744, and 0.753 for the cases 1, 4*, and 2, respectively.

- Compared to 49.3 % Pu-quality in the conventional FA, the discharge Pu_{qual} is larger than 57 % in the three low moderated FA designs making at least a second recycling feasible.

- The worst void reactivity coefficient of around −30 pcm / %-Void (minimum during exposure) is obtained for case 4*. It is more negative for case 2 (−40 pcm / %-Void) and case 1 (−55 pcm / %-Void).

Additionally, the fuel composition influence is investigated in the geometry of case 2:

- Fuel with the lower plutonium qualities of 55 % and 50 % requires an enrichment increase to approximately 5.6 % to attain cycle lengths comparable to case 2. The lower plutonium quality results in higher cycle average conversion ratios of 0.78 and 0.794 for case 5* and case 6*, respectively.

- However, the VC for these cases is with −15 pcm / %-Void and −5 pcm / %-Void for case 5* and case 6*, respectively, less negative.

Validation studies have shown that the deterministic approach seems to be appropriate for coolant void ranges up to 80 %. CASMO-4 and TRITON calculations agree within an expected range of deviation. Due to the yet unexplained differences at high void contents above 80 % void in the active coolant channel more investigations are needed to apply corresponding generated material contents e.g. to transient calculations with high void fractions in the core, which are required for safety performance studies.

As consequence, the 10x10 lattice geometry of case 2 will be used as starting point for the later on performed core design studies because it reveals the best conversion ratio within the investigated parameter range and also shows appropriate safety parameters. It has been considered to use also a 9x9 lattice, which has an even better CR, but a lower number of fuel rods is inducing higher linear heat generation rates and, therefore, limits the reactor power. The Pu_{qual} of 65.1 % (vector 1) is selected for the core design studies due to the much better void reactivity coefficient. Lower plutonium qualities can be considered in later stages if the VC for core designs with 65.1 % quality shows large enough margins to accept the penalty of more than 20 pcm / %-Void seen between cases 2 and 5*.

5 Validation of energy discretization for few-group cross-section generation

5.1 Motivation

The neutron energy spectrum in low moderated reactor core designs is harder than in conventional LWR. In addition it is harder for MOX fuel in comparison to UOX fuel. In a near critical infinite pin lattice with UOX fuel with 1 wt% ^{235}U enrichment and a moderator to fuel volume ratio (MFR) of 2 for example, representing the conditions in a conventional LWR lattice, about 87 % of all fissions happen below the most commonly used thermal energy threshold of 0.625 eV (value determined from two-group material constants calculated with NEWT). In a low moderated lattice with a MFR of 1 and 3.75 wt% enriched MOX fuel, however, the thermal fission fraction is reduced to around 50 % which is illustrated for different fuels (enrichment adjusted to obtain k_{inf} of approximately unity) and moderation in Fig. 5.1.
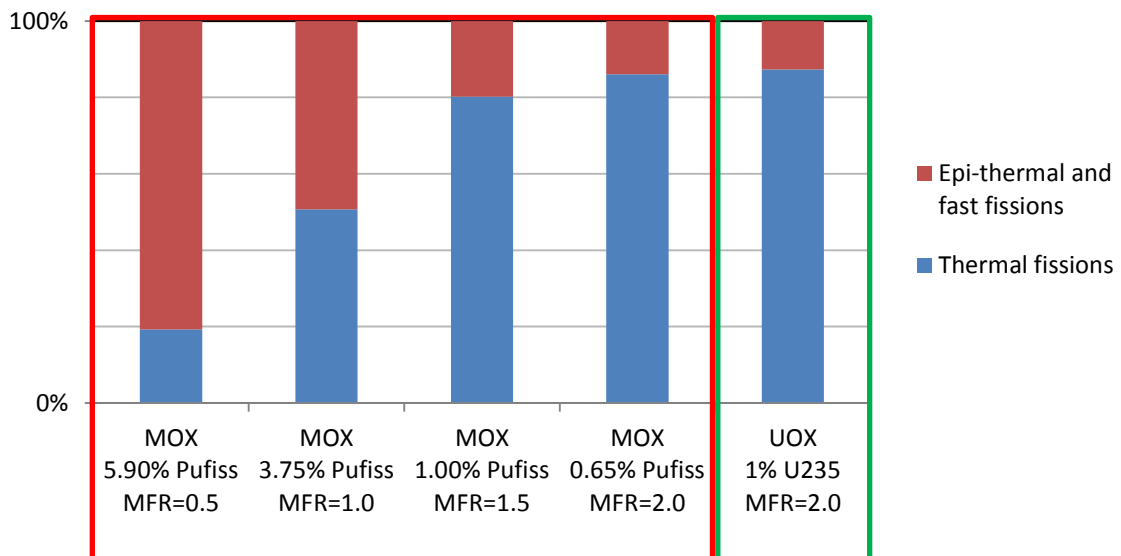
Fig. 5.1: Distribution of fission reactions in infinite lattice unit cell calculation on thermal (blue) and fast (red) energy group depending on MFR and fuel composition (MOX fuel framed red; UOX fuel framed green). The energy threshold for material constant condensation is 0.625 eV.

The study goal in this context focuses on the development of reduced moderation fuel assemblies with effective MFR between 1 and 1.5. This is smaller than the geometric MFR shown in Tab. 4.2, since an average void content of around 40 % in the fuel assembly channel

is present in the full core. Therefore, the importance of fission reactions occurring at higher incident neutron energy in the cross-section processing has to be re-evaluated.

The shift of the neutron flux to higher energies is illustrated in Fig. 5.2 for the cases included in Fig. 5.1. Here the increasing importance of the epi-thermal energy range becomes obvious for low moderated lattices. Therefore, it has to be validated if the most commonly used energy group structure of two energy groups with a cutoff energy of 0.625 eV is suitable in 3D reactor simulations with nodal codes to validate the design of the low moderated reactor cores or if a larger number of energy groups is required to provide a credible data basis.
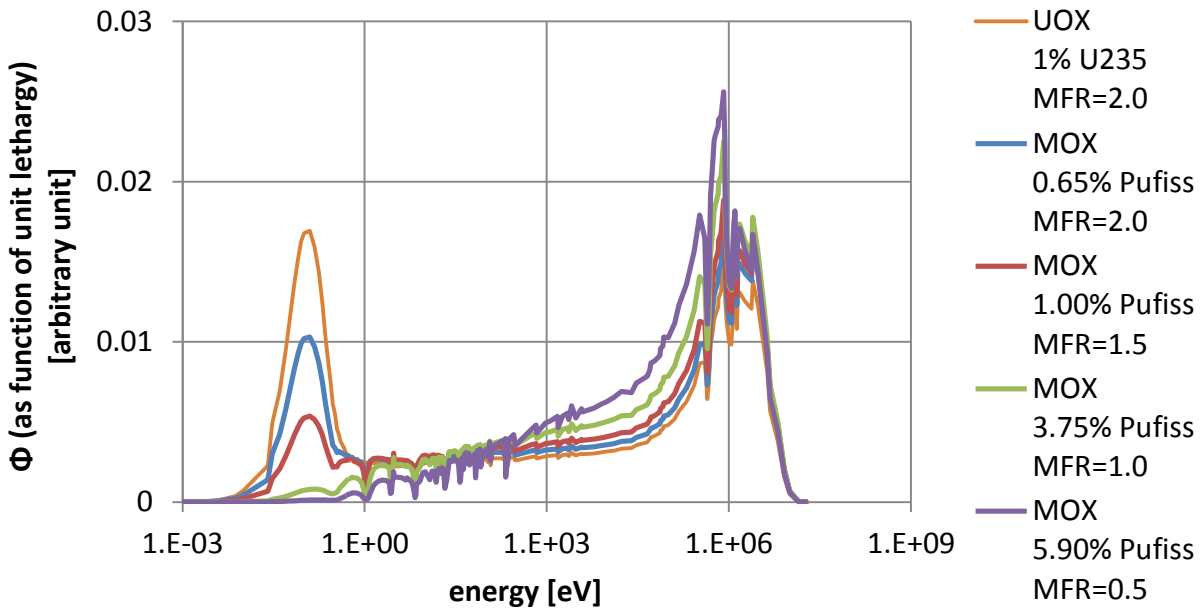
Fig. 5.2: 238 group neutron flux energy spectrum in infinite lattice unit cell calculations depending on MFR and fuel composition.

5.2   Investigation methodology

The straightforward way to test the quality of a homogenized few-group cross-section library is to compare the nodal calculation for representative cases employing these cross-sections with an "accurate" transport solution. Here, the transport solver NEWT is used to generate reference transport solutions for different test models. The few-group homogenized cross-sections used by the nodal core simulator PARCS are also prepared with NEWT from infinite lattice fuel assembly calculations with subsequent B1 correction. By using the same transport solver to obtain the reference solution and the few-group material constants, deviations between the results due to differences in basic nuclear data and the transport method can be excluded. The total error depends on spatial and energy discretization and homogenization, generated correction factors (ADF) and the nodal method itself [53]. NEWT

and PARCS have been selected for this validation study due to their flexibility for generation and use of few-group material constants with different energy structures.

In addition to the deterministic reference solution, the Monte Carlo Code KENO-VI is used to solve the larger test models for comparison. While good agreement can be expected for predicted eigenvalues between KENO-VI and NEWT using the same ENDFB-VII multi-group cross-sections, lower predicted k_{eff} is likely for KENO-VI calculations employing continuous energy nuclear data. This effect is observed and discussed in chapter 4.4.

To check the whole computational chain consistently, various procedures should be executed starting in TRITON by checking the transport eigenvalue with that computed with the homogenized material constants. As next step, the transfer of the cross-sections from TRITON to the PMAXS library format is automatically proofed by the cross-section interface GenPMAXS internally, which is useful for large libraries with several histories and branches. The smallest test case possible in PARCS is a two node problem with reflective boundary conditions and uniform thermal-hydraulic conditions as defined in TRITON to check if PARCS is providing cross-section look-up tables and interpolations in a consistent manner.

If this principal functionality is approved successfully, more challenging test cases are required to assess the cross-section quality for more realistic conditions. A simple test is to use an infinite lattice colorset (2x2 FA lattice with reflective boundary conditions and one axial layer), which is composed in a heterogeneous way to induce sufficiently large flux gradients and, thus, challenge the core simulator. This is accomplished by building the colorset of differently enriched or burned FAs and by introducing local absorbers like a control rod in one or more corners. Comparing the nodal solution to a transport solution verifies the suitability of the computed diffusion coefficient and the assembly discontinuity factors (ADFs).

As final procedures, 2D-slices of quarter cores are used to analyze the cross-sections against realistic finite problems with leakage. Such models should be of similar size as the full-core to be analyzed later, because otherwise the impact of the neutron leakage is too dominant and the diffusion approximation is not anymore applicable. On the other hand, it takes very long to obtain a reference solution for large problems and, therefore, a compromise has to be found. Here, at first a quarter of an intermediate size square core model with 5x5 fuel assemblies and one row of reflector assemblies is used with less heterogeneity (e.g. no corner FA, no control rods) before a large more realistic quarter core model with 9x9 fuel assemblies with cylindrical outer shape and one row of reflector assemblies is tested.

All calculations with NEWT and KENO are executed on the same geometry models and material conditions and with cross-sections of the ENDF-B/VI evaluation. In NEWT, only the multi-group (MG) library with 238 energy groups is used, while KENO is run both in multi-group, as well as, in continuous energy (CE) mode with the corresponding library versions. In NEWT, the recommended options for spatial discretization (4x4 cells per pin cell), angular discretization (S_6), and scattering order were applied (P_2 in water, P_1 in all other materials) [76]. For single FA calculations more detailed options give only slightly improved results but considerably increase the runtime. A similar behavior is expected for colorsets. For the large core slice models investigated, a finer discretization is unfeasible because the mesh generation in NEWT gets very slow (no parallelization yet). For example, for the 10x10 quarter core slice presented below, the mesh generation took more than one month. For KENO calculations, the selected number of generations, number of skipped generations and number of neutron per generation has been chosen to reduce the standard deviation in k_{eff} below 10 pcm. The corresponding standard deviation in the individual fuel assembly powers is between 0.1 % and 0.25 % in KENO-MG and between 0.3 % and 0.55 % in KENO-CE calculations. The smaller uncertainty is found in FA with higher power because of a better statistics originating from a larger number of neutrons.

Few-group cross-sections have been prepared from single lattice TRITON transport calculations in the common 2 energy group structure and additionally in finer 4 and 11 energy group structures. The selected group boundaries are summarized in Tab. 5.1 and the resulting 11 group energy boundaries are illustrated in Fig. 5.3.

Tab. 5.1 Energy boundaries and energy group width for different few-group cross-section libraries

Upper energy boundary, eV	2 group structure	4 group structure	11 group structure
2.000e7			1
2.354e6			2
4.000e5		1	3
1.700e4			4
9.500e3			
5.500e2	1		5
1.000e2		2	6
3.000e1			7
1.000e1			8
4.000		3	9
1.770			10
0.625	2	4	11

While in the 2-group and the 4-group library all or 99.9 %, respectively, of all fission neutrons are born in energy group one, for the 11-group cross-section library fission neutrons are born in groups 1 to 3. In addition, the slowing down and capture effects during slowing down are modeled more detailed with finer energy group structures. These effects reduce the group collapsing error incorporated in cross-section libraries with less energy resolution. For the cross-section generation for fuel assemblies and reflector assemblies, the guidelines described in [76] were followed. PARCS is run with different diffusion solvers for comparison.
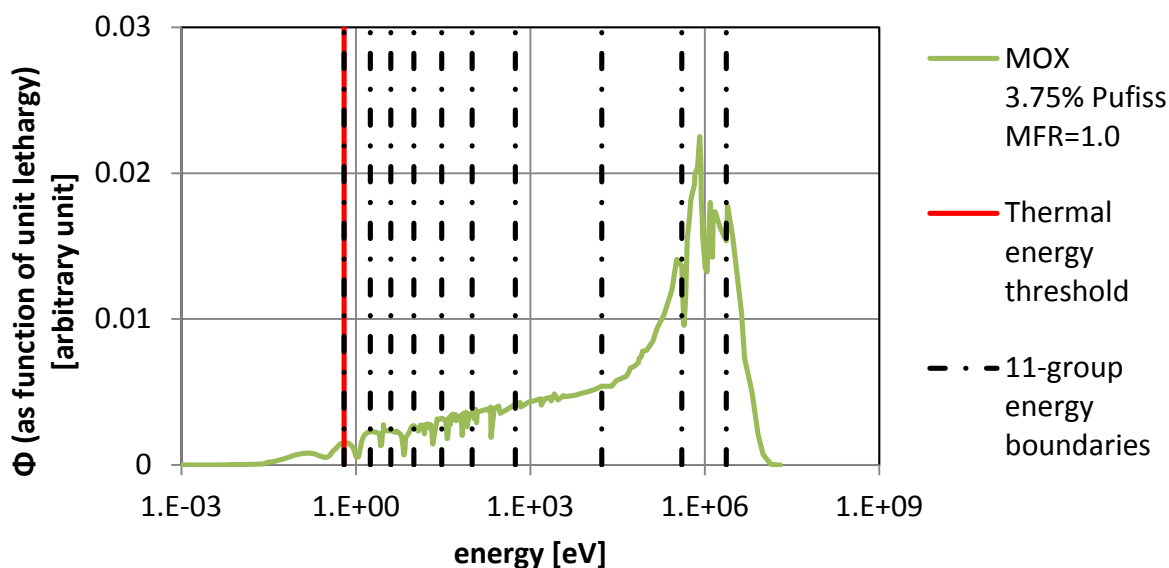
Fig. 5.3: 238 group neutron flux energy spectrum in an infinite lattice low moderated MOX fuel unit cell. The black dashed lines illustrate the selected energy boundaries for the 11-group cross-section library.

A possible compromise for higher accuracy while still using the common two group energy structure might be to move the two-group threshold of 0.625 eV upwards to higher energies like ~1.77 eV or ~4 eV to include the next important resonances located in the epi-thermal energy range in the thermal group. These two suggested new threshold values are selected in such a way to lie between large resonances of [240]Pu at 1.07 eV, [242]Pu 2.67 eV and [238]U at 6.67 eV. They are both used as energy group boundaries in the 11 group library and can also be seen in Fig. 5.3. However, due to the obtained results with more energy groups presented below, this approach has not been pursued further.

The power profile deviation between the reference and the other cases will be given in the two error metrics power-weighted error (PWE) and the error-weighted error (EWE) [97]. While for the PWE, given in equation (5.1), the local bundle power error is weighted with the reference bundle power, the EWE, given in equation (5.2), weights the error with itself and is,

thus, decoupled from the actual power distribution. The PWE reduces the importance of the low power region error and enhances the high power region error. The EWE, on the other hand, is more similar to the root-mean-square error and emphasizes the maximal errors. However, both the PWE as well as the EWE cannot give information about the sign of the error and, therefore, the local deviations have always to be considered.

$$\text{PWE} = \frac{\sum_i |e_i| \text{Ref}_i}{\sum_i \text{Ref}_i} \quad , [\%] \tag{5.1}$$

$$\text{EWE} = \frac{\sum_i |e_i|^2}{\sum_i |e_i|} \quad , [\%] \tag{5.2}$$

where

$$e_i = 100 * \frac{\text{Calc}_i - \text{Ref}_i}{\text{Ref}_i} \quad , [\%] \tag{5.3}$$

In these equations, Calc_i and Ref_i are the calculated and the selected reference power form factor, respectively. For KENO calculations, the standard deviation of the PWE and EWE is determined by using the standard deviation instead of the error e_i in equations (5.1) and (5.2).

5.3   2x2 colorsets

Small 2x2 FA models (denoted here as colorset) with large flux gradients arranged in an infinite lattice are suitable to test the quality of few cross-sections without too much modeling effort for the nodal and lattice physics codes. A representative selection of six is presented here to highlight leading effects. The different colorset configurations shown in Fig. 5.4 are composed of low moderated FA with 10x10 fuel pins (geometry of case 2 in Tab. 4.2).

Different average enrichment levels of 1 wt%, 2.5 wt%, and 4 wt% Pu$_{\text{fiss,}}$ in the following also referred to as low, medium and high enrichment, respectively, are used to create heterogeneity in the models. In cases A1, A2, and A3, two FA with medium and two FA with high enrichment are arranged in a checkerboard grid. Even larger heterogeneity is created in cases B1, B2, and B3 by using fuel assemblies of all three enrichment levels in a checkerboard like configuration. In cases A2 and B2 one control rod (CR) is inserted in the FA at position (1, a) and a second CR is inserted in cases A3 and B3 at position (1, b). Control rod crosses in the model are located at the outwards facing corners enabling individual insertion of no or up to 4 CR in the model. The inserted control rods further increase the heterogeneity induce flux gradients in the models. Therefore, they allow investigating the influence of absorbers on the

results. The thermal-hydraulic conditions in all calculations are set to constant mean BWR typical conditions as: active coolant density of 0.4572 g/cm³ (corresponding to 40 % void content) at 560.47 K coolant temperature and 800 K fuel temperature.
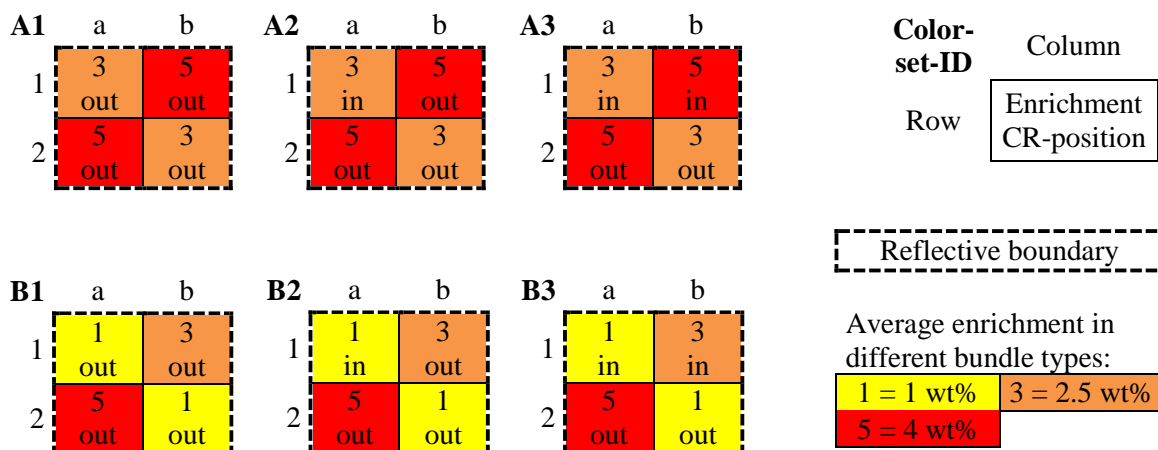
Fig. 5.4: Configuration for six different colorsets consisting of 2x2 fuel assemblies with different enrichment and control rod insertion.

The global results of k_{eff} for all colorset calculations with NEWT and PARCS with different nodal solvers and material constant libraries and ADF definition are shown in Tab. 5.2. Relative differences of k_{eff} between PARCS with different options and the reference NEWT calculation for each colorset are summarized in Tab. 5.3.

Tab. 5.2 Summary of k_{eff} results for all colorsets

Code	Method	XS-structure	k_{eff}, [-]					
			A1	A2	A3	B1	B2	B3
NEWT	ESC	238g, isotopic	1.09963	1.05317	1.00546	1.05167	1.00307	0.95485
PARCS	HYBRID	2g, homogenized	1.10058	1.05296	1.00386	1.05038	1.00089	0.95097
PARCS	NEMMG	2g, homogenized	1.10057	1.05294	1.00386	1.05030	1.00079	0.95089
PARCS	NEMMG	4g, homogenized	1.09984	1.05276	1.00384	1.04982	1.00080	0.95066
PARCS	NEMMG	11g, homogenized	1.09914	1.05253	1.00393	1.04951	1.00095	0.95098
PARCS	NEMMG	2g, homogenized, w/o ADF	1.10078	1.04943	0.99913	1.05207	0.99800	0.94681

In general the predicted eigenvalue by PARCS is adequate. It is less accurate for the more challenging cases B1 to B3 with more different fuel types and larger spectral mismatch between neighboring fuel assemblies. The differences in k_{eff}, which is for the colorset cases with reflective boundary conditions in fact k_{inf}, between PARCS calculations with the HYBRID and the NEMMG solver using the same two-group cross-sections are negligible. The HYBRID solver uses the analytical nodal method which is more accurate as the nodal

expansion method (NEM) in the NEM-multi-group solver NEMMG. However, only the NEMMG solver can handle larger number of energy groups in the cross-sections.

Tab. 5.3 Summary of k_{eff} difference to the reference NEWT calculation for all colorsets in [pcm]

Code	Method	XS-structure	dk_{eff}, [pcm]					
			A1	A2	A3	B1	B2	B3
NEWT	ESC	238g, isotopic	-	-	-	-	-	-
PARCS	HYBRID	2g, homogenized	94.1	−20.6	−160.5	−128.8	−217.7	−388.3
PARCS	NEMMG	2g, homogenized	93.2	−22.7	−160.9	−136.3	−227.8	−396.2
PARCS	NEMMG	4g, homogenized	20.6	−40.8	−162.8	−185.1	−226.5	−418.5
PARCS	NEMMG	11g, homogenized	−49.9	−63.9	−153.6	−215.9	−211.4	−386.8
PARCS	NEMMG	2g, homogenized, w/o ADF	114.5	−373.6	−633.3	40.1	−506.6	−803.9

Using higher number of energy groups with the NEMMG solver produces mostly a lower eigenvalue with less than 150 pcm difference between results for the 2 group and the 11 group calculations. The highest differences between results for different group structure are observed for the uncontrolled cases A1 and B1. Exceptions are especially cases A3 and B3 showing a fluctuating more or less constant trend.

For all colorsets except for B1, the eigenvalue of the reference transport calculation is predicted more accurate by PARCS if ADF are used than if they are omitted. In the control rod free colorsets A1 and B1, omitting ADF leads to slightly higher predicted eigenvalues compared to calculations with ADF. If one or two control rods are used, k_{eff} predicted by PARCS without ADF is 300 or 500 pcm lower relative to results obtained with ADF.

The reasons of the different effects in each colorset caused by different energy group structure in the cross-sections and by ADF are the multiple sources of errors which cancel out each other depending on the problem and the prepared few-group cross-sections. These sources of errors include spatial discretization, spatial homogenization, group collapsing and transport error [53]. Increasing for example the number of energy groups improves the group collapsing error contribution to the total error. However, without improving other sources of error, too, by e.g. using a finer mesh on pin-by-pin level, a higher order method like simplified transport and creating the few-group cross-section with appropriate spectrum, the error cancelation can impact the total solution accuracy both in positive and negative way. Regarding the effect of ADF, the assumptions for which they are created have to be considered. In the single FA calculation for generation of few-group cross-sections and ADF reflective boundary

conditions are usually applied. Thus, for the generation of ADF, zero current boundary conditions are assumed, which becomes invalid in real problems with large flux gradients.

An overview of the global PWE and EWE of the nodal powers obtained with PARCS relative to the NEWT transport calculation for each colorset is provided in Tab. 5.4. The corresponding reference fuel assembly power form factors and relative deviations between PARCS calculations with two-group cross-sections with different solvers and ADF options to NEWT are presented in Fig. 5.5.

Tab. 5.4 Summary of PWE and EWE results relative to the reference NEWT calculation for all colorsets in [%]

Code	Method	XS-structure	PWE, [%]						EWE, [%]					
			A1	A2	A3	B1	B2	B3	A1	A2	A3	B1	B2	B3
NEWT	ESC	238g, isot.	-	-	-	-	-	-	-	-	-	-	-	-
PARCS	HYBRID	2g, homog.	1.2	0.7	1.4	2.7	1.8	3.1	1.2	1.1	2.6	2.9	2.6	4.0
PARCS	NEMMG	2g, homog.	1.3	0.8	1.5	2.9	2.0	3.3	1.3	1.1	2.7	3.1	2.7	4.2
PARCS	NEMMG	4g, homog.	1.2	0.7	1.5	2.8	1.8	3.3	1.2	1.1	2.6	3.0	2.7	3.9
PARCS	NEMMG	11g, homog.	1.2	0.7	1.4	2.8	1.9	3.3	1.2	1.2	2.5	3.1	2.7	3.8
PARCS	NEMMG	2g, homog., w/o ADF	0.1	2.4	3.5	0.4	2.3	3.3	0.1	4.8	3.9	0.4	5.2	4.0

PARCS reproduces the power shape appropriately for the cases A1 and A2 with absolute local deviations to NEWT between 0.4 % and 1.3 % if ADF are applied. Larger local deviations are found for cases A3, B1 and B2 of up to 3.5 %. Maximal local errors in the nodal power of 5 % between PARCS with 2-group cross-sections with ADF to NEWT are found in the most heterogeneous case B3. As for the eigenvalue, the difference between HYBRID and NEMMG solvers for two-group cross-sections is negligible.

Interestingly, if ADF are omitted, the power shape is predicted much more accurate for the uncontrolled cases A1 and B2, but less precise for cases A2, A3, and B2 with some inserted CR. Although the global error metrics PWE and EWE do not indicate this, the local power distribution is also predicted very differently for case B3 depending on the use of ADF.

In colorset A1 and B1, low powers are over-predicted by PARCS and correspondingly high power under-predicted. However, this effect is stronger in case B1 due to the larger spectral mismatch between neighboring FA. The same can be observed in the uncontrolled FA of cases A2 and B2, but the very low power in the controlled FA is predicted by PARCS even lower as by NEWT. In the most heterogeneous cases A3 and B3 with two control rods

inserted in differently enriched neighboring FA, the power shape is predicted least accurate by PARCS, irrespective of the group structure or model chosen.

A1

	a	b
1	**0.947**, 1.3, 1.3, 0.1	**1.053**, −1.1, −1.2, −0.1
2	**1.053**, −1.1, −1.2, −0.1	**0.947**, 1.3, 1.3, 0.1

A2

	a	b
1	**0.686***, −1.1, −1.0, 6.8	**1.123**, −0.3, −0.4, −1.6
2	**1.123**, −0.3, −0.4, −1.6	**1.068**, 1.3, 1.4, −0.9

A3

	a	b
1	**0.726***, −0.4, −0.3, 5.0	**0.833***, −3.0, −3.1, 3.9
2	**1.287**, −0.1, −0.1, −2.9	**1.153**, 2.5, 2.6, −2.7

B1

	a	b
1	**0.873**, 3.1, 3.3, −0.4	**1.062**, −1.5, −1.6, 0.4
2	**1.192**, −3.2, −3.4, 0.3	**0.873**, 3.1, 3.3, −0.4

B2

	a	b
1	**0.604***, 0.5, 0.6, 7.3	**1.131**, −0.6, −0.7, −1.4
2	**1.276**, −2.3, −2.5, −1.2	**0.989**, 3.4, 3.6, −1.3

B3

	a	b
1	**0.639***, 1.4, 1.6, 5.3	**0.818***, −4.7, −4.8, 3.9
2	**1.476**, −1.6, −1.8, −2.2	**1.067**, 5.0, 5.2, −3.1

ID	Column
	Power form factor determined with NEWT, [-]
row	Relative error of power form factor as $(\text{PARCS}_{2g,\text{HYBRID}} - \text{NEWT}) / \text{NEWT}$, [%]
	Relative error of power form factor as: $(\text{PARCS}_{2g,\text{NEMMG}} - \text{NEWT}) / \text{NEWT}$, [%]
	Relative error of power form factor as: $(\text{PARCS}_{2g,\text{NEMMG, w/o ADF}} - \text{NEWT}) / \text{NEWT}$, [%]

Fig. 5.5: Power form factors determined with NEWT for all colorsets and relative errors of the power form factors determined with PARCS with two different nodal solvers (HYBRID and NEMMG) and two different material constant libraries (2g homogenized cross-sections with and without ADF). * indicates inserted control rod in fuel assembly.

In Fig. 5.6, the reference fuel assembly power form factors and relative deviations between PARCS calculations with few-group cross-sections in different number of energy groups to NEWT are depicted. The corresponding global error metrics PWE and EWE for these calculations are included in Tab. 5.4. Using a larger number of energy groups has almost no effect on the local power distribution. The FA power error alters by less than 0.4 % for all FA in all cases except for two FA in case B3. However, the changes are not in all cases improvements.

The larger local errors in cases with inserted control rods and in the more complex cases of the B colorset series indicates potential for improvement of the cross-section generation process. Especially enhancements in ADF generation could improve the results substantially. Fuel assemblies with inserted CR could e.g. be embedded in a more appropriate environment for cross-section generation. However, due to the many possible combinations in a real core, a

corresponding parameterization is very challenging [82]. Recent development trends consider for example online cross-section generation taking into account leakage to the current surrounding FAs for a more realistic prediction of the real local neutron flux distribution and spectrum [98].

A1	a	b		A2	a	b		A3	a	b
1	**0.947**	**1.053**		1	**0.686***	**1.123**		1	**0.726***	**0.833***
	1.3	−1.2			−1.0	−0.4			−0.3	−3.1
	1.3	−1.1			−1.3	−0.3			−0.3	−3.0
	1.3	−1.1			−1.4	−0.2			−0.3	−2.9
2	**1.053**	**0.947**		2	**1.123**	**1.068**		2	**1.287**	**1.153**
	−1.2	1.3			−0.4	1.4			−0.1	2.6
	−1.1	1.3			−0.3	1.3			−0.1	2.5
	−1.1	1.3			−0.2	1.3			−0.2	2.5

B1	a	b		B2	a	b		B3	a	b
1	**0.873**	**1.062**		1	**0.604***	**1.131**		1	**0.639***	**0.818***
	3.3	−1.6			0.6	−0.7			1.6	−4.8
	3.2	−1.3			0.5	−0.4			1.7	−4.2
	3.2	−1.3			0.6	−0.3			1.9	−3.9
2	**1.192**	**0.873**		2	**1.276**	**0.989**		2	**1.476**	**1.067**
	−3.4	3.3			−2.5	3.6			−1.8	5.2
	−3.4	3.2			−2.6	3.4			−2.1	5.1
	−3.5	3.2			−2.6	3.4			−2.3	5.0

ID	Column
row	**Power form factor determined with NEWT, [-]**
	Relative error of power form factor as $(PARCS_{2g,,NEMMG} - NEWT) / NEWT$, [%]
	Relative error of power form factor as: $(PARCS_{4g,,NEMMG} - NEWT) / NEWT$, [%]
	Relative error of power form factor as: $(PARCS_{11g,,NEMMG} - NEWT) / NEWT$, [%]

Fig. 5.6: Power form factors determined with NEWT for all colorsets and relative errors of the power form factors determined with PARCS with the nodal NEMMG solver and three different energy group structures in the material constant libraries (2g, 4g, and 11g homogenized cross-sections with ADF). * indicates inserted control rod in fuel assembly.

5.4   6x6 mini quarter core model

A simple 5x5 quarter core slice surrounded by one row of reflector assemblies hax been investigated as second test set to include leakage in the model and approach the real problem size by an intermediate step. To minimize errors introduced by modeling deficiencies for CR and corner reflectors [86] a square core model is used without inserted CR. The model configuration is depicted in Fig. 5.7.

The same three bundle enrichment levels and TH conditions as for the prior described colorset test cases have been used and arranged in the geometry. For the KENO calculations 2000

active generations, 1000 inactive generations and 10^5 neutrons per generation are used. This is a total of $2*10^8$ active neutron histories providing an appropriate statistics.
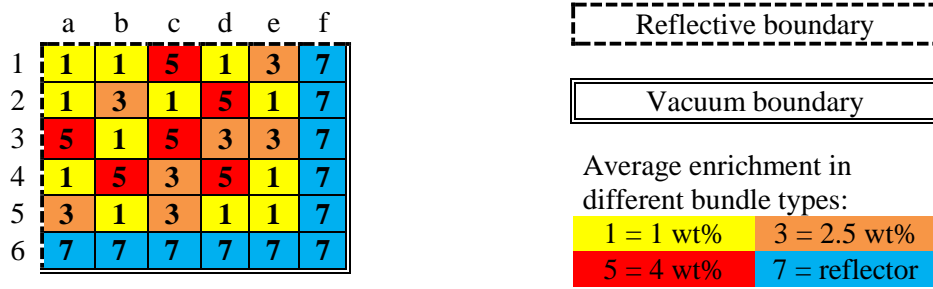
Fig. 5.7: Configuration for 6x6 quarter core slice test case with enrichment distribution, reflector assembly positions and boundary conditions.

The results for k_{eff} determined with NEWT, KENO, and PARCS with different cross-section libraries for the investigated 6x6 mini quarter core are summarized in Tab. 5.5. In addition, differences in k_{eff} to the reference NEWT calculation and global PWE and EWE are included. In Fig. 5.8 the corresponding radial power profile for the NEWT calculation is included and on the left relative errors of FA powers to KENO-MG, PARCS with two-group cross-sections with ADF and to PARCS with two-group cross-sections without ADF are shown. On the right of Fig. 5.8, relative deviations of PARCS calculations with different few-group cross-sections to NEWT are compared.

Tab. 5.5 Summary of results for 6x6 mini quarter core slice

Code	Method	XS-structure	k_{eff}, [-]	dk, [pcm]	PWE, [%]	EWE, [%]
NEWT	ESC	238g, isotopic	0.99997	ref	ref	ref
KENO-MG	MC	238g, isotopic	$1.00149 \pm 5^*$	151	1.02 ± 0.14	3.08 ± 0.16
KENO-CE	MC	CE, isotopic	0.99364 ± 5	−633	0.99 ± 0.26	3.01 ± 0.31
PARCS	HYBRID	2g, homogenized	0.99626	−372	3.67	4.43
PARCS	NEMMG	2g, homogenized	0.99617	−380	3.72	4.39
PARCS	NEMMG	4g, homogenized	0.99660	−338	3.61	4.30
PARCS	NEMMG	11g, homogenized	0.99721	−276	3.46	4.03
PARCS	NEMMG	2g, homogenized, w/o ADF	0.99741	−256	1.58	2.60

*standard deviation

Comparing the reference NEWT results with the KENO-MG calculations shows adequate agreement between the codes both for k_{eff} as well as for the power weighted error. The larger error weighted error of 3 % of KENO relative to NEWT comes from deviations at the core corner where the power is very low. KENO generally tends to predict larger maximal and lower minimal values of the local power. The absolute deviation of local power form factors between KENO and NEWT is within ± 0.02. In Fig. 5.8 on the left, asymmetry of the KENO

power profile can be observed since the deviations to the symmetric NEWT power profile is asymmetric. This is caused by the statistical character of Monte Carlo calculations. KENO-CE predicts almost identical power distribution as KENO-MG. The rather strong under-prediction of k_{eff} with KENO-CE can be explained with the deficiencies for harder spectrum MOX configurations discussed in chapter 3.2, which should be improved for the next program version of SCALE.

Left table:

	a	b	c	d	e
1	**1.361** / 1.0±0.2 / 3.9 / 1.1	**1.308** / 0.9±0.2 / 5.0 / 0.6	**1.647** / 1.3±0.2 / −3.6 / 0.3	**0.938** / −0.2±0.1 / 4.0 / −1.7	**0.803** / −0.7±0.1 / −1.0 / 4.4
2	**1.308** / 1.0±0.2 / 5.0 / 0.6	**1.596** / 1.2±0.2 / −1.6 / 0.8	**1.122** / 0.3±0.1 / 5.6 / −0.8	**1.259** / 0.4±0.2 / −5.2 / −1.7	**0.610** / −1.7±0.1 / 5.1 / 2.9
3	**1.647** / 1.4±0.2 / −3.6 / 0.3	**1.122** / 0.3±0.1 / 5.6 / −0.8	**1.423** / 0.6±0.2 / −4.6 / −1.6	**0.960** / −0.4±0.1 / −1.0 / −2.3	**0.677** / −2.0±0.1 / −2.6 / 2.5
4	**0.938** / −0.1±0.1 / 4.0 / −1.7	**1.259** / 0.4±0.2 / −5.2 / −1.7	**0.960** / −0.3±0.1 / −1.0 / −2.3	**0.853** / −0.9±0.1 / −6.3 / −3.9	**0.418** / −4.1±0.1 / 1.8 / −0.3
5	**0.803** / −0.5±0.1 / −1.0 / 4.4	**0.610** / −1.6±0.1 / 5.1 / 2.9	**0.677** / −2.0±0.1 / −2.6 / 2.5	**0.418** / −4.0±0.1 / 1.8 / −0.3	**0.284** / −7.0±0.1 / −0.3 / 1.1

Right table:

	a	b	c	d	e
1	**1.361** / 3.9 / 4.0 / 4.0	**1.308** / 5.0 / 4.4 / 4.4	**1.647** / −3.6 / −3.9 / −3.8	**0.938** / 4.0 / 3.4 / 3.6	**0.803** / −1.0 / 0.5 / −0.2
2	**1.308** / 5.0 / 4.4 / 4.4	**1.596** / −1.6 / −1.7 / −1.6	**1.122** / 5.6 / 4.5 / 4.4	**1.259** / −5.2 / −5.0 / −4.6	**0.610** / 5.1 / 6.1 / 5.4
3	**1.647** / −3.6 / −3.9 / −3.8	**1.122** / 5.6 / 4.5 / 4.4	**1.423** / −4.6 / −4.8 / −4.5	**0.960** / −1.0 / −1.6 / −1.3	**0.677** / −2.6 / −1.3 / −2.0
4	**0.938** / 4.0 / 3.4 / 3.6	**1.259** / −5.2 / −5.0 / −4.6	**0.960** / −1.0 / −1.6 / −1.3	**0.853** / −6.3 / −6.2 / −5.5	**0.418** / 1.8 / 3.1 / 2.8
5	**0.803** / −1.0 / 0.5 / −0.2	**0.610** / 5.1 / 6.1 / 5.4	**0.677** / −2.6 / −1.3 / −2.0	**0.418** / 1.8 / 3.1 / 2.8	**0.284** / −0.3 / 3.3 / 2.5

column (left) — example cells legend:

Power form factor determined with NEWT, [-]

Relative error of power form factor (± std.dev.) as:
(KENO−MG − NEWT) / NEWT, [%]

Relative error of power form factor as:
(PARCS$_{2g,,NEMMG}$ − NEWT) / NEWT, [%]

Relative error of power form factor as:
(PARCS$_{2g,,NEMMG,w/o\ ADF}$ − NEWT) / NEWT, [%]

column (right) — example cells legend:

Power form factor determined with NEWT, [-]

Relative error of power form factor as:
(PARCS$_{2g,,NEMMG}$ − NEWT) / NEWT, [%]

Relative error of power form factor as:
(PARCS$_{4g,,NEMMG}$ − NEWT) / NEWT, [%]

Relative error of power form factor as:
(PARCS$_{11g,,NEMMG}$ − NEWT) / NEWT, [%]

Fig. 5.8: Power form factors determined with NEWT for 6x6 core model and deviation of power form factors determined with other methods relative to NEWT are shown. In example cells at the bottom of this figure, the content of the cells is illustrated.

A general comparison of the global results in Tab. 5.5 for the different combinations of PARCS solvers and cross-section libraries relative to the NEWT calculation reveals rather small differences between k_{eff}, PWE and EWE. The solution accuracy of both the HYBRID and the NEMMG are comparable as already seen for the colorset study above. Increasing the number of energy groups from 2 to 11 improves k_{eff} prediction by 100 pcm but does not significantly affect the power error. Omitting ADF improves k_{eff} even slightly and reduces the

PWE and EWE significantly by 2 %. For colorsets A1 and B2 which also have no control rods inserted as this mini core, similar effect of k_{eff} increase end PWE and EWE reduction has been observed if ADF are not considered in the calculation. If ADF are used in PARCS, it is notable that in low enriched bundles the power tends to be over-predicted, while in high enriched bundles the power tends to be under-predicted relative to the NEWT calculation (cp. enrichment distribution in Fig. 5.7). If, on the other hand, ADF are omitted, such a particular trend depending on bundle enrichment cannot be observed and the general error profile in the core is much smoother except for the outer core boundary to the reflector. Improvements of the power distribution could be achieved by more appropriate ADF generation with SCALE at least for this specific application. Further investigations going more into detail are necessary to identify individual error sources. In general, the effect of error cancelation discussed above is also valid for this problem.

5.5   10x10 quarter core model

The most representative test case for full-core calculations investigated here is a 2D-slice of a quarter core with 73 low moderated FAs consisting of 10x10 fuel pins and TH conditions as mentioned above. In Fig. 5.9, the general core layout with local bundle enrichment type, positions of inserted CR, and the position of reflector assemblies is depicted. Due to the problem size, the different average bundle enrichments of 1 wt%, 2.5 wt% and 4 wt% Pu_{fiss}, the locally inserted CR and the leakage, this model is challenging for a nodal simulator and is suitable to test the cross-sections for core level applications. In the NEWT and KENO models, the available geometry shapes restrict the outer model geometry to a cuboid and do not allow following the actual curvature of the core surface. Normally bodies containing void can be defined in both codes but because of convergence problems no results could be obtained using this option. Therefore, the south-east corner of the model shown in Fig. 5.9 is filled with water (7^+ nodes) in the transport calculations but not in PARCS. Tests between PARCS calculations with and without these additional nodes have shown a negligible effect on the results if reflector nodes are added in the corner of the core lattice of less than 5 pcm in k_{eff} and less than 0.1 % in the nodal power distribution in the whole core except for the two adjacent corner fuel nodes at the symmetry axis next to the reflector, where the error is increased to 0.5 %. Even if a second reflector row is added, the local deviation stays below 20 pcm in k_{eff} and smaller than 0.5 % in the local power distribution in the whole core except for the fuel nodes facing the south and east reflector where it rises to about 1.3 %. For the KENO calculations of this model 400 active generations, 200 inactive generations and 10^6

neutrons per generation were used. This is a total of $4*10^8$ active neutron histories leading to appropriate statistics.
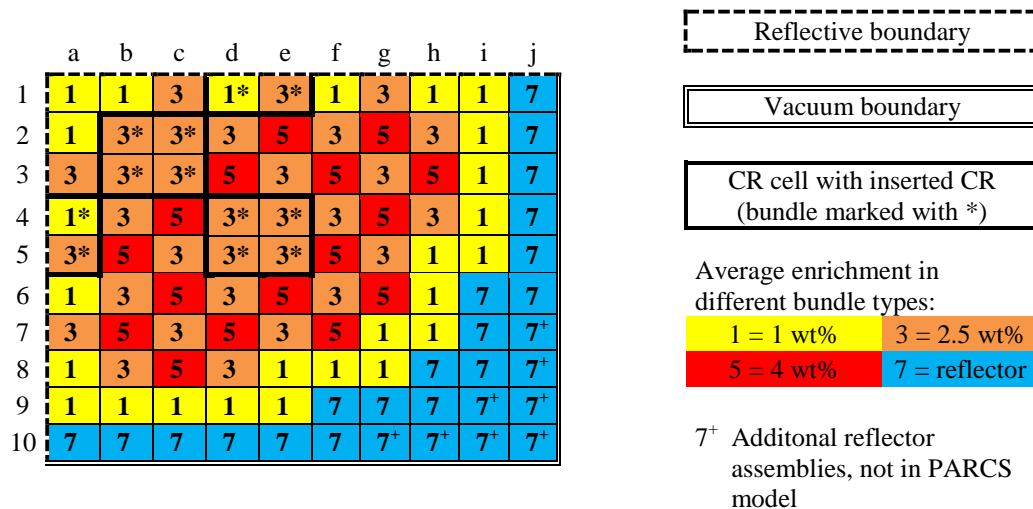
Fig. 5.9: Configuration for 10x10 quarter core slice test case with enrichment distribution, reflector assembly positions and boundary conditions.

The global results for the investigated 10x10 quarter core and global differences to the reference NEWT calculation are summarized in Tab. 5.6. In Fig. 5.10 the corresponding radial power profile is given together with the deviation of the local power form factors of selected PARCS calculations to the reference. Comparing the reference NEWT results with the KENO calculations shows adequate agreement between the codes and similar behavior as for the 6x6 case. Again almost identical deviation of the power distribution relative to the reference solution can be observed for KENO-CE as for KENO-MG.

Tab. 5.6 Summary of results for 10x10 quarter core slice

Code	Method	XS-structure	k_{eff}, [-]	dk, [pcm]	PWE, [%]	EWE, [%]
NEWT	ESC	238g, isotopic	1.00517	ref	ref	ref
KENO-MG	MC	238g, isotopic	$1.00728 \pm 3^{*}$	212	1.03 ± 0.18	2.69 ± 0.19
KENO-CE	MC	CE, isotopic	0.99861 ± 5	-656	1.13 ± 0.32	2.46 ± 0.36
PARCS	HYBRID	2g, homogenized	1.00264	-253	2.65	4.58
PARCS	NEMMG	2g, homogenized	1.00256	-261	2.65	4.40
PARCS	NEMMG	4g, homogenized	1.00270	-247	2.92	5.92
PARCS	NEMMG	11g, homogenized	1.00300	-217	2.80	5.55
PARCS	NEMMG	2g, homogenized, w/o ADF	1.00085	-431	2.86	6.35

*standard deviation

	a	b	c	d	e	f	g	h	i
1	**0.686**	**0.667**	**0.847**	**0.547***	**0.863***	**1.103**	**1.352**	**0.879**	**0.589**
	0.6	3.3	−1.1	2.1	−5.8	4.6	−0.7	4.0	6.3
	1.0	3.4	−0.8	1.7	−5.7	4.3	−0.8	4.1	8.9
	1.2	3.5	−0.6	1.7	−5.7	4.4	−0.6	4.6	8.6
2	**0.667**	**0.590***	**0.651***	**1.058**	**1.440**	**1.454**	**1.560**	**1.102**	**0.598**
	3.3	−3.5	−3.4	1.4	−2.3	0.3	−2.7	−0.1	6.6
	3.4	−3.4	−3.7	0.9	−2.6	−0.4	−3.0	−0.2	8.6
	3.5	−3.3	−3.8	0.7	−2.6	−0.5	−2.9	0.1	8.1
3	**0.847**	**0.651***	**0.740***	**1.280**	**1.336**	**1.678**	**1.400**	**1.233**	**0.590**
	−1.1	−3.4	−4.1	−1.7	1.6	−2.9	1.3	−3.1	6.6
	−0.8	−3.7	−4.8	−1.9	0.8	−3.3	0.4	−3.1	8.2
	−0.6	−3.8	−5.0	−2.0	0.6	−3.3	0.3	−2.7	7.6
4	**0.547***	**1.058**	**1.280**	**0.847***	**0.955***	**1.393**	**1.503**	**1.024**	**0.537**
	2.1	1.4	−1.7	−0.3	−3.7	1.3	−2.7	−0.5	5.6
	1.7	0.9	−1.9	−0.9	−4.0	0.6	−3.0	−0.6	7.7
	1.6	0.7	−2.0	−1.0	−4.0	0.6	−2.9	−0.3	7.3
5	**0.863***	**1.440**	**1.336**	**0.955***	**0.930***	**1.474**	**1.194**	**0.719**	**0.479**
	−5.8	−2.3	1.6	−3.7	−2.1	−2.6	0.2	3.9	6.5
	−5.7	−2.6	0.8	−4.0	−2.6	−2.7	−0.3	4.2	10.2
	−5.7	−2.6	0.6	−4.0	−2.6	−2.6	−0.1	4.4	8.9
6	**1.103**	**1.454**	**1.678**	**1.393**	**1.474**	**1.210**	**1.133**	**0.607**	
	4.6	0.3	−2.9	1.3	−2.6	0.6	−4.3	5.1	
	4.3	−0.4	−3.3	0.6	−2.7	−0.1	−4.0	6.8	
	4.4	−0.5	−3.3	0.6	−2.6	0.0	−3.6	6.4	
7	**1.352**	**1.560**	**1.400**	**1.503**	**1.194**	**1.133**	**0.607**	**0.447**	
	−0.7	−2.7	1.3	−2.8	0.2	−4.3	4.2	6.3	
	−0.8	−3.0	0.4	−3.0	−0.3	−4.0	4.4	10.1	
	−0.6	−2.9	0.3	−2.9	−0.1	−3.6	4.7	8.7	
8	**0.879**	**1.102**	**1.233**	**1.024**	**0.719**	**0.607**	**0.447**		
	4.0	−0.1	−3.1	−0.5	3.9	5.0	6.3		
	4.1	−0.2	−3.1	−0.6	4.2	6.8	10.1		
	4.6	0.1	−2.8	−0.3	4.4	6.4	8.7		
9	**0.589**	**0.598**	**0.590**	**0.537**	**0.479**				
	6.3	6.6	6.6	5.6	6.5				
	8.9	8.5	8.1	7.7	10.2				
	8.6	8.1	7.6	7.3	8.9				

column

row	Power form factor determined with NEWT, [-]	
	Relative error of power form factor as:	$(PARCS_{2g,,NEMMG} - NEWT) / NEWT$, [%]
	Relative error of power form factor as:	$(PARCS_{4g,,NEMMG} - NEWT) / NEWT$, [%]
	Relative error of power form factor as:	$(PARCS_{11g,,NEMMG} - NEWT) / NEWT$, [%]

Fig. 5.10: Power form factors determined with NEWT for 10x10 quarter core model and deviation of power form factors determined with PARCS and number of energy group in cross-sections relative to NEWT are shown. In example cell at the bottom of this figure, the content of the cells is illustrated. * indicates a fuel assembly with inserted control rod

Compared to NEWT, KENO tends to predict larger values in high power regions especially in the second and third outermost FA rows (< 1.5 % local deviation corresponding to ~0.02 higher power form factor with KENO) and predict smaller values in fuel assemblies with low power in the core center (> −7 % local deviation, corresponding to ~0.04 lower power form

factor with KENO). As observed for the previous investigations, the different PARCS calculations vary only negligibly for larger number of energy groups in the few-group cross-section library. The value of k_{eff} is improved by 50 pcm if 11 instead of 2 energy groups are used but the weighted error increases in this case. Increased local error in the power distribution can especially be found in the FA next to the reflector. The indifferent influence of the energy group structure in the cross-sections in the local and global results is caused by the error cancelation effects discussed in detail above.

This result is essential because it proves that the energy resolution of the common two-group cross-sections does not have to be increased to describe the harder neutron spectrum in low moderated BWR cores as investigated in this context.

The influence of fuel and reflector ADF on results for this 10x10 core model has been assessed as for the colorset test cases and the 6x6 minicore. Withdrawing ADF flattens the radial power profile especially in regions around inserted CR and in corner FA at the reflector. Compared to the PARCS calculation with ADF, this leads to a systematically higher predicted power in controlled FAs and lower predicted power in FAs next to controlled ones. Using the ADF generated with TRITON improves the global results in general. However, a similar dependence of the local error on the bundle type can be observed as for the 6x6 core model. This is a result of the applied assumptions for ADF generation assuming zero net current between adjacent fuel assemblies which is strictly only valid for an infinite core lattice. For the controlled bundles and the reflector region, this approximate correction improves the prediction, but apparently deteriorates the results for the checkerboard-like uncontrolled FA lattice in the second and third row.

5.6   Implications for core design studies

The negligible influence of the energy group structure on the results obtained with the core simulator PARCS suggests that the common two-group energy structure of the homogenized cross-sections is sufficient to model low moderated reactor cores at least at uniform thermal-hydraulic conditions of a BWR core.

Potential for improvements regarding the ADF generation with SCALE has been identified during the validation studies. The observed tendency to under-predict high power peaks is specifically problematic for the estimation of local safety parameters and, thus, has to be improved, if conservative assumptions shall be minimized.

To further extend the cross-section validation, the next steps should include:

- Investigation of the error trends of the power distribution of a model with more realistic material compositions combining fresh and burnt fuel and
- validation for different thermal-hydraulic conditions like higher void content.

5.7   Complementary code-to-code comparison for a full-core model

The comparison of the computational route of TRITON / PARCS with that of CASMO-4 / MICROBURN-B2 for a full-core model used to determine an equilibrium cycle showed that larger power peaks are predicted in the core with CASMO-4 / MICROBURN-B2. The general agreement between both routes is, however, very good considering the differences between the individual tools (i.a. basic nuclear data, methodology in lattice code, nodal method, and thermal-hydraulic model). Selected results of this code-to-code comparison are summarized in Appendix B. A detailed code-to-code comparison of CASMO-4 / MICROBURN-B2 and TRITON / PARCS for a core model with uniform core conditions would be useful to eliminate uncertainties arising from TH models.

6 Design studies on low moderated BWR cores

The goal of the design studies is to develop a low moderated core design with improved fuel utilization fulfilling a variety of relevant neutronic core safety parameters and operational parameters. Starting point and reference for comparison is a full-MOX BWR core design analyzed in [13] and described in more detail below. For the low moderated core designs, the FA designs identified as the most promising ones in chapter 4.6 are adopted.

6.1 Methodology for investigation

6.1.1 Computational route and model

The lattice code CASMO-4 is used to generate homogenized and condensed two energy group cross-section libraries using the cutoff energy of 0.625 eV between fast (group 1) and thermal (group 2) neutrons. These libraries are used in the 3D core simulator MICROBURN-B2 to perform the core analysis including TH feedback. All investigations with MICROBURN-B2 are performed for a quarter core model assuming rotational symmetry with 196 radial FA subdivided in 24 axial nodes (784 FA in full core).

6.1.2 Optimizing the equilibrium cycle

The feasibility of the investigated core designs is assessed on the basis of equilibrium cycles. To reach such an equilibrium cycle, several consecutive cycles are run. Since the starting conditions have no impact on the equilibrium state, a core loaded with 100 % fresh fuel assemblies is selected as starting condition for this procedure. The least reactive fuel assemblies are discharged at the end of each cycle according to a given ranking map. The remaining ones are rearranged corresponding to the same map and a fresh batch of FA is loaded. This is repeated until the burnup distribution in the core doesn't change anymore. Typically this occurs after fifteen to twenty cycles if the iterations are started from a homogeneous core with only fresh FAs.

The fissile plutonium and gadolinia enrichment in the fuel is adjusted iteratively and manually in the preceding CASMO-4 calculations to maintain

- low control rod (CR) density throughout the cycle and
- low radial (f_{rad}) and axial (f_{ax}) power peaking factors.

For all cases (reference core design as well as low moderated core designs), the same reloading and re-shuffling reactivity ranking map is used, as well as the same batch size and cycle length in equivalent full power hours (efph). The coast down is adjusted by fine tuning from case to case. Due to the fact that the target core eigenvalue for the investigated low moderated core designs is unknown, the equilibrium cycle is designed to have a k_{eff} of unity throughout the whole cycle. This is the same approach as applied in [13] for the full-MOX BWR core and is an acceptable simplification, since k_{eff} is around $1 \pm 100\,pcm$ in actual cycles for the reference BWR.

6.1.3   Operational parameters

Several operational features need to be taken into account to optimize a core design. The most important parameters are:

1.   Maximal core pressure loss

Since the reduced moderation core is to be incorporated into an existing Gen-II BWR, no changes of the recirculation pumps and of the reactor pressure vessel internals are accepted. Consequently, the core must be designed in such a way that the core pressure drop is comparable to or less than the one of the reference core. Because pumps can maintain a higher pressure head at lower flow rates a slightly increased pressure loss could be accepted if the core flow rate is reduced.

2.   Fuel economy

To obtain an economically competitive concept, the average discharge burnup should be targeted to be in the range of the discharge burnup of about 51 MWd/kgHM that corresponds to the one of the reference full-MOX BWR core. The energy generated per cycle is used as additional measure to determine the utilization of the plants' capacity of energy output, because the core heavy metal inventory and the nominal core power vary between designs.

6.1.4   Global core safety parameters

The following global safety parameters for the stationary core conditions were evaluated and compared to the ones of the reference core:

1.   Stuck-rod cold shutdown margin

The capability of a safe shutdown of the reactor has to be ensured at any time, especially at the most reactive core state which is the cold zero power (CZP) and xenon free core in a

BWR. Additionally it is assumed that the most effective control rod remains stuck outside of the core. Regulatory guidelines require the stuck-rod cold shutdown margin (CSDM) of the core eigenvalue at this state to the target eigenvalue k_{target} at which the core becomes critical to be at least -1 %. To account for calculation uncertainties it is mostly required to be more negative than -1.5 %. The CSDM is determined according to the equation

$$\text{CSDM} = \frac{k_{\text{stuck rod}} - k_{\text{target}}}{k_{\text{stuck rod}}} < -0.015 \,. \tag{6.1}$$

For each core design the computed eigenvalue has a bias from the real eigenvalue, which depends on core state, burnup, and other parameters. Accordingly, the CSDM has to be determined not relative to $k_{target} = 1$, but relative to a corrected unbiased value of k_{target} different from unity corresponding to the real CZP xenon free critical eigenvalue. This value can be determined for existing reactors from measurements during reactor startup and extrapolation to subsequent core loadings. Unfortunately, k_{target} is unknown for both the reference full-MOX BWR core and the low moderated core designs. Based on experience with core design for the reference plant, a target value of $k_{target} = 0.991$ has been chosen for the full-MOX core. Therefore, it is also selected for the low moderated core designs as a reasonable starting point.

2. Void reactivity coefficient

There are three options in MICROBURN-B2 to compute the void reactivity coefficient (VC) for a whole core corresponding to the variation of the three thermal-hydraulic boundary conditions core inlet coolant temperature, core inlet coolant mass flow rate, and core exit pressure. Since mainly the axial coolant density distribution in the core depends strongly on the chosen type of variation and the corresponding reactivity feedback depends also on local factors like fuel burnup and history effects, the calculated VC around the operation point will be different depending on the selected parameter change. One can use it to compare different core designs to each other and assess the individual effect of the three parameters around the operation point, but full-core transient analyses are crucial to assess the core behavior in relevant accident scenarios. In MICROBURN-B2, the VC is calculated depending on the linear change of the core average coolant void content between the nominal state and one varied state as

$$\text{VC} = \frac{\Delta k}{\Delta \text{Void (\%)}} \,. \tag{6.2}$$

3. Doppler reactivity coefficient

The Doppler reactivity coefficient (DC) is determined in MICROBURN-B2 by varying the fuel temperature uniformly in negative and positive direction (by default $\pm 25\ °F = \pm 13.9\ °C$) and then applying the following formula to the two temperature intervals:

$$DC = \frac{\Delta k}{\Delta T_{fuel}}. \tag{6.3}$$

Averaging the two obtained coefficients is equal to computing a quadratic fit through all three value pairs and to determine the DC at the operating point from this fit.

4. Power reactivity coefficient

With the power reactivity coefficient (PC), the combined reactivity effect accompanying a reactor power change can be captured. The coolant boundary conditions remain constant but due to the power change the coolant and the fuel properties change. In MICROBURN-B2 the approach to determine the PC is similar to that described for the DC. By imposing a user defined power fraction change in negative and positive direction (by default $\pm 10\ \%$ of the nominal thermal power) two additional states are created to be utilized for linear fits determined with the formula

$$PC = \frac{\Delta k}{\Delta P}. \tag{6.4}$$

5. Isothermal temperature reactivity coefficient

To assess the core start-up behavior, the isothermal temperature reactivity coefficient (ITC) is used. There are two approaches for its determination. The detailed approach is to determine a critical core conditions by control rod pattern adjustment for various isothermal core states between the cold (20°C) and hot (286°C) temperature and then impose a small isothermal temperature variation at each state to determine the corresponding local ITC. However, investigations have shown that it is sufficient to use a simplified procedure to determine the ITC change during the reactor heatup phase. In this method the CZP critical control rod pattern is used for all isothermal core states in the heatup range. For each state the core eigenvalue is computed and a polynomial function is fitted through the corresponding temperature-eigenvalue value pairs to determine the dependence of the ITC on the temperature via derivation. The ITC is usually positive at low temperatures due to the strong over moderation. It has to become negative at a temperature enough below the operating temperature of 286 °C for each of four different bounding core conditions to achieve inherent

safe feedback at full power operation. These bounding conditions are begin of cycle (BOC) without xenon, BOC with maximal xenon concentration (approximately 8 hours after shutdown), end of cycle (EOC) without xenon, and finally EOC with maximal xenon concentration.

6.1.5   Local safety parameters

1. Linear heat generation rates

Fuel mechanics limits the maximal linear heat generation rate (LHGR) in MOX fuel to approximately 400 W/cm for fresh fuel. Due to increasing pellet cladding interaction (PCI) in high burnup fuel, this limit is decreasing with exposure. Here, no explicit thermal-mechanical assessment was done. Instead, the burnup dependent LHGRs for each case are compared to the full-MOX core and are assumed to be adequate if they are equal or lower to the ones of the reference core. This assumption is appropriate since fuel rod dimensions are comparable.

2. Boiling transition

The safety margin to boiling transition in BWRs is measured in terms of the CPR. It is currently not predictable for the investigated low moderated FA with MICROBURN-B2 due to the lack of an appropriate design specific CPR correlation on FA level. Instead, the maximum core exit void content is used as a simplified preliminary design criterion for the local coolability. In the low moderated core designs the core flow rate is adjusted accordingly to maintain a maximal exit void in the range of the full-MOX BWR.

Assessment of the CPR has been done subsequently with the sub-channel code SUBCHANFLOW for selected FA designs and peak operating conditions obtained from the neutronic core calculations (see chapter 7).

3. Fuel centerline and cladding surface temperature

Local temperatures in the fuel rod are especially considered in transient analyses. Fuel centerline temperatures have to stay below the melting point and the cladding surface temperatures have to stay below the limiting temperature for the exothermic Zircaloy-water-oxidation reaction, which generates both hydrogen (explosion risk) and heat.

6.2   Reference full-MOX BWR core

The starting point and reference core design for the performed investigations is a 100 % MOX core design. The description and results for this core design are summarized in [12] and

discussed extensively in [13] (core design "V1/v7"). In chapter 1.2, the general design parameters of the reference NPP Gundremmingen are provided.

In this design, the uprated power of 4000 MW$_{th}$ is used as nominal operation power. The target cycle burnup used to design this core with a heavy metal inventory of 139 t is set to 9.7 MWd/kgHM. This corresponds to approximately 8406 equivalent full power hours (efph) using the currently licensed rated core power of 3840 MW$_{th}$ as full power level (this is due to the setting in the simulation model). The actual cycle length depends naturally on the nominal power and the coastdown and is with 339 days about 11 days shorter as the equivalent full power value for this case. During nominal power operation, the flow rate is reduced slightly to 97.5 % of the rated value of 14306 kg/s to have a higher void content in the core and to improve generation of plutonium. During the last 56 equivalent full power days (efpd) of the cycle, the flow is increased stepwise to 111 % of the rated flow to improve neutron moderation and, thus, increase the core reactivity. This strategy of moderation control during the cycle is called spectral shift. In addition to the flow adjustment, the power is decreased stepwise by up to 10 % of the nominal thermal power during a 27 efpd long coastdown at the end of thy cycle.

The subcooling of the coolant at the core inlet is dependent on the steam flow rate (equal to the feedwater flow rate) and the coolant recirculation within the reactor pressure vessel (RPV). Higher core power results, in contrary to intuitive expectation, in a lower coolant enthalpy at the core inlet. This is caused by the increased amount of "cold" feedwater added to the constant recirculation flow. MICROBURN-B2 has the ability to automatically compute the core inlet coolant temperature based on core power and core recirculation flow rate.

In every depletion step during the equilibrium cycle, the insertion of control rods is manually adjusted to obtain critical conditions. Due to the use of burnable poison rods in the FA only a small control rod fraction of below 5.5 % is needed during the cycle to control the excess reactivity. The control rods do not contain absorber material in the uppermost part leaving about 6 cm of the FA top uncovered by CR even at full insertion. Because the CR-worth in approximately the upper and lower 10 % of the FA is reduced due to the low local power and leakage effects near the core surface, the general approach is to not fully insert them at any time during normal operation, but to keep them about 10 % withdrawn to be more flexible and effective in power maneuvering.

The ATRIUM^{TM} 10XM (A10) fuel assembly design (see also section 4.2) is used in the reference core. In axial steps of about 50 cm, 8 spacers with mixing vanes are used to assure a

wetted rod surface and to distribute the coolant void in the radial direction. The upper half of the fuel assembly has a larger flow area than the lower one, due to the empty rod positions above the part-length rods, which are only present in the lower half of the FA. Part-length fuel rods are used to improve the moderation in the upper highly voided core regions to increase the burnup and to reduce the flow velocity and, thus, the pressure loss. Flow holes in the fuel assembly foot piece regulate the coolant bypass flow fraction to around 11 % during full power operation. The water channel flow fraction is designed to be roughly 3 % of the coolant recirculation flow rate. This results in a remaining active channel flow rate of approximately 12000 kg/s in the major part of the cycle before it is increased stepwise during coastdown to almost 14000 kg/s at EOC. In the outermost FA row of the core, where the power is low, a smaller inlet throttle is used to reduce the active coolant flow fraction through the fuel channel and redirect coolant to the hotter core center, which also induces a more uniform void fraction at the core outlet.

The fresh FAs contain MOX fuel with 65.1 % Pu_{qual} (Pu-vector 1 in Tab. 4.3) with a content of ~4.43 wt% Pu_{fiss} (actual content depends on the gadolinia content and the presence or absence part-length rods) in the fuel. The fresh batch is loaded in the core at the dark blue positions presented in Fig. 6.1 for the equilibrium cycle core layout. One fresh fuel batch consists of 148 FA (37 FA in quarter core), which is divided into three streams with differing burnable poison rod (BPR) setup. Fresh FA with 12 Gd rods with 3 wt% Gd enrichment are introduced in the core center to flatten the core power profile (batch name MH, for MOX with high Gd content), while only 6 Gd rods with 2.5 wt% Gd enrichment are used in the peripheral fresh FA, where the power is generally lower (batch name ML, for MOX with low Gd content). In selected fresh FA positions, the Gd content in the lower FA half is increased to suppress the bottom power peak characteristic for BWR reactors (batch name MM, for MOX with medium Gd content). The fuel matrix in Gd pins consists of low enriched (0.5 wt% ^{235}U) uranium tails accumulated during fuel enrichment.

The applied optimized "super-low-leakage" loading strategy can be seen in Fig. 6.1 with almost three rows of highly burnt and, therefore, low reactivity FA at the core periphery [13]. The unloaded batch of burned FA at the end of the cycle consists of 44 FA with six irradiation periods and 104 FA with 5 irradiation periods. The average discharge burnup at the end of cycle is 51.4 MWd/kgHM.
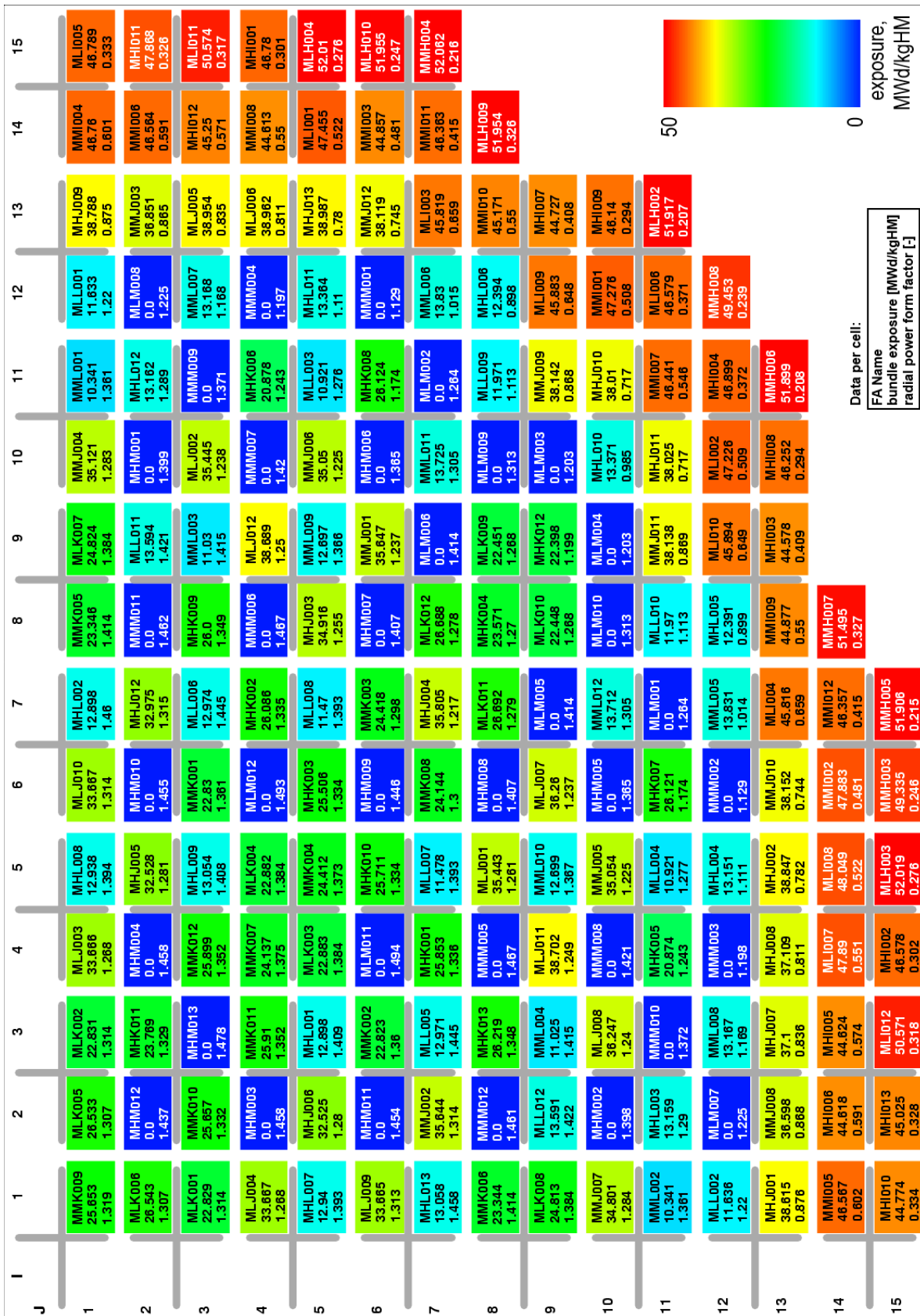
Fig. 6.1: Quarter core layout of the reference full-MOX BWR equilibrium core. Each cell contains FA name, BOC bundle exposure [MWd/kgHM] and radial power form factor. The first two letters MH, MM and ML in the FA name correspond to MOX fuel with high, medium and low gadolinia content, respectively. The third letter is the batch-ID, where later letters of the alphabet refer to younger batches. The FAs in each batch are numbered consecutively.

Loading and re-shuffling patterns are generally optimized iteratively obeying the following rules:

- do not put FA with high reactivity next to each other,
- do not put fresh FA in a control rod cell used to compensate excess reactivity,
- adjust reactivity ranking (switch FA positions) to obtain low radial power form factor,
- achieve low leakage core by putting the least reactive FA to the core periphery and
- if the number of FA per batch has to be changed, a whole set of four FA has to be added or subtracted to maintain the rotational quarter core symmetry.

In the following sections, more detailed results for the full-MOX core design are presented as comparison along with the results for the investigated low moderated core design to quantify safety performance and fuel utilization.

6.3   Investigated low moderated core designs

The development of a low moderated BWR core is an iterative procedure. Changing the geometry influences strongly the operation parameters and various adjustment possibilities exist to achieve a feasible core design. The different low moderated core designs investigated are presented in the following in more detail. The basic approach is to change the reference full-MOX BWR core design step wise to obtain a feasible low moderated core design fulfilling preferably all important operational and safety design criteria. In the current studies it is assumed that the reference BWR core is completely unloaded and freshly loaded only with low moderated MOX FAs, hereby concentrating recycled fuel in one reactor and avoiding challenges resulting from a mixed core loading with conventional UOX or MOX fuel assemblies. The design of a first core is out of the scope of the present studies.

The safety assessment will be presented in subchapter 6.4 while the fuel utilization is discussed in subchapter 6.5. Design parameters for the full-MOX core and the low moderated core designs are summarized in Tab. 6.1 and the fuel assembly parameters are listed in Tab. 6.2. Detailed cycle thermal-hydraulic boundary conditions are plotted in Fig. A.1 to Fig. A.3. In Fig. A.4, the design equilibrium cycle eigenvalue achieved by manual adjustment of the control rods is shown. The variation of the density of the control rods in the core during the cycle is presented in Fig. A.5.

Tab. 6.1 Overview of main core design parameters

		Full-MOX	HC10-1	HC10-2	HC12-1	HC12-2
Core height	cm	371	371	371	230	270
Rated core power	MW	3840	3840	3100	3290	3840
Nominal core power	MW	4000	4000	3100	3290	3840
Batchsize	-	148				
Gd-Design	-	52 high Gd, 48 medium Gd, 48 low Gd bundles				
Maximal CR density	%	5.4	2.1	2.1	4.7	5.1
Fresh FA Pu$_{fiss}$ content	wt%	4.43	5.01	4.53	6.93	6.73
Fresh FA ^{235}U content	wt%	0.27	0.24	0.25	0.24	0.24
Core HM inventory	t	135.34	199.04	199.83	116.16	136.39
HM inv. in fresh FA	kg	176.85	257.89	257.93	151.92	178.34
Pu$_{fiss}$ inv. in fresh FA	kg	7.84	12.92	11.68	10.53	12.01
Av. cycle burnup	MWd/kgHM	9.7	6.6	5.4	9.7	9.6
Av.discharge burnup	MWd/kgHM	51.4	35.2	28.4	51.2	50.9
Cycle length (rel. to rated core power)	efph	8406*	8400*	8400	8400	8400
	efpd	350.25	350	350	350	350
Cycle energy generation	TWh	32.3	32.2	26.0	27.6	32.3
Nominal core flow rate	kg/s	13948	12350	9990	10735	12920
Active flow fraction	%	85.8	88.7	89.2	90.9	90.7
Bypass frac.	%	10.9	11.3	10.8	9.1	9.3
Active flow rate	kg/s	11967	10954	8911	9758	11718
Bypass flow rate	kg/s	1520	1396	1079	977	1202

*corresponds to 337 days at 4000 MW$_{th}$ nominal core power [13]

Tab. 6.2 Fuel assembly parameters

		ATRIUM^{TM} 10XM	HC10	HC12
Rod pitch (P)	mm	> 12.84	12.84	10.70
Rod diameter (D)	mm	10.28	11.44	9.30
P / D	-	> 1.249	1.122	1.151
Cladding thickness	mm	0.62	0.69	0.56
Pellet diameter	mm	8.87	9.87	8.02
Rod to rod gap	mm	> 2.56	1.4	1.4
Moderator to fuel volume ratio (MFR)*	-	2.57	1.55	1.69
MFR with 40 % void in fuel channel*	-	1.92	1.15	1.25
Fuel cross-sectional area*	cm²	56	77	73
Active channel flow area*	cm²	91	76	81
Bypass flow area**	cm²	54	42	42
Heated perimeter	cm	294	359	421
Wetted perimeter	cm	359	411	472
Bundle HM mass for 371 cm length	kg	177	258	246

*value for full lattice including part-length rods **including internal water channel

6.3.1   General design aspects applied to all low moderated core designs

The same quarter core model with 196 radial FA and 24 axial nodes described before is used for the low moderated core designs. Also the control rod (CR) design and the radial core geometry remain unchanged. To reduce the optimization effort, the general cycle design strategy is adapted from the one of the reference full-MOX core:

- cycle length of 8400 equivalent full power hours (350 efpd),
- 148 fresh fuel assemblies per batch,
- 3 streams per batch with low, medium and high Gd content and
- use of the identical reactivity ranking map for refueling and shuffling.

For each core design, the Pu_{fiss} enrichment in the fresh fuel, the core flow rate at end of cycle and the power coastdown are individually adjusted to obtain a critical equilibrium cycle. Most designs have still potential for fine tuning of these parameters but their effect on the general conclusions here is negligible.

The high BOC reactivity of conventional MOX-FA requires the use of burnable poison rods (BPR) in the FAs because otherwise the control rod density in the core would need to be too high and the cold shutdown margin requirements could not be met especially at BOC. Investigations have shown that the higher conversion and the slower decline of reactivity with burnup in low moderated FA diminishes this drawback significantly, making BPR not to an essential requirement. Nevertheless, BPR are used in the low moderated designs to keep the control rod density in the core and the corresponding CR burnup at a minimum.

No changes are applied to the general design of the internals of the reactor pressure vessel and also the model for the lower and upper tie plate of the FA is kept the same. For all FAs in one core design the same axial thermal-hydraulic design is applied. To model the pressure loss of spacers, the loss coefficients of the A10 FA are used as a first approach. In core designs with adjusted core height, the same number of spacers with reduced distance is used. For future detailed thermal-hydraulic studies advanced spacers or possibly wire wrappers have to be considered and investigated in more detail. As in the reference core, the bypass flow is established mainly through artificial flow holes in the foot piece of the FA, but also through various leakage paths in the core support plate (CSP) itself and between the CSP, the fuel support, the lower tie plate (LTP) and the fuel channel. Due to the reduced flow cross-section in the low moderated FA designs and the removal of internal water structures as additional flow paths, the bypass flow fraction is increased, if the same leak flow path resistances are used as in the reference core. To maintain the nominal bypass flow fraction of

approximately 10 %, the flow holes in the FA foot piece of low moderated FA are scaled down (form loss coefficient increased by approximately 3.5), while the remaining leak paths have been found to have a minor influence on the flow distribution and, thus, remain unchanged. The form loss coefficients of the throttle at the bundle inlet are adopted from the full-MOX core design as well as those for lower and upper tie plate (UTP).

6.3.2   Core design HC10-1

The first step in the investigations is to replace the reference fuel bundles with 371 cm long low moderated FA with 10x10 fuel rod lattice. The tightest 10x10 lattice design considered in the FA design studies presented in Chapter 4 (1.4 mm rod to rod gap) is chosen, because it shows appropriate FA-based safety features and conversion properties. The radial geometry parameters of this FA type, denoted below by HC10, are summarized in Tab. 6.2. Compared to the A10, the HC10 has nine more fuel rods replacing the internal water channel of the A10, the fuel rods are thicker than those in the A10 and no part-length rods are used in the HC10.

These modifications lead to a significantly increased core inventory of 199 t compared to the 31 % lower inventory in the reference core of 135 t. Although the average enrichment in a fresh FA don't have to be increased much from 4.43 to 5.01 wt% Pu_{fiss} for this design (both use plutonium with 65.1 % Pu_{qual}), the plutonium inventory in the bundle is increased by 65 %. This increased heavy metal (HM) inventory makes one FA significantly more expensive.

Applying the same BPR strategy (three streams with low, middle and high Gd content) and loading pattern as for the reference core, a very low maximal CR density in the whole cycle of 2.1 % can be achieved. The required BPR content in the three streams of this design is significantly lower than in the reference assembly due to the reduced excess reactivity in the low moderated fuel. The exact Gd content per stream is shown in Tab. A.2.

The nominal core power is set to the uprated reactor power of 4000 MW_{th} as in the reference core resulting in the same volumetric core power density. Due to the increased HM inventory (+31 %), the HM mass specific power density is decreased accordingly and cycle and discharge burnup (6.6 and 35.2 MWd/kgHM, respectively) will inevitably be lower than in the full-MOX BWR core.

To remove the generated heat from the reactor core without significant increase of the exit void content compared to the reference core, the active core coolant flow rate has to be

comparable in both cases. Due to the tighter fuel rod lattice, the core pressure loss is increased at BOC by 1.41 bar to 3.27 bar and at EOC by 1.56 bar to 3.77 bar. The higher EOC pressure loss is caused by the flow rate increase at EOC which is adjusted similar to the one of the full-MOX core. The pressure loss during the cycle is illustrated in Fig. A.6. The core average void content depicted in Fig. A.7 and Fig. A.8, as well as, the maximal local exit void content shown in Fig. A.9, are increased negligibly by 0.5 % in the HC10-1 core in comparison to the reference core.

Core design HC10-1 is only practicable with design changes of the core recirculation pumps and the core support structures because of the strongly increased pressure loss. The low discharge burnup caused by the low power density has potential for improvement.

6.3.3   Core design HC10-2

The geometrical core design and, thus, the core HM inventory of case HC10-2 are identical to case HC10-1. The primary design goal for core HC10-2 is to achieve a reduction of the high pressure loss with a lower flow rate. It can also be achieved by reducing the coolant density, but since this deteriorates the conversion ratio, the coolant density distribution in the core is kept approximately constant. For case HC10-2, the power and flow rate are both reduced iteratively to obtain a core pressure loss below 1.9 bar at BOC and below 2.3 bar at EOC (with core flow rate increase during coastdown) as in the reference core. To achieve this, the nominal flow rate and nominal core power are reduced by 27.5 % and 22.5 %, respectively. Then, the axial coolant void profile and the local exit void fraction can be maintained similar as in the reference and HC10-1 core design.

With the constant cycle length of 350 efpd and the lower rated core power of 3100 MW_{th} (1 efpd = 3100 MWd instead of 3840 MWd as in the reference core) the discharge exposure is 28.4 MWd/kgHM. The generated energy during the one-year cycle is decreased according to the lower rated power from 32.3 TWh to 26.0 TWh. The average fresh fuel enrichment can be reduced to 4.53 wt% due to the lower power output but the fissile Pu content in a fresh FA is still about 49 % higher than in the 4.43 % enriched conventional MOX FA. With the selected fuel assembly enrichment, reloading strategy and cycle length, no coastdown is necessary. This has no significant influence on this study and could easily be changed by slightly reducing the fuel enrichment.

The BPR design for this core, shown in Tab. A.3, is directly adopted from core HC10-1. The lower reactivity in core HC10-2 in comparison to the reactivity in core HC10-1 leads to

extremely low control rod requirement especially at BOC. After 40 days almost all CR are withdrawn from the core as shown in Fig. A.5. To improve the core design HC10-2, the number of BPR could be slightly reduced to have more excess reactivity during the first quarter of the cycle and thereby gain more flexibility. In general it is preferable to have at least some CR partially inserted in the core for better reactivity control because of the low reactivity worth of CR in the upper and lower core periphery.

Although this core design appears feasible with the reduced pressure loss, major drawbacks are first of all the increased HM inventory in the core inducing higher fabrication costs, larger fuel amount to recycle and decreased burnup and secondly the reduced thermal core power implies less generated electrical power output and, thus, reduced plant profitability.

6.3.4   Core design HC12-1

In design HC12-1 the disadvantage of low burnup for cases HC10-1 and HC10-2 is compensated by a significant HM inventory reduction. For the HC10 bundle this could be achieved by a core height reduction of about 31 % for a target core power of 4000 MW_{th} (core height derived from fresh bundle masses and reference core height: 177 kg/258 kg*371 cm = 255 cm). This would result in a heavy metal mass specific power density as in the reference core and 46 % higher volumetric power density making a FA design with more fuel rods necessary to assure LHGR margins.

Therefore, the HC12 bundle design with 12x12 fuel pins is utilized for this case (see chapter 4, case 4). In comparison to the HC10 bundle, it has slightly decreased fuel cross-section area and an increased active flow area, which is favorable for the pressure loss but due to the better moderation disadvantageous regarding the conversion ratio. The thinner fuel rods have a diameter of 9.3 mm. Using the HC12 bundle and a target core power of 4000 MW_{th} would only require a core height reduction of 28 % (core height derived from fresh bundle masses and reference core height: 177 kg/246 kg*371 cm = 267 cm) to obtain the reference specific power density and burnup. Taking into account the expected pressure drop increase as observed in case HC10-1, power and flow rate reduction have to be considered. Assuming a power reduction of 22.5 % as for case HC10-1 would result in a corresponding additional core height reduction (core height of 207 cm) to achieve the reference discharge exposure. However, scoping studies have shown that friction loss increase is not as strong as for core design HC10-1 due to the shorter core height and the enlarged flow cross-section. Power

reduction to 3290 MW$_{th}$ and additional core height reduction to a final core height of 230 cm are sufficient to achieve the target discharge exposure of 51.2 MWd/kgHM.

The corresponding reduction of HM inventory to 116 t and the increased neutron leakage due to the increased core surface to volume ratio (advantageous for void reactivity coefficient) requires increasing the fissile plutonium content in the bundles to an average value of 6.93 wt%. In comparison to the full-MOX core, this is a 34 % higher amount of plutonium per fresh bundle. Additionally the maximal Pu$_{fiss}$ content in the center fuel rods with the highest enrichment level of this design is very high with 11.45 wt% resulting in pin plutonium content of 17.6 wt% (65 % plutonium quality). This can in principle be handled by the existing manufacturing processes (at least on lab scale) and the bundle average plutonium content of 10.7 % is kept below the recommended level of 13 % (see chapter 2.4). However, current industrial facilities for fuel recycling probably have to be improved.

Due to the smaller rod diameter, the number of BPR and the gadolinia content in the BPR in fresh fuel is increased to bind appropriate amount of excess reactivity (cp. Tab. A.4) and model the equilibrium cycle with very similar control rod demand as in the reference core design shown in Fig. A.5. The maximal exit void fraction is similar to the already presented cores by design but the core average void content is reduced e.g. at BOC from 44 % to 40 % because of the shorter core height and, thus, increased weight of the lower core part with subcooled coolant for core averaging. The pressure loss in this design is even lower than in the full-MOX core (1.66 bar at BOC and 1.95 bar at EOC) indicating some potential for power and flow increase, although the fuel enrichment would have to be further increased. Alternatively, only the coolant flow rate could be increased to improve the heat removal and give better safety margin against boiling transition.

Major drawback of core design HC12-1 is the reduced power output of 27.6 TWh during one cycle at normal operation and the potential safety penalties due to the high plutonium content in the fuel.

6.3.5 Core design HC12-2

The final core design HC12-2 utilizes a core height of 270 cm (height of 267 cm determined in last section rounded up) to obtain the core heavy metal inventory of 136 t as in the reference core and to achieve a target discharge burnup of around 51 MWd/kgHM. Using the reference rated power of 3840 MW$_{th}$ together with the reference cycle length of 8400 efph

results in a discharge burnup of 50.9 MWd/kgHM and cycle energy generation of 32.3 TWh equal to the full-MOX core.

The increased pressure loss in the tighter lattice limits the nominal operation power to 3840 MW$_{th}$ (4000 MW$_{th}$ in reference core design). To avoid the strong pressure drop increase at end of cycle, the coolant flow rate increase is omitted in this core design leading to core pressure loss below 2.42 bar during the whole cycle. Maximal local exit void content and core average void content are almost identical as for case HC12-1.

Fresh fuel enrichment of 6.73 wt% Pu$_{fiss}$ is required in this core design and the corresponding fissile inventory in fresh fuel bundles is, thus, 53 % larger as in the conventional MOX FA used in the reference core. The required higher enrichment is disadvantageous in a once-through fuel cycle but has to be viewed in the context of multi-recycling. Due to the increased conversion ratio a higher overall-use of initial uranium is achieved.

The gadolinia rod design for the three fuel streams summarized in Tab. A.5 is adopted directly from core design HC12-1 and the resulting control rod density in the core during the cycle is almost identical in both designs and lower than in the reference full-MOX core.

This core design represents the best compromise between slight core power reduction to reduce the larger pressure loss in the tighter fuel lattice and adequate fuel burnup.

6.4 Steady state safety-related investigations

6.4.1 General parameters

The major safety related differences in the core designs introduced in the last chapters are found in the void reactivity coefficient (VC) and the stuck-rod cold shutdown margin (CSDM). Tab. 6.3 shows a comparison of safety parameters for all designs. The core average void content and exit void content are similar by design (see Fig. A.7 and Fig. A.9), but the core average void content is slightly decreased in the shorter HC12 cores. This decrease is caused by a slightly lower average exit void fraction (e.g. 0.715 in HC10-1 and 0.695 in HC12-2) and the stronger influence of the lower core region with subcooled coolant. The differences in the axial void fraction shape can be seen in Fig. A.8. The maximal linear heat generation rate (LHGR) depicted in Fig. A.12 is smaller in the low moderated cores than in the reference core. This is due to the increased number of rods in the bundle designs and the lower nominal power in some core designs, which both results in a smaller specific power per

rod. Radial (f_{rad}) and axial peaking factors (f_{ax}) are comparable and have still some potential for optimization (see Fig. A.10 and Fig. A.11). The Doppler reactivity coefficient (DC) is slightly increased due to harder neutron spectrum and corresponding reduced resonance escape probability (see Fig. A.15). A reduction of the power reactivity coefficient (PC) can be observed which correlates with the void coefficient discussed in more detail below (see Fig. A.16). Investigation of the isothermal temperature coefficient (ITC) in all low moderated core designs is promising. The ITC has been evaluated to change its sign for temperatures below 150 °C in all core designs and the four core states (BOC and EOC core with zero and maximum xenon concentration in each). The sign change appears at about 40 °C lower temperatures for xenon free cores than for high xenon concentrations. Detailed results are included in Fig. A.17 to Fig. A.20.

Tab. 6.3 Cycle maximal values of selected parameters for different core designs

		Full-MOX	HC10-1	HC10-2	HC12-1	HC12-2
Average void content	%	44.3	44.90	44.00	41.40	42.10
Max. bundle exit void content	%	85	86.1	86.2	85.8	86.5
LHGR	W/cm	399	370	272	326	317
f_{rad}	-	1.494	1.471	1.45	1.507	1.512
f_{ax}	-	1.271	1.341	1.340	1.308	1.294
DC	pcm/K	−2.28	−2.60	−2.69	−2.70	−2.72
PC	pcm/MW	−1.15	−0.80	−1.07	−0.70	−0.58
Limiting Temperature for sign change of ITC	°C	-	120	120	140	150

6.4.2 Void reactivity coefficient

As explained in 6.1.4 there are different methodologies available in MICROBURN-B2 to determine the void reactivity coefficient (VC). The variation of one of the three thermal-hydraulic boundary conditions flow rate, inlet enthalpy, and exit pressure will result in different void distribution change and corresponding reactivity effect. The approach to vary the enthalpy of the coolant at the core inlet leads to comparable results as changing the core coolant flow rate: the VC is reduced but still clearly negative. As shown in Fig. 6.2, the VC for the low moderated cases is between −30 and −60 pcm / %-Void change, compared to around −80 pcm / %-Void change in the reference full-MOX core. For the full-MOX and the HC10 core designs the VC is predicted about −10 pcm / %-Void smaller if it is determined by flow variation as presented in Fig. A.13. Interestingly, the VC is predicted to be about 5 pcm / %-Void higher for the HC12 cases when it is determined with flow rate variation instead of inlet enthalpy variation.
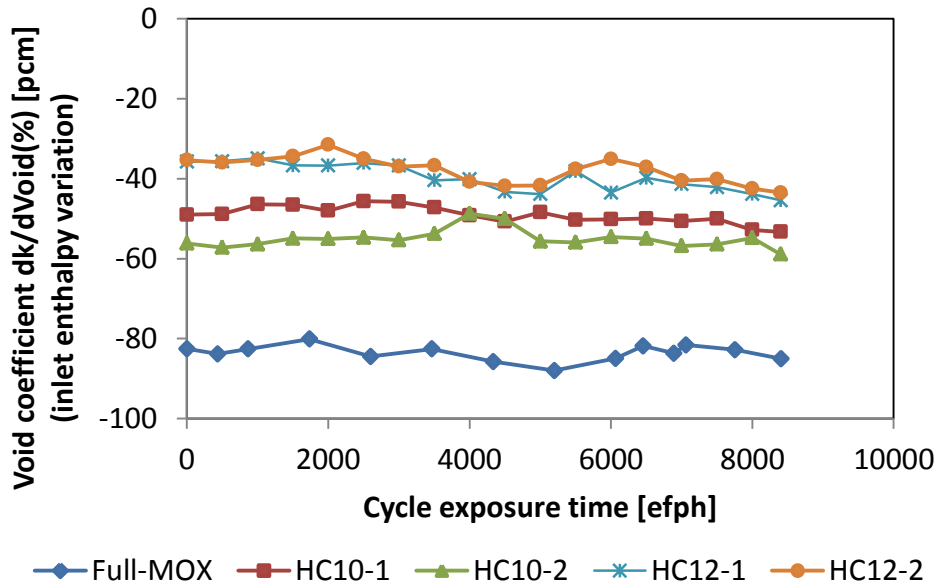
Fig. 6.2: Coolant void reactivity coefficient determined with inlet coolant enthalpy variation during equilibrium cycle as function of exposure time

If the VC is determined by varying the core pressure, smaller but still negative values are obtained for the full-MOX core (−55 to −60 pcm / %-Void) and core designs HC10-1 and HC10-2 (−25 to −35 pcm / %-Void) as shown in Fig. A.14. For the core design HC12-1 and HC12-2, values around unity are obtained (+10 to −10 pcm / %-Void). A closer look on the calculation results for the two HC12 core designs reveals inconclusive results for the VC obtained with pressure variation. Changing the sign of a small pressure variation leads to a predicted VC with unchanged sign and positive or negative VC depends, therefore, on the calculation procedure. Additionally the default pressure variation used in MICROBURN-B2 to calculate this VC is with 10 % of the nominal pressure quite large and the small effect on k_{eff} is in the range of the numerical error. Therefore, no distinct conclusion can be drawn from this calculation. The phenomenon should be further investigated in full-core calculations for relevant transients with pressure variation.

6.4.3 Stuck-rod cold shutdown margin

One very interesting effect observed for the low moderated designs is the strong improvement of the stuck-rod cold shutdown margin (CSDM) from −1.5 % at BOC in the MOX core to less than −4 % at BOC in all low moderated cores as it is presented in Fig. 6.3 as function of the cycle exposure for the equilibrium cycle. It is determined as the relative difference of k_{eff} to the selected value of $k_{target} = 0.991$ (see section 6.1.4). It has to be kept in mind that this value for k_{target} is only a preliminary assumption and can be wrong both for the

full-MOX as well as for the low moderated core designs. The actual bias of the computed to the real eigenvalue can only be determined from comparison of computation and measurements in a real core usually done during startup (see discussion in section 2.2.3). The wave like appearance of the CSDM in Fig. 6.3 is caused by the varying control rod insertion during the cycle (see Fig. A.5)
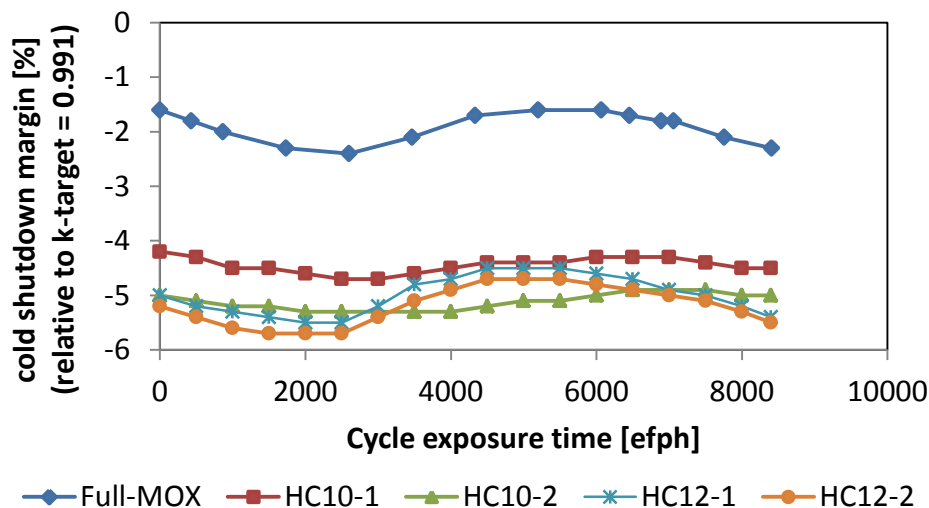
Fig. 6.3: Stuck-rod cold shutdown margin during equilibrium cycle as function of exposure time.

   In modern Gen-II BWR core designs usually the upper part of the reactor core dominates the CSDM behavior. Small changes in this part like changing the gadolinia design can affect the CSDM strongly. The upper half of the reference BWR core design is especially characterized by empty rod positions due to part-length rods enhancing the moderation increase between highly voided nominal and cold core conditions. In the low moderated core designs no part-length rods are used and the effect of moderation increase can be assumed to be less pronounced. The individual factors influencing the improvement of the CSDM results differ in strength in the investigated core designs. These factors have been analyzed in more detail at begin of cycle (BOC) in all core designs by separating step-by-step the single reactivity effects between the nominal hot full power (HFP) core state with equilibrium xenon concentrations and all rods out (ARO) of the core and the shutdown cold zero power (CZP) xenon free core state with all rods in (ARI) except for the most reactive one which is stuck outside of the core. In Fig. 6.4 and Fig. 6.5 the k_{eff} values for the different cores and conditions of this study are illustrated and the individual effects will be explained in the following. The exact values corresponding to the figures are additionally summarized in Tab. A.6.
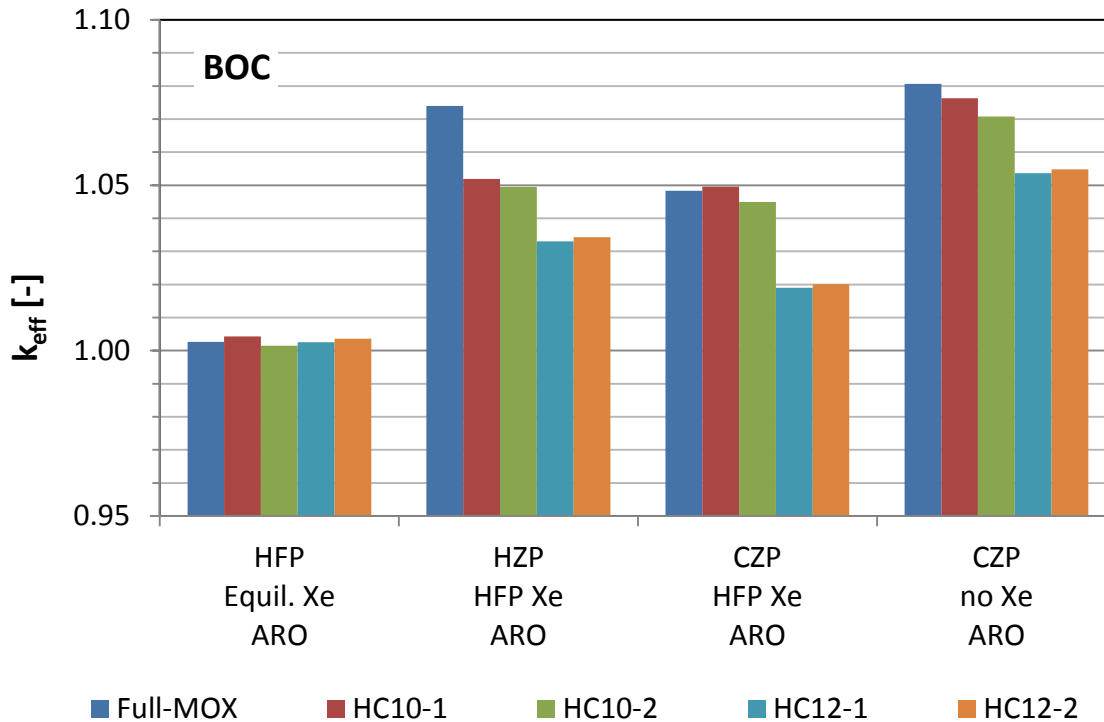
Fig. 6.4: Comparison of the core k_{eff} at begin of cycle (BOC) for different core states from the nominal hot full power (HFP) operation conditions with all rods out (ARO) and equilibrium xenon concentrations to the cold zero power (CZP) condition with ARO and without any xenon.

At BOC a small fraction of CRs is inserted in all cores to compensate the excess reactivity and to obtain critical conditions. The first data set included in Fig. 6.4 shows the core effective eigenvalue at nominal HFP core condition, with voided coolant (average void fraction larger than 0.40 in all cores), equilibrium xenon concentration in the core (although xenon builds up during the first days it is considered to be in equilibrium at BOC in the calculation), and CRs in ARO position. The second data set shows the obtained core k_{eff} if the core is set to an isothermal temperature of 260°C and is used here as intermediate hot zero power (HZP) condition between HFP and CZP. This temperature is slightly below the actual hot zero power operation conditions of 285°C but it is the largest temperature that can be used by MICROBURN-B2 to do an isothermal calculation without explicit thermal-hydraulic calculation. In the third and fourth data set the computed k_{eff} at an isothermal temperature of 20°C representing CZP is shown. In data sets 2 and 3 the equilibrium xenon concentrations in the HFP core are used to obtain k_{eff} and in data set 4 all xenon is removed from the cores.

Comparison of data sets 1, 2 and 3 in Fig. 6.4 for the full-MOX core shows a strong under moderation at HFP compared to much better moderation at HZP ($dk_{eff} = k_{eff,HZP} - k_{eff,HFP} = +0.071$) turning into over moderation at CZP ($dk_{eff} = k_{eff,HFP} - k_{eff,CZP} = -0.026$). The large difference between the HFP and HZP result comes mainly from the void decrease from

~ 45 % to 0 % and the negative void reactivity coefficient but also from the fuel temperature decrease and the corresponding negative Doppler reactivity effect. The difference between HZP and CZP is caused by the increasing moderator density and the fuel temperature decrease due to the temperature reduction. The value of $dk_{eff} = +0.071$ between HZP and CZP seems too large if the reactivity coefficients are assumed to be constant (approximately $+0.04$ due to void change and $+0.01$ due to fuel temperature change) but can be explained by their non-linear behavior. It was observed e.g. in [13] that the void reactivity coefficient becomes more negative for decreasing void content in the BWR core. The inverse proportionality of the Doppler reactivity coefficient to the square root of the fuel temperature is well documented in open literature (see section 2.2.6).

The coolant conditions at which the change from under to over moderation appears is strongly dependent on the amount of inserted CRs which cause significant moderator displacement. A comparison of k_{eff} between HZP and CZP with ARI instead of ARO and HFP equilibrium xenon concentration shows for example a difference in k_{eff} of less than -0.001 instead of -0.026. The xenon concentration in the core additionally affects the change which was shown in the ITC assessment in section 6.4.1. Computing dk_{eff} between HZP and CZP in a xenon free core with ARI results even in a positive difference of $+0.008$. This result agrees with the value shown in the ITC assessment for a similar full-MOX core design in [12] which was done for xenon free core states with CZP critical CR pattern with approximately 80 % CR-density in the core resembling closely ARI conditions.

For the HC10 core designs the HFP to HZP difference in k_{eff} is significantly reduced to approximately $+0.048$ compared to $+0.071$ in the reference core design mainly due to the reduced void reactivity coefficient. This effect is even stronger for the HC12 than for the HC10 core designs ($+0.03$) because the VC is even lower. Transition from HZP to CZP has a similar but less pronounced over moderation effect in the HC12 core designs compared to the full-MOX core (-0.014 compared to -0.026). In the HC10 cores, there is almost no over moderation effect observable between HZP and CZP (-0.002 and -0.005 in core design HC10-1 and HC10-2, respectively). The reduced over moderation effect can be explained with the lower moderator to fuel ratio in the HC12 lattice compared to the ATRIUM^{TM} 10XM FA, which is even lower in the HC10 lattice.

The temperature below which the core becomes over moderated can be approximately determined with the sign change of the ITC summarized in Tab. 6.4 for the investigated core designs with xenon free core at BOC (see section 6.1.4 for discussion of results for the ITC

and Fig. A.17 to Fig. A.20 for the ITC as function of the isothermal core temperature for different core states in the four low moderated core designs). In core design HC10-1, the ITC changes its sign at the lowest temperature of 66 °C and the corresponding over moderation observed between HZP and CZP in Fig. 6.4 is very low. As the temperature for the ITC sign change in the remaining core designs increases, the over moderation effect at CZP gets stronger.

Tab. 6.4 Temperature sign change of ITC in xenon free core at BOC for different core designs. The applied control rod pattern in each core is individually adjusted to obtain a critical core at CZP.

		Full-MOX	HC10-1	HC10-2	HC12-1	HC12-2
Temperature for sign change of ITC in xenon free core at BOC	°C	~140	66	82	99	93

Based on the comparison of data sets 3 and 4 in Fig. 6.4 it can be stated that the xenon worth $(dk_{eff} = k_{eff, \text{HFP equil. Xe}} - k_{eff, \text{no Xe}})$ in the core designs HC10-1 and HC10-2 is reduced from -0.032 in the full-MOX core to -0.027 and -0.026, respectively. In both HC12 cores, the xenon worth is slightly larger than the one in the full-MOX core (-0.035 dk_{eff}). The xenon worth is comparable in all core designs and the small differences result from deviations in the moderation, the power density and the geometry (self-shielding in fuel rods).

The xenon free CZP effective core eigenvalues for the different core designs with different CR pattern are shown in Fig. 6.5. Data sets 1, 2 and 3 show k_{eff} with ARO, with ARI assuming stuck rod and with ARI, respectively.

The worth of all rods except the stuck rod ($dk_{eff} = k_{eff,\text{stuck-rod}} - k_{eff,\text{ARO}}$) is the smallest for the full-MOX core (-0.105). Its absolute value is about 0.01 larger for the core designs HC12-1 and HC12-2 with values of -0.114 and -0.115, respectively. For the HC10-1 and HC10-2 core design, the reactivity worth of the CRs is further improved to -0.129 and -0.132, respectively. Since the insertion of CR combines the effect of absorber insertion and moderator displacement, it is difficult to quantify the single effects. The lower the MFR in the core is, the stronger is the moderation displacement effect of inserting the CR. Therefore, the moderation reduction is the strongest in the HC10 core designs and the weakest in the reference core. The deterioration of the reactivity worth of the CR absorbers in the low moderated core designs may not be very strong because of the unchanged water gap outside of the fuel channel where the thermal neutron flux can recover. To quantify the individual moderator displacement effect on the reactivity, CR without absorber materials can be used in further studies.
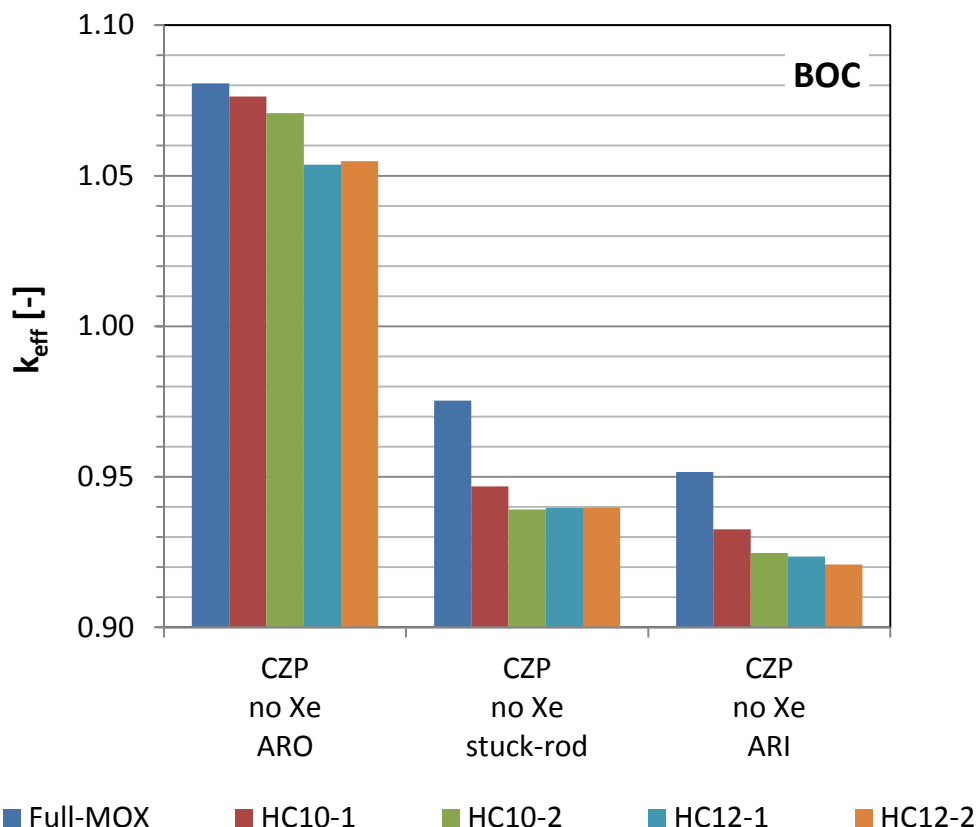
Fig. 6.5: Comparison of the core k_{eff} at BOC for the xenon free core with different control rod positions all rods out (ARO), all rods in (ARI) except for the most reactive CR stuck outside of the core, and ARI.

Interestingly, by comparing data sets 2 and 3 in Fig. 6.5 the stuck-rod (same rod in all core designs) shows to have the smallest worth in the HC10 core design and the largest worth in the full-MOX BWR core. Since the worth of the most reactive CR depends strongly on local factors like loading pattern and burnable poison design and the worth of all rods is a global parameter, this does not necessarily contradict the already obtained results. For the CSDM, only the reactivity worth of ARI except for the stuck rod is relevant.

In summary, the increased CSDM results on the one hand from the smaller excess reactivity released in the low moderated core designs between HFP with equilibrium xenon concentrations and CZP xenon free core conditions with ARO (dk_{eff} = 0.072, 0.069, 0.051, and 0.051 in the core designs HC10-1, HC10-2, HC12-1, and HC12-2, respectively, compared to dk_{eff} = 0.078 in the reference core design). On the other hand, the CSDM is increased by the higher CR worth with stuck rod out in the low moderated core designs (dk_{eff} = −0.129, −0.132, −0.114, and −0.115 in the core designs HC10-1, HC10-2, HC12-1, and HC12-2, respectively, compared to dk_{eff} = −0.105 in the reference core design). The increased CR worth is mainly caused by the larger relative moderator displacement in the low moderated

core designs especially in the upper half of the core which is characterized only in the reference core by empty rod positions due to the use of part-length fuel rods.

6.5 Assessment of fuel utilization

After demonstrating the general neutronic feasibility of the investigated low moderated core designs in the last sections, now the fuel utilization will be assessed. The characteristic parameters for all investigated core designs are summarized in Tab. A.7. In addition, core average values for Pu_{fiss} enrichment and content and Pu_{tot} content in the core for begin and end of cycle are included as well as the plutonium consumption.

6.5.1 Fissile inventory ratio

The conversion ratio used on fuel assembly level to quantify the fuel utilization is, however, difficult to compute on full-core level because the isotopic reaction rates are not available after homogenizing cross-sections per FA. Instead, the fissile inventory ratio (FIR) quantifying the conservation of fissile inventory in the core relative to begin of the cycle can be used. The FIR as function of exposure for one cycle is shown in Fig. 6.6 for the different core designs. Better comparison of the designs varying in size and core power is ensured by using total generated power in units of TWh as time scale instead of equivalent full power hours which depend on the nominal core power.
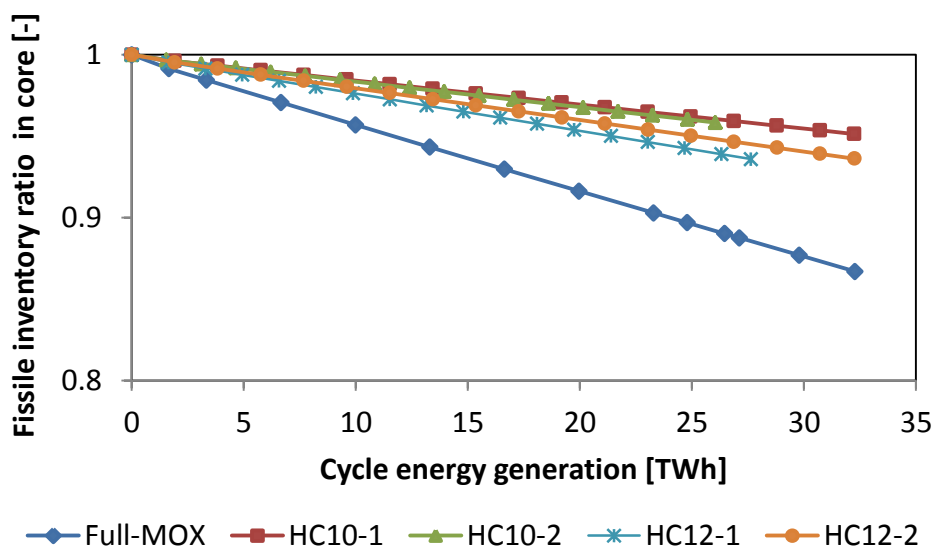
Fig. 6.6: Fissile plutonium inventory ratio (instantaneous value relative to begin of cycle value) during equilibrium cycle as function of generated energy.

It can be observed that all low moderated core designs are characterized by a moderate decrease of FIR during the cycle compared to the reference full-MOX core. This is the main motivation for the development of a low moderated BWR. The best fuel utilization is achieved in the HC10-1 core design (FIR = 0.951 for 32.3 TWh generated energy) with the lowest moderator to fuel ratio. Compared to core HC10-1, the FIR in core HC10-2 has only slightly more negative gradient but it is still slightly higher at EOC due to the lower burnup and cycle length (0.958). Because the MFR in the core design HC12-2 is higher than in the HC10-1, the end of cycle FIR is reduced to 0.936. Due to the shorter core height and the increased enrichment in core HC12-1 compared to core HC12-2, the FIR in core HC12-1 shows the steepest decline among the low moderated core designs. However, both HC12 core designs have the same fissile conservation at EOC.

6.5.2 Consumption of fissile plutonium

The low moderated core designs are characterized by a lower net consumption of fissile plutonium during one cycle in comparison to the reference full MOX core as can be observed in Fig. 6.7. There the plutonium consumption is presented as function of exposure for the reference core and the four investigated low moderated core designs.
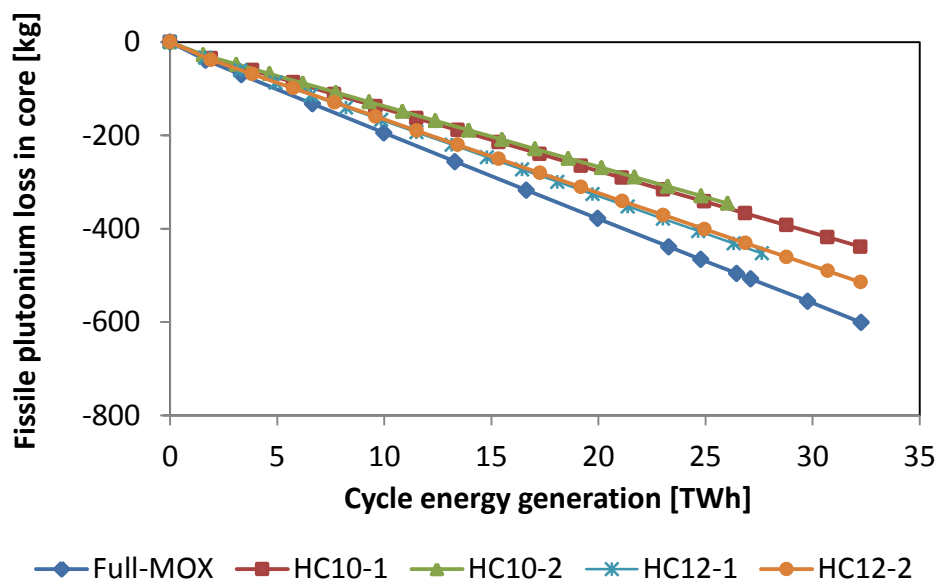
Fig. 6.7: Fissile plutonium consumption during one cycle as function of generated energy.

The reason for it is the effect of a harder neutron spectrum and better conversion ratio leading to a reduced slope for the HC10 and HC12 core designs compared to the full-MOX core. The net consumption of fissile plutonium of −601 kg in the references core is reduced by around 15 % to −515 kg for core HC12-2 and by more than 25 % to −439 kg for the HC10-1 core.

The improvement in fuel utilization in core HC10-2 relative to the full-MOX core is comparable to that one in core HC10-1 if they are compared at the exposure of 26 TWh for EOC of core HC10-2. For core design HC12-1, a similar observation can be made if it is compared to the HC12-2 design.

6.5.3   Discharge plutonium quality

Besides the obvious reduction in fissile plutonium consumption in a low moderated reactor core, another important advantage is the high discharge plutonium quality (Pu_{qual}; fissile fraction in plutonium) of such cores. This can be seen in Fig. 6.8, where the batch average Pu_{qual} in the batches 1 to 6 of the individual core designs is shown. The batches 1 to 5 consist of 148 FA, while batch 6 contains only 44 FA. Fresh fuel has a Pu_{qual} of 65 % in all cores.
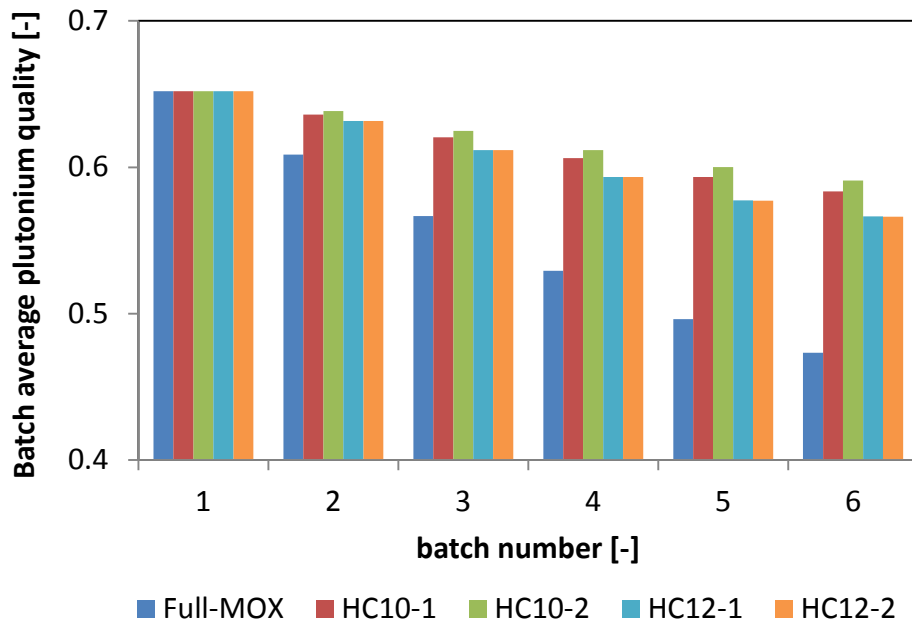
Fig. 6.8: Batch average plutonium quality in all batches of different core designs. Batch 1 (fresh fuel) to 5 consist of 148 fuel assemblies. Batch 6 contains 44 fuel assemblies.

The significantly slower reduction of the Pu_{qual} in the low moderated cores can already be observed after one cycle in batch two. In the reference core design, the Pu_{qual} of 65 % in fresh fuel is reduced to around 47 % in batch 6. In the investigated low moderated BWR cores, the BOC Pu_{qual} of 65 % is reduced only to values between 59 % (HC10-2) and 56 % (HC12-2). Since secondary recycling of MOX fuel with low Pu_{qual} is technically challenging because of criticality safety, radiation and high heat load (cp. chapter 2.4), the higher discharge Pu_{qual} is an important advantage of the low moderated core designs making a second fuel recycling more feasible. Additionally, the second generation MOX fuel fabricated from recycled MOX

fuel with low Pu_{qual} would require very high total plutonium content leading to a significant degradation of the reactivity coefficients. The second generation plutonium could for example be used in a full-MOX BWR core as described in [12]. There, feasibility of full-MOX BWR cores could be demonstrated even with plutonium qualities as low as 50 % in fresh fuel.

6.5.4 Remarks on fuel cycle economics

The increased recycling effort for higher HM inventory in the core designs HC10-1 and HC10-2 is an important factor for the economic viability but it is not relevant for the fuel utilization in the reactor itself. Nonetheless, since the discharge burnup in these two low moderated cores is strongly reduced compared to the one of the reference core, it can be assumed that the fuel cycle costs will increase.

Because of similar HM inventory and identical burnup in fuel discharged from the reference core and the two HC12 core designs, a similar amount of fuel has to be handled in an assumed second recycling. However, more plutonium has to be processed during recycling due to the higher enrichment in core designs HC12-1 and HC12-2 compared to the reference core design.

Due to the high uncertainties in costs for individual steps during recycling it is difficult to predict the fuel cycle costs accurately. For multiple recycling of plutonium, the costs will likely increase if higher heat loads have to be handled or shielding has to be improved in manufacturing facilities. A detailed assessment of fuel cycle economics is not in the frame of this work, but should be subject of follow-up studies.

7 Thermal-hydraulic analysis of selected low moderated fuel assemblies with SUBCHANFLOW

7.1 Goal

In the frame of core design analysis of LWR also local safety criteria have to be assessed to ensure sufficient safety margins to non acceptable operational regimes. In BWR, especially the critical power ratio (CPR) determining the margin to boiling transition has to be determined. For presently used fuel assembly designs, empirical correlations obtained from experimental investigations can be utilized to determine the CPR in each FA from average TH conditions with numerical codes. However, for the development of new designs, FA specific CPR correlations are not available a priori and hence preliminary design studies have to be done on more detailed geometry resolution using the most appropriate available correlations. The sub-channel code SUBCHANFLOW is used to perform the thermal limit assessment of the reduced moderator BWR FA designs proposed using the more general correlations for heat transfer and critical power implemented there. SUBCHANFLOW also predicts the fuel rod centerline and cladding temperature, the FA pressure drop and the void fraction among other thermal hydraulic parameters that permit the evaluation of the FA designs.

7.2 Methodology

The sub-channel analysis of FAs (or reactor cores) needs both geometrical data of the FA and thermal-hydraulic boundary conditions at the inlet (mass flow rate, coolant temperature) and outlet (pressure) of the FA. In addition, the 3D power distribution in the FA has to be provided as well as the temperature-dependent thermo-physical properties of the materials (fuel, gap, and cladding) for the mathematical solution of the heat conduction problem. Based on the fuel rod lattice, the fluid domain is subdivided into sub-channels as shown in Fig. 7.1 for a representative part of a BWR fuel assembly inside the fuel channel.
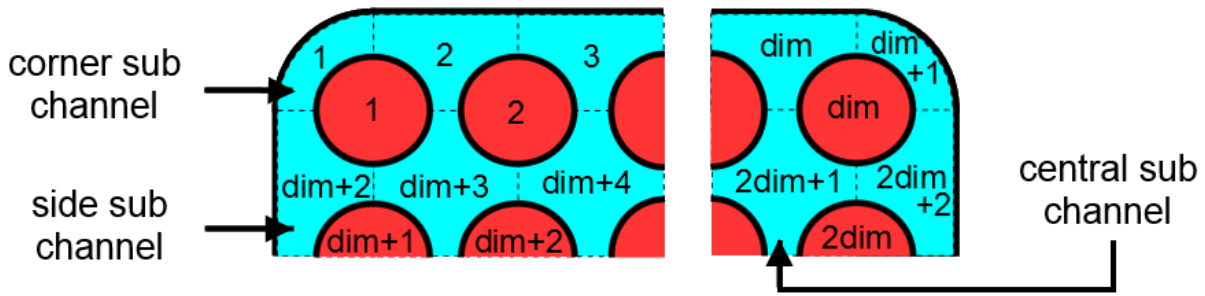
Fig. 7.1: Schematics of enumeration of sub-channels and fuel rods in SUBCHANFLOW for a fuel lattice with dim*dim fuel rods surrounded by a fuel channel box with rounded corners and indication of the three appearing sub-channel types. Only a fraction of the whole FA is shown.

The dimension of the fuel rods, their position in the lattice and the geometry of the surrounding fuel channel wall are used to derive important thermal-hydraulic parameters for each individual sub-channel. These parameters include flow area, heated and wetted perimeter, gap width between fuel rods, flow paths to neighboring sub-channels, and distance of the current sub-channel center to neighboring sub-channel centers. In addition, individual local form losses can be entered for each sub-channel and axial level to model e.g. spacer grids or the FA tie plates. Since all fuel rods of one fuel bundle are arranged in a square lattice surrounded by a fuel channel box, there is no cross-flow between neighboring fuel assemblies in a BWR. They are thermal-hydraulically coupled only via the lower and upper plenum and leak paths to the bypass at the lower and upper end of the FA. Therefore, single BWR FA can be investigated individually if the thermal-hydraulic boundary conditions at inlet and outlet are provided.

The geometrical dimensions of the investigated low moderated FA are fixed by the previous neutron physical design studies which also dictate the thermal-hydraulic boundary conditions and 3D pin power distribution. It is possible to simply define an axial power shape in SUBCHANFLOW and superimpose a radial pin power profile. However, for this study the pin power reconstruction method is used in MICROBURN-B2 to determine a more realistic 3D pin power profile in each FA. The number of axial nodes used in the SUBCHANFLOW for this study is 24 for compatibility with the neutronic core model of MICROBURN-B2. In this way e.g. power distributions can easily be transferred between both codes. Standard thermo-physical properties for MOX fuel and Zircaloy cladding are included in SUBCHANFLOW. For the fuel rod gap conductance, a conservative value of 6000 W/m²K is used.

Besides the problem specific input like geometry and material data, different correlations and models to determine two-phase flow domain, coolant void fraction, pressure drop, heat

transfer and the critical heat flux (CHF), etc. are available. For this study, the correlations summarized in Tab. 7.1 are selected, which give good results for two-phase flow applications based on former experience [89]. The chosen equal volume turbulent mixing model includes a void drift model, for which the recommended void drift coefficient of 1.4 is selected. In addition, three different correlations (EPRI, BIASI, BARNETT) implemented in SUBCHANFLOW for the prediction of the CHF, which are relevant for the TH operating conditions and geometries of BWR, are validated using experimental data of the OECD BFBT benchmark and used to assess the CPR in the selected low moderated FAs.

Tab. 7.1: Overview of empirical correlations and models selected in SUBCHANFLOW for the present investigations.

Subcooled void	Bowring
Boiling void	Chexal-Lellouche
Two-phase friction	Armand friction
Turbulent friction	Blasius
Heat transfer	Dittus-Boelter
Critical heat flux (CHF)	EPRI, BIASI, BARNETT
CHF shape factor	no power profile correction
Fuel rod gap model	simplified
Lateral transport model	Rogers-Rosehart
Turbulent mixing model	Equal volume exchange

The CHF is determined for each connected pair of fuel rod and sub-channel from the TH conditions in the sub-channel by the empirical correlations. Its ratio to the actual heat flux from the fuel rod to the coolant in the sub-channel is called critical heat flux ratio (CHFR; see chapter 2.3.3). For each fuel rod connected to multiple sub-channels SUBCHANFLOW determines the minimal value of this ratio. The absolute minimum in the FA is called minimal critical heat flux ratio (MCHFR). The relevant boiling transition safety criterion in BWR is the critical power ratio (CPR), which is determined iteratively by SUBCHANFLOW by increasing the total power until the MCHFR reaches unity.

7.3 Validation of critical heat flux correlations of SUBCHANFLOW for critical power ratio prediction

The validation of the CHF models of SUBCHANFLOW is done using the test data obtained from the NUPEC BWR Full-size Fine-mesh Bundle Test (BFBT) Benchmark [99]. In total 44 tests are simulated. These tests were performed under BWR-relevant thermal hydraulic conditions as follows: pressures of 5.5 to 8.6 MPa, flow rates of 2.8 to 18.1 kg/s,

and sub cooling of the coolant of 25 to 126 kJ/kg. The test assembly was an 8x8 BWR fuel assembly with a central water tube occupying 2x2 rod positions.

A basic input deck for SUBCHANFLOW representing the BFBT bundle geometry is developed. The different thermal-hydraulic boundary conditions of the 44 tests are entered as tables in the SUBCHANFLOW input deck. All 44 cases were then automatically run by SUBCHANFLOW consecutively as stacked cases. The predicted critical power for each case can finally be requested by the user in a separate file. This procedure is done once with each CHF correlation and the corresponding results are illustrated in Fig. 7.2.
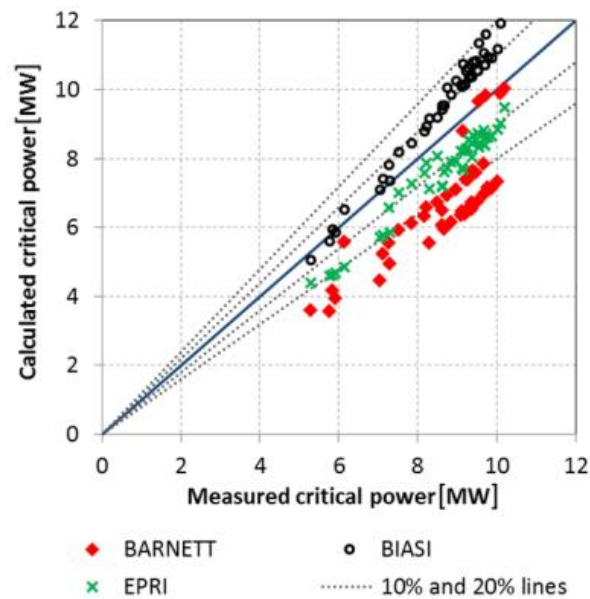
Fig. 7.2: Comparison of measured critical power and by SUBCHANFLOW predicted critical power with different boiling transition correlations for 44 cases of the BFBT benchmark.

In general, it can be stated that the critical power obtained with the EPRI and BIASI correlations are adequate, while the BARNETT correlation significantly under-predicts depending on the pressure. It must be noted that these results are also sensitive to the selected cross-flow mixing models. For the presented results, the Rogers-Rosehart turbulent mixing model with the recommended void drift coefficient of 1.4 is used to obtain the best agreement with the measurements.

The best predictions are achieved with the EPRI CHF correlation, with which the critical power is generally underestimated by approximately 10 %. On the contrary, with the BIASI correlation, the critical power tends to be over-predicted by up to 20 %. Finally, the BARNETT correlation under-predicts the majority of the test data by more than 20 % except for the experiments at 5.5 bar pressure which reproduce the critical power very accurately. The reason for this is the fact that this correlation combines three different CHF correlations

depending on the pressure. Based on the presented results it can be stated that the BARNETT CHF correlation is the most conservative one for pressures of 7 MPa as present in BWR at operation conditions, followed by the EPRI correlation.

For academic purposes, however, all three CHF correlations will be used for the investigations of the low moderated FA design in the frame of this dissertation.

7.4   Definition of the selected fuel assemblies and operation conditions

For this analysis, the hottest fuel assemblies predicted for two distinct time points of the equilibrium cycle of the four reduced moderator core designs investigated in chapter 6 are chosen to be modeled with SUBCHANFLOW. The two time points of the equilibrium cycle are selected based on the experience gained from the reference full-MOX BWR core analysis. In that core, the limiting MCPR values are obtained for the last time step with nominal core power and flow rate before flow rate increase and coastdown - called end of nominal cycle (EONC) below - and for the last time step with nominal power before coastdown and with small flow rate increase – called end of full power (EOFP) below. Because the burnable poison contents and corresponding control rod density is varying between the low moderated core designs, the peak power may be reached at a different point of time and location in the respective core even though the fuel shuffling is controlled with the same reactivity ranking map in all core designs.

The thermal-hydraulic and geometrical data needed for the analysis of the peak power fuel assemblies with SUBCHANFLOW is derived from the core analysis mentioned before performed with MICROBURN-B2 including pin power reconstruction. In Tab. 7.2, the FA name, its position in the core, the point of time in the cycle and the defining TH parameters of the individual cases are presented for EONC and in Tab. 7.3 for EOFP. Because there is no flow rate increase in core design HC12-2, EONC and EOFP are identical and the data is only given in Tab. 7.3. The position of each FA corresponds to the core map shown in Fig. 6.1. The characteristic geometrical parameters of each selected FA designs are summarized in Tab. 7.4. Based on these data, each low moderated fuel assembly type is modeled with SUBCHANFLOW to perform the thermal-hydraulic analysis. The main results obtained with this sub-channel code will be discussed in the next subchapter.

Tab. 7.2: Thermal-hydraulic data for the peak power bundle in different core designs at the last timestep with nominal operating conditions (before flow rate increase and coastdown)

		HC10-1	HC10-2	HC12-1	HC12-2
FA name	-	MHM013	MHM012	MMM011	
FA position (I, J)		(3, 3)	(2, 2)	(8, 2)	
Cycle exposure	efph	7000	7500	7000	no spectral shift
Core power	MW	4000	3100	3290	
f_{rad}	-	1.447	1.427	1.453	
FA power	MW	7.381	5.641	6.098	
Flow rate	kg/s	13.927	10.110	11.399	
Inlet enthalpy	kJ/kg	1218.799	1207.828	1211.764	

Tab. 7.3: Thermal-hydraulic data for the peak power bundle in different core designs at the last time step with full power operation (before coastdown)

		HC10-1	HC10-2	HC12-1	HC12-2
FA name	-	MHM013	MHM013	MHM013	MHM013
FA position (I, J)		(3, 3)	(3, 3)	(3, 3)	(3, 3)
Cycle exposure	efph	7500	8000	7500	7500
Core power	MW	4000	3100	3290	3840
f_{rad}	-	1.471	1.450	1.507	1.512
FA power	MW	7.503	5.733	6.323	7.406
Flow rate	kg/s	15.403	10.690	12.134	13.447
Inlet enthalpy	kJ/kg	1224.143	1211.949	1216.019	1217.765

Tab. 7.4: Geometry parameters of investigated low moderated FA designs

		HC10-1	HC10-2	HC12-1	HC12-2
Active height	m	3.710	3.710	2.300	2.700
Rod pitch (P)	cm	1.284	1.284	1.070	1.070
Rod diameter (D)	cm	1.144	1.144	0.930	0.930
P / D	-	1.122	1.122	1.151	1.151

		HC10-1	HC10-2	HC12-1	HC12-2
Hydraulic diameter of…					
… corner sub-channel	mm	7.095	7.095	6.146	6.146
… side sub-channel	mm	9.236	9.236	8.233	8.233
… central sub-channel	mm	8.890	8.890	7.700	7.700

7.5   Selected results for the thermal-hydraulic analysis

The evaluation of the thermal hydraulic analysis is focused on safety parameters such as the maximal fuel and cladding temperature and the critical power (MCHFR and CPR). The parameters predicted by SUBCHANFLOW using three CHF correlations are summarized in Tab. 7.5 for the EONC FAs and in Tab. 7.6 for the EOFP FAs. The provided MCHFR is predicted for the nominal FA power given above while the CPR is determined by SUBCHANFLOW by iterative increase of the FA power until the MCHFR becomes unity somewhere in the FA.

Tab. 7.5: Global SUBCHANFLOW results for the peak power bundle in different core designs at the last timestep with nominal operating conditions before flow rate increase (EONC).

		HC10-1	HC10-2	HC12-1	HC12-2
max. T_{fuel}	K	1705.9	1317.4	1627.2	-
max. T_{clad}	K	570.6	568.7	570.5	-
EPRI CHF correlation:					
MCHFR at nominal conditions	-	1.068	1.191	1.167	-
CPR	-	1.058	1.179	1.154	-
BARNETT CHF correlation:					
MCHFR at nominal conditions	-	0.751	0.817	0.798	-
CPR	-	0.829	0.825	0.807	-
BIASI CHF correlation:					
MCHFR at nominal conditions	-	2.813	4.406	3.038	-
CPR	-	1.436	1.554	1.534	-

Tab. 7.6: Global SUBCHANFLOW results for the peak power bundle in different core designs at the last time step with full power operation before coastdown (EOFP).

		HC10-1	HC10-2	HC12-1	HC12-2
max. T_{fuel}	K	1652.0	1319.5	1682.8	1652.5
max. T_{clad}	K	570.9	569.0	570.8	570.9
EPRI CHF correlation:					
MCHFR at nominal conditions	-	1.111	1.207	1.157	1.062
CPR	-	1.099	1.194	1.146	1.051
BARNETT CHF correlation:					
MCHFR at nominal conditions	-	0.824	0.884	0.795	0.720
CPR	-	0.832	0.812	0.868	0.731
BIASI CHF correlation:					
MCHFR at nominal conditions	-	2.962	4.590	2.886	2.607
CPR	-	1.508	1.591	1.519	1.413

The maximal predicted fuel (T_{fuel}) and cladding surface (T_{clad}) temperatures are sufficiently below the safety limits i.e. melting point or threshold temperatures for e.g. Zircaloy-water oxidation reaction (see chapter 2.3.1). As already observed for the validation studies for the different CHF correlations, the predicted MCHFR and CPR are the lowest for the BARNETT correlation, while they are the highest for the BIASI correlation. The values predicted by SUBCHANFLOW when the EPRI correlation is used lie between the ones predicted with BIASI or BARNETT correlation.

It is assumed here that the most reliable results are obtained with the EPRI CHF correlation because the predicted critical power is closest to the measurements as shown in chapter 7.3 and the predicted values are still conservative. The predicted CPR values obtained in the investigated FA are larger than unity by 5 % in the EOFP peak power FA in core HC12-2 up

to almost 20 % in the EOFP peak power FA in core HC10-2. This means that at steady state no boiling transition is predicted. Whether these margins are sufficient considering the uncertainties e.g. due to the small rod to rod gap and anticipated power increase during transients has to be further investigated. In open literature [68], a minimal CPR of 1.3 is suggested for BWR steady state conditions. For comparison, in the reference BWR full-MOX core, the minimal CPR is larger than 1.5.

Using the BIASI correlation, very good values for the CPR above 1.4 for all case are obtained. However, considering the non-conservative character of this correlation and the involved uncertainties, the safety margin is not acceptable. On the contrary, the BARNETT CHF correlation predicts already exceeded critical power by around 20 % for all cases. The lowest CPR value of 0.731 is predicted for the peak power FA in core HC12-2.

 Assessing the local MCHFR at each rod indicated potential for local improvements. In Fig. 7.3, the MCHFR is presented for each rod in the lattice of the peak power FA at EONC in core HC10-1.

	1	2	3	4	5	6	7	8	9	10
1	1.146	1.185	1.105	1.069	1.073	1.074	1.068	1.102	1.100	1.130
2	1.185	1.153	1.182	1.137	1.152	1.152	1.139	1.185	1.160	1.181
3	1.105	1.182	1.158	1.183	1.191	1.191	1.185	1.161	1.186	1.111
4	1.069	1.137	1.183	1.197	1.202	1.202	1.199	1.188	1.145	1.079
5	1.074	1.152	1.191	1.202	1.207	1.209	1.206	1.197	1.161	1.087
6	1.074	1.152	1.191	1.202	1.209	1.212	1.210	1.199	1.162	1.087
7	1.068	1.139	1.185	1.199	1.207	1.210	1.206	1.194	1.151	1.085
8	1.103	1.185	1.161	1.188	1.197	1.199	1.194	1.172	1.200	1.126
9	1.100	1.160	1.186	1.145	1.161	1.162	1.151	1.200	1.173	1.209
10	1.131	1.181	1.111	1.079	1.087	1.087	1.085	1.126	1.209	1.172

Fig. 7.3: Radial map of the MCHFR for each rod in the peak power FA in core HC10-1 for EONC (CPR=1.058) predicted by SUBCHANFLOW by using the EPRI CHF correlation.

The lowest MCHFR values (red color) are reached in the middle of the peripheral rod rows where also large powers are reached in the rods and their neighbors. The highest rod power is reached in the rod at position (2, 2) but the MCHFR is still higher as in the peripheral rods because especially the neighboring burnable poison pins at positions (1, 2) and (2, 1) have low power. The largest margin to CHF is obtained in the central fuel rods with the lowest power in the FA (green color). The local MCHFR gradients between neighboring fuel rods are consistent with the pin power profile and the gradients there are mainly caused by the different enrichment levels in the different fuel pins. The axial location of boiling transition depends on the fuel rod and is usually in one of the three uppermost calculation nodes.

In the peak power FA at EOFP of core HC12-2 similar observations can be made. The predicted MCHFR for the local fuel rod are presented in Fig. 7.4. The smallest values (red color) are obtained in the peripheral fuel rods in the middle of the FA sides. They are comparable to the MCHFR values presented in Fig. 7.3. The central MCHFR values, however, are smaller as in the HC10-1 lattice. Small values follow again the boundary between different enrichment levels.

	1	2	3	4	5	6	7	8	9	10	11	12
1	1.183	1.202	1.125	1.062	1.062	1.064	1.064	1.065	1.067	1.179	1.222	1.198
2	1.202	1.143	1.144	1.079	1.100	1.107	1.107	1.101	1.078	1.145	1.145	1.222
3	1.126	1.144	1.091	1.075	1.095	1.101	1.101	1.097	1.076	1.093	1.145	1.180
4	1.062	1.079	1.075	1.103	1.114	1.117	1.118	1.115	1.106	1.077	1.079	1.068
5	1.063	1.100	1.095	1.114	1.121	1.124	1.124	1.122	1.116	1.098	1.102	1.066
6	1.065	1.107	1.101	1.117	1.124	1.126	1.127	1.125	1.119	1.103	1.110	1.067
7	1.065	1.108	1.102	1.118	1.125	1.127	1.127	1.125	1.119	1.103	1.110	1.067
8	1.065	1.101	1.097	1.116	1.122	1.125	1.125	1.123	1.117	1.099	1.103	1.067
9	1.068	1.078	1.077	1.106	1.116	1.119	1.119	1.117	1.107	1.078	1.081	1.070
10	1.180	1.146	1.093	1.077	1.098	1.104	1.104	1.099	1.079	1.095	1.148	1.182
11	1.223	1.146	1.146	1.079	1.103	1.110	1.110	1.103	1.081	1.148	1.148	1.225
12	1.199	1.223	1.180	1.069	1.067	1.068	1.068	1.068	1.070	1.182	1.225	1.201

Fig. 7.4: Radial map of the MCHFR for each rod in the peak power FA in core HC12-2 for EOFP (CPR=1.051) predicted by SUBCHANFLOW by using the EPRI CHF correlation.

7.6   Discussion of results

The generalized boiling transition correlations used in the above investigations have been determined for FAs used in Generation II BWR. Due to the differences between the design of Gen-II BWR FA and the design of low moderated FA, the applicability of those correlations for low moderated fuel assemblies is limited. Appropriate experiments for the low moderated FA are needed to derive appropriate correlations that can be implemented in the codes for the correct prediction of critical power. Additionally, the effect of spacers on the dryout behavior is not modeled by SUBCHANFLOW and has to be considered in further investigations. Conventional grid spacers with mixing vanes should be investigated, as well as, wire-wrap spacers, which are more suitable for tight pitched lattices. Despite of this, the performed investigations allow the identification of critical safety parameters and underline the importance of neutronic and thermal hydraulic investigations to find an optimized fuel assembly design.

Improvement of the local MCHFR could be achieved by flattening the fuel pin power profile in the fuel lattice and by widening the lattice. Safety margin to critical power can be improved

by reducing the FA power or increasing the flow rate. However, these measures will require reevaluation of the low moderated core designs investigated in chapter 6.

8 Summary and conclusions

The main objectives of this dissertation are the neutronic development of a reduced moderation core with square lattice fuel assemblies for a Gen-II BWR nuclear power plant (reference plant), the evaluation of its key safety features, and the demonstration of the advantages of such a core in terms of improved fuel utilization without deterioration of the safety margins compared to a Gen-II BWR full-MOX core design.

First of all, low moderated fuel assembly designs have been developed and optimized with respect to fuel utilization and selected neutronic safety parameters using lattice physics codes in chapter 4. The outer fuel assembly dimensions are not changed to maintain the compatibility with the reference plant. By removing internal water structures and increasing the fuel rod diameter, the ratio of moderator to fuel is reduced. Due to the harder neutron spectrum, the conversion ratio of fertile to fissile isotopes is increased from below 0.68 to around 0.75 in fuel assembly designs with equivalent reactivity. Among the investigated fuel assembly designs, the best fuel utilization is achieved with the lattice dimension of 10x10 and with the lowest investigated fuel rod coolant gap width of 1.4 mm. Increasing the lattice dimension tends to decrease the fuel utilization and to make the void reactivity coefficient less negative. Using MOX fuel with lower plutonium quality significantly deteriorates the value of the void coefficient.

In an additional validation study of the lattice codes for low moderated fuel assemblies and the typical BWR void fraction range, a good agreement between different codes has been determined. However, for very high void contents exceeding 85 %, differences between the numerical codes are observed, which necessitate further investigation.

To validate the energy discretization of the few group condensed and homogenized cross-sections used in 3D core simulators, various representative test cases have been systematically assessed compared to reference neutron transport solutions in chapter 5. It has been demonstrated, that increasing the number of energy groups from two to four or eleven does not improve the calculation results. Therefore, the common two-group energy structure of the cross-sections with an energy threshold of 0.625 eV is still appropriate to model the more epi-thermal neutron spectrum in the low moderated core designs.

Extensive core design studies have been conducted in chapter 6 starting with the previously developed fuel assembly design with 10x10 fuel rods. An optimized low moderated core has been developed in several iterations. The optimization has been done in comparison to a reference full-MOX BWR core with the aim to achieve comparable values for the operational parameters core pressure loss, coolant void content, cycle length, discharge burnup and cycle energy generation.

The final core design has a core height of 270 cm and consists of fuel assemblies with 12x12 fuel rods. Although a smaller number of thicker fuel rods has proven to yield a better fuel utilization, the high power density in a short core requires the applied larger lattice dimension. The evaluated inherent neutronic safety features are demonstrated to be adequate. The void reactivity coefficient of below -30 pcm / %Void is less negative than in the reference core design but it is still sufficiently negative. The cold shutdown margin is evaluated to be more then -4 %. This is a significant improvement compared to the reference full-MOX BWR. On the one hand, it is caused by the reduced excess reactivity release between hot full power and cold zero power core conditions in the low moderated core. On the other hand, the control rod worth is significantly increased due to the stronger relative moderator displacement during their insertion.

Compared to the reference core, the fissile plutonium consumption during one cycle is reduced by around 15 % and the discharge plutonium quality is significantly increased from 47.3 % to 56.6 %, which makes a second recycling feasible. However, the smaller core size (increased leakage) and lower moderation (less reactivity) necessitates higher enrichment and, thus, the fuel costs are increased.

Finally, the thermal limits of boiling transition and peak cladding surface and fuel centerline temperature have been assessed for selected hot fuel assemblies of the low moderated core designs. The EPRI critical heat flux correlation has been identified to be most appropriate and still a conservative correlation to reproduce experimental results of the investigated test cases. The critical power ratio in the low moderated peak power FA calculated with the EPRI correlation is larger than unity in all cases (> 1.05). However, the hereby provided safety margin to boiling transition is insufficient to cover uncertainties in the calculation or power changes during postulated transients. Therefore, power reduction, larger fuel rod coolant gap or other measures to improve the heat transfer will be necessary to enlarge the safety margins e.g. to values of the critical power ratio above 1.3 in the whole core.

The major conclusions to be drawn from the present work are the following:

- The neutronic feasibility of a reduced moderation core with square lattice fuel assemblies for a Gen-II BWR could be demonstrated for steady state core conditions.
- The consumption of fissile nuclides is decreased by 15 % in comparison to a full-MOX BWR. However, the significantly increased enrichment required to obtain sufficient reactivity for an equivalent cycle yields substantially higher fuel assembly costs. Therefore, the presented core design can only be beneficial in a closed fuel cycle with multiple recycling of the fuel.
- The thermal-hydraulic assessment indicates insufficient margin to boiling transition. Thus, appropriate measures to improve the safety have to be considered in further investigations. This includes improvement of the investigation methodology and design changes.

Based on the performed investigations, the following areas for further developments, optimizations and evaluations should be pursued. The listed order of appearance does not quote any prioritization:

- Analysis of selected limiting transient scenarios,
- assessment of FA design modifications to enlarge the safety margins (e.g. CPR),
- experimental investigation to determine more suitable boiling transition correlations and
- fuel cycle cost assessment taking into account multiple recycling.

Appendix A   Additional data and results of core design studies

A.1   Fuel assembly design in investigated BWR cores

Nomenclature of gadolinia design: 6G2.5 for example means there are 6 burnable poison rods in the bundle with a Gd_2O_3 enrichment of 2.5 wt% in each.

Tab. A.1: Bundle design data for full-MOX core design

Gd design:	6G2.5 (low Gd)		6G2.5* / 8G3.25** (medium Gd)		12G3.0 (high Gd)	
	Pu_{fiss}	^{235}U	Pu_{fiss}	^{235}U	Pu_{fiss}	^{235}U
av. enrichment, wt%	4.47	0.26	4.48	0.26	4.35	0.27
bundle HM-mass, kg	177.01		176.92		176.59	
no. of reloads	48		48		52	

	Pu_{fiss}	^{235}U
fissile per batch, wt%	4.43	0.27

* upper part of fuel assembly w/o part-length fuel rods

**lower part of FA with part-length fuel rods

Tab. A.2: Bundle design data for core design HC10-1

Gd design:	4G2.0 (low Gd)		6G2.0 (medium Gd)		6G3.5 (high Gd)	
	Pu_{fiss}	^{235}U	Pu_{fiss}	^{235}U	Pu_{fiss}	^{235}U
av. enrichment, wt%	5.13	0.24	5.10	0.25	5.10	0.24
bundle HM-mass, kg	258.05		257.98		257.66	
no. of reloads	48		48		52	

	Pu_{fiss}	^{235}U
fissile per batch, wt%	5.11	0.24

Tab. A.3: Bundle design data for core design HC10-2

Gd design:	4G2.0 (low Gd)		6G2.0 (medium Gd)		6G3.5 (high Gd)	
	Pu_{fiss}	^{235}U	Pu_{fiss}	^{235}U	Pu_{fiss}	^{235}U
av. enrichment, wt%	4.54	0.24	4.52	0.25	4.52	0.25
bundle HM-mass, kg	258.05		257.98		257.77	
no. of reloads	48		48		52	

	Pu_{fiss}	^{235}U
fissile per batch, wt%	4.53	0.25

Tab. A.4: Bundle design data for core design HC12-1

Gd design:	8G2.5 (low Gd)		10G3.0 (medium Gd)		14G4.5 (high Gd)	
	Pu_{fiss}	^{235}U	Pu_{fiss}	^{235}U	Pu_{fiss}	^{235}U
av. enrichment, wt%	6.94	0.24	6.93	0.24	6.92	0.25
bundle HM-mass, kg	152.15		152.03		151.61	
no. of reloads	48		48		52	

	Pu_{fiss}	^{235}U
fissile per batch, wt%	6.93	0.24

Tab. A.5: Bundle design data for core design HC12-2

Gd design:	8G2.5 (low Gd)		10G3.0 (medium Gd)		14G4.5 (high Gd)	
	Pu_{fiss}	^{235}U	Pu_{fiss}	^{235}U	Pu_{fiss}	^{235}U
av. enrichment, wt%	6.74	0.24	6.73	0.24	6.72	0.25
bundle HM-mass, kg	178.61		178.47		177.98	
no. of reloads	48		48		52	

	Pu_{fiss}	^{235}U
fissile per batch, wt%	6.73	0.24

A.2 Core thermal-hydraulic conditions
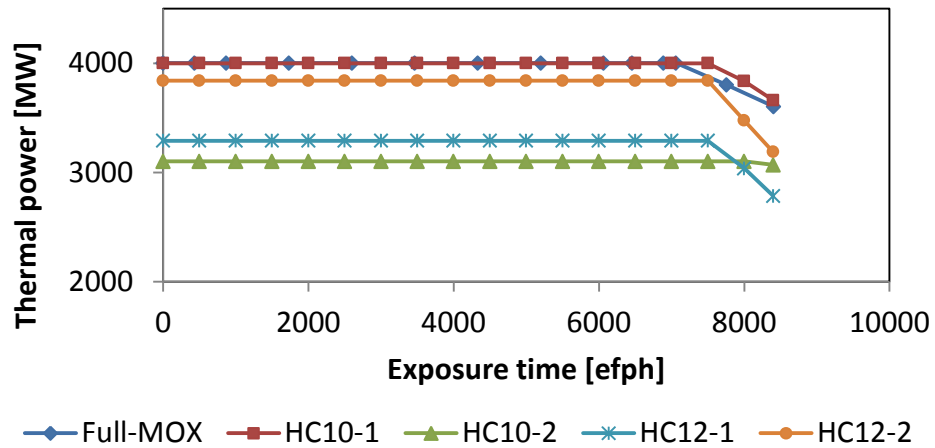
Fig. A.1: Thermal core power during equilibrium cycle as function of exposure time.
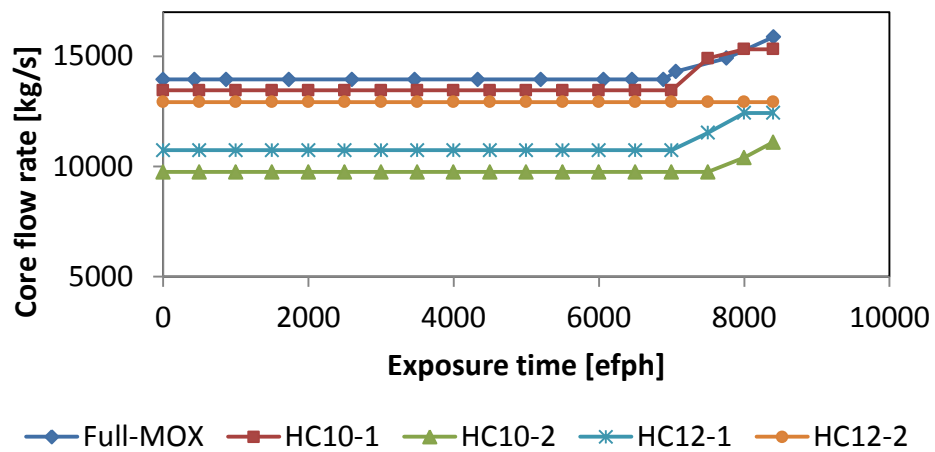
Fig. A.2: Core flow rate during equilibrium cycle as function of exposure time.
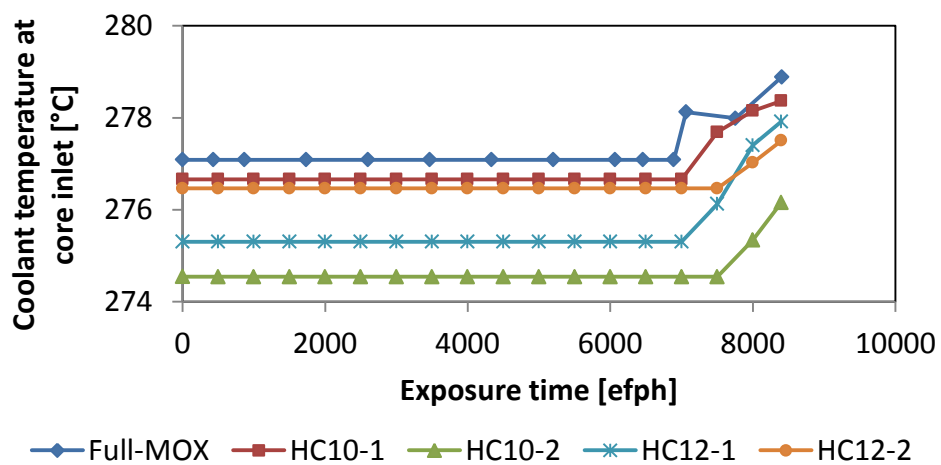
Fig. A.3: Core inlet coolant temperature during equilibrium cycle as function of exposure time.

A.3   Results of core design studies
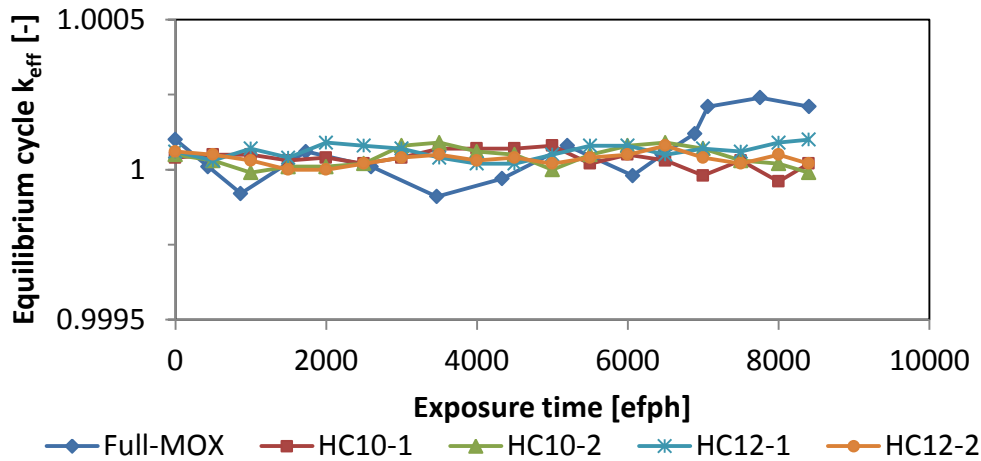
Fig. A.4: Equilibrium cycle k_eff of investigated core designs as function of exposure time.
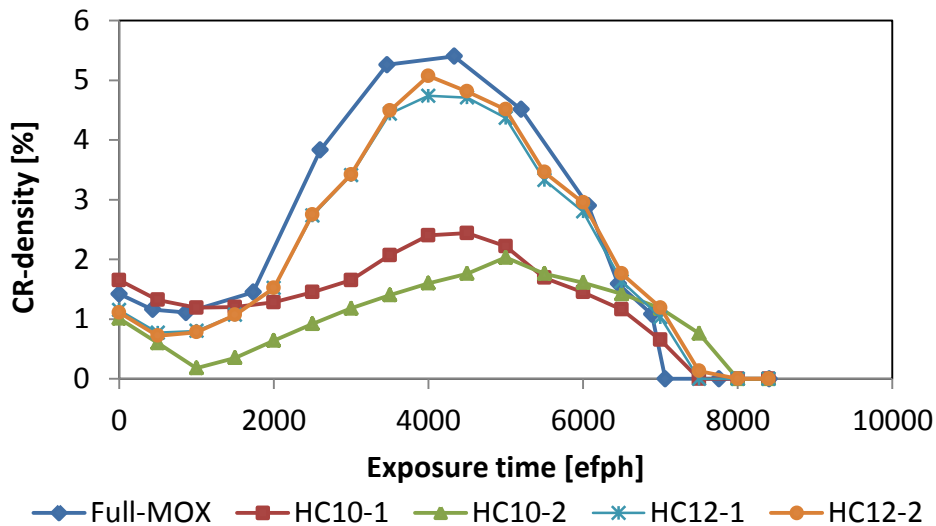
Fig. A.5: Cycle CR-density during equilibrium cycle as function of exposure time.
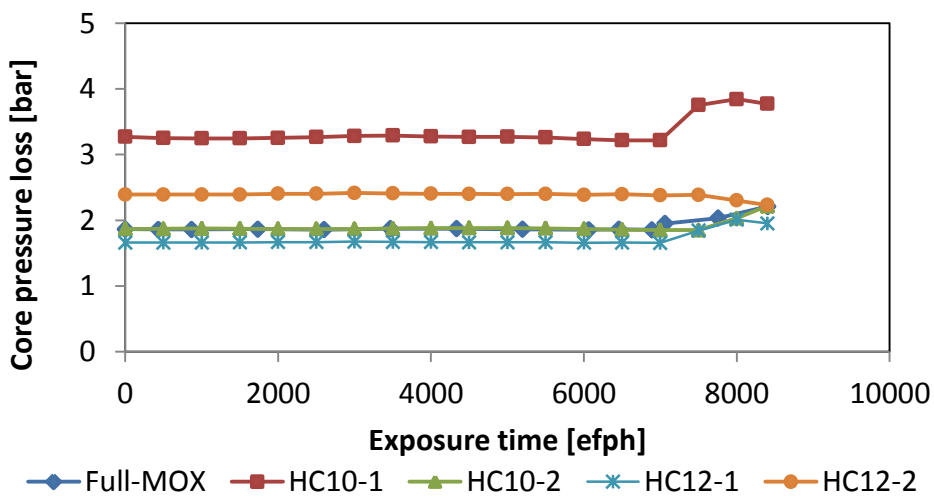
Fig. A.6: Core pressure loss during equilibrium cycle as function of exposure time.
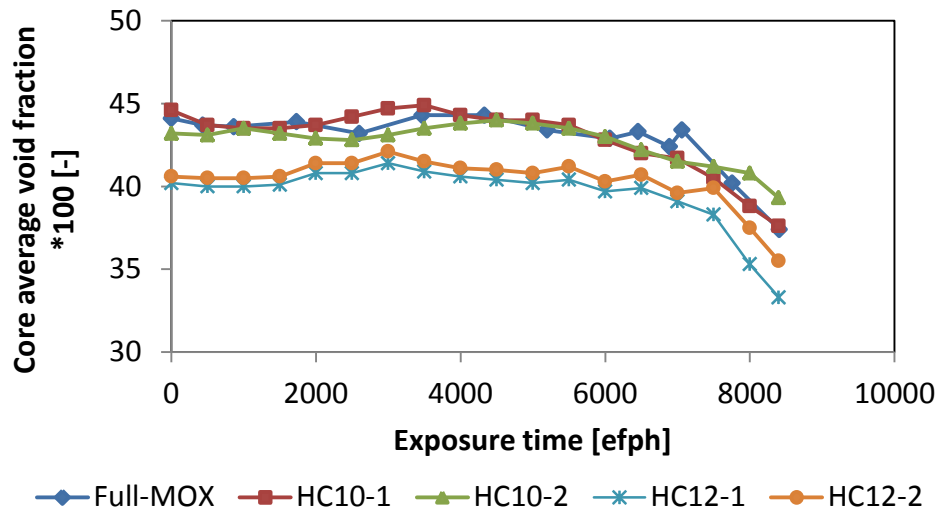
Fig. A.7: Core average coolant void fraction during equilibrium cycle as function of exposure time.
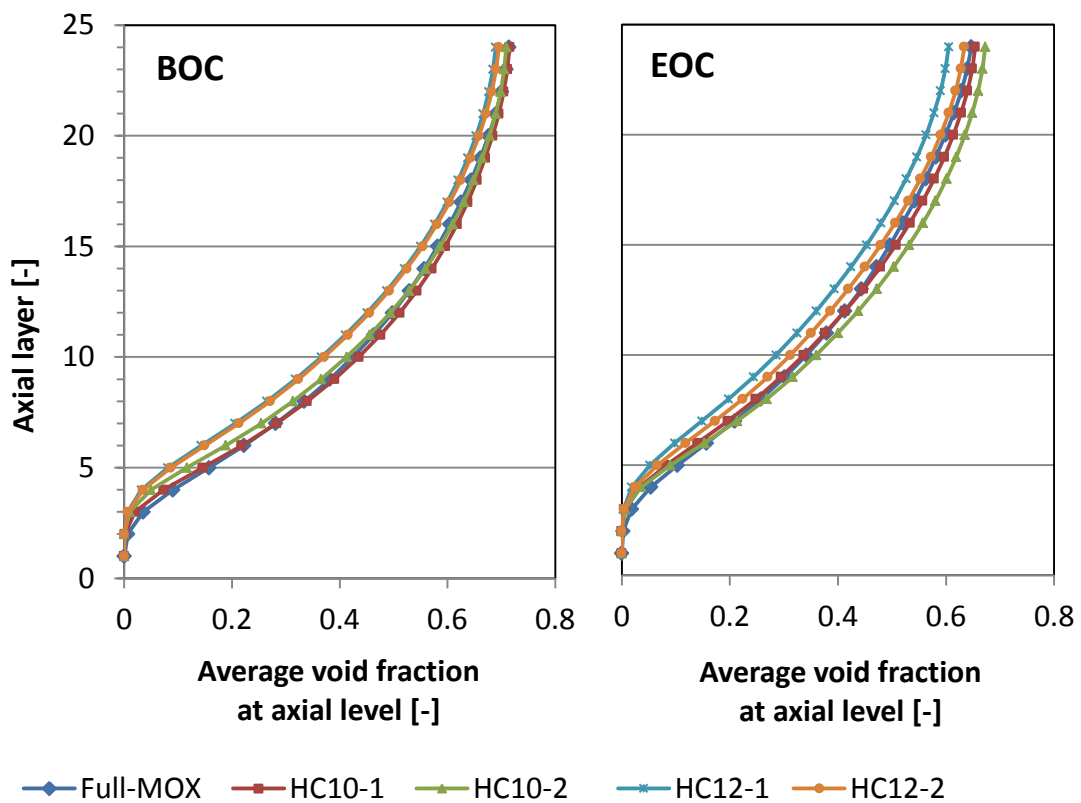
Fig. A.8: Average coolant void fraction at different axial height at begin (left) and end (right) of equilibrium cycle.
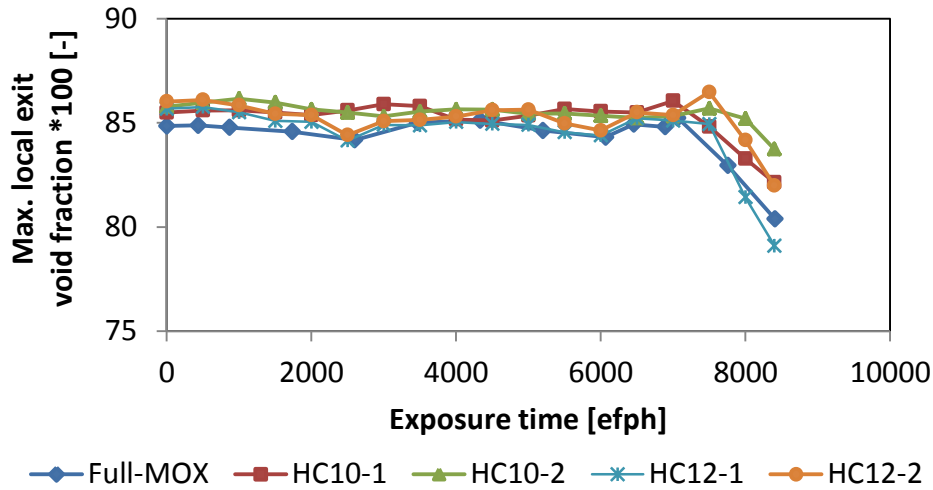
Fig. A.9: Maximum local exit coolant void fraction during equilibrium cycle as function of exposure time.
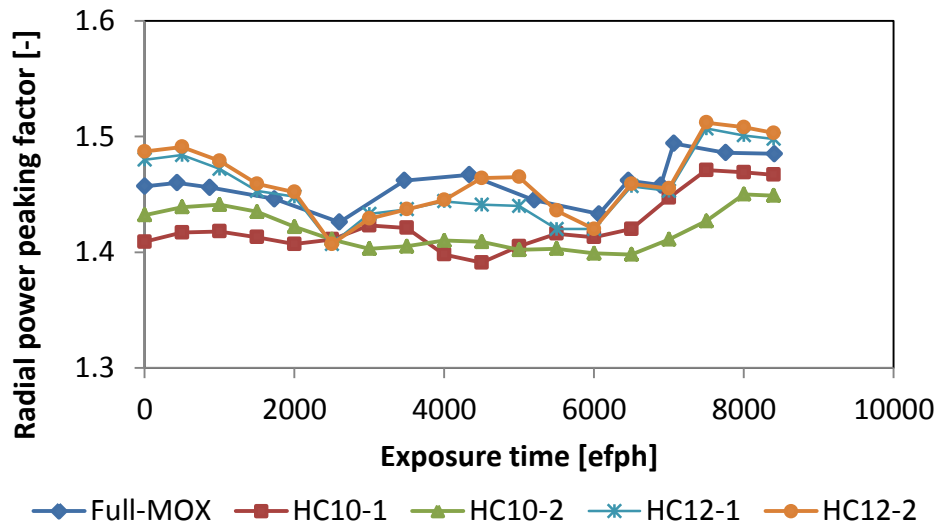
Fig. A.10: Radial power peaking factor during equilibrium cycle as function of exposure time.
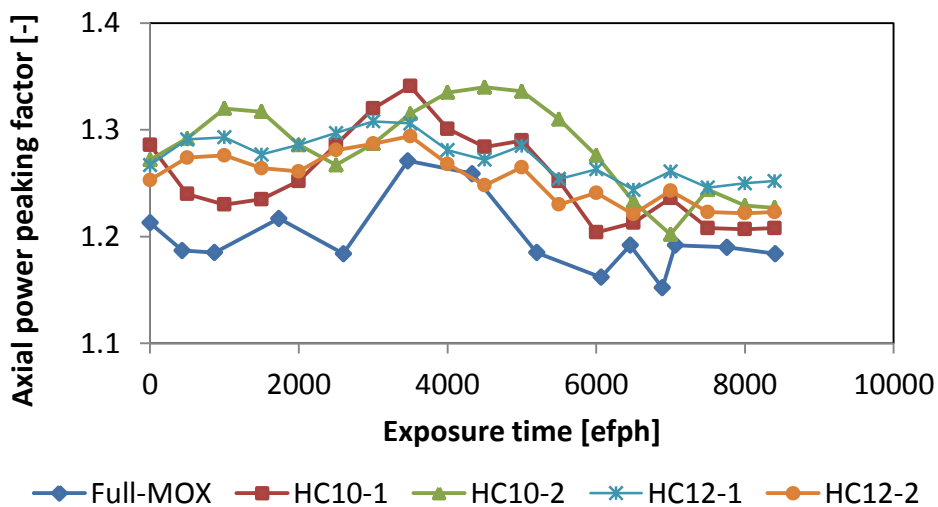
Fig. A.11: Axial power peaking factor during equilibrium cycle as function of exposure time.
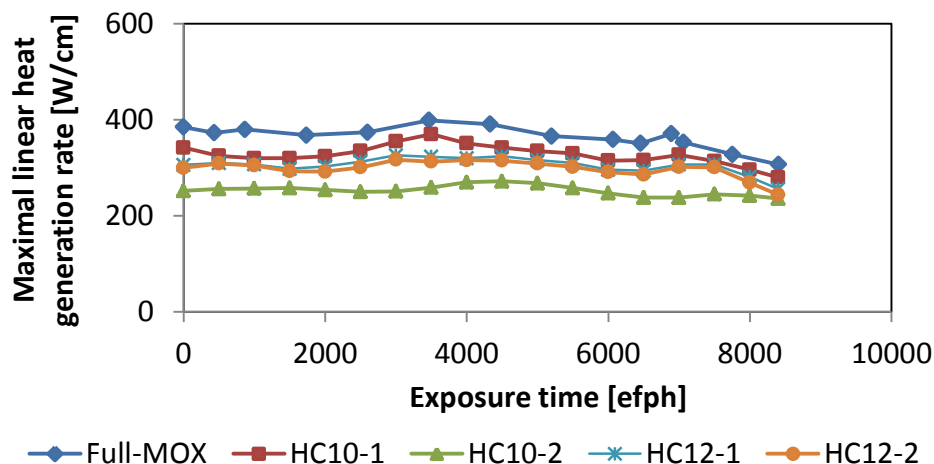
Fig. A.12: Maximal linear heat generation rate during equilibrium cycle as function of exposure time.
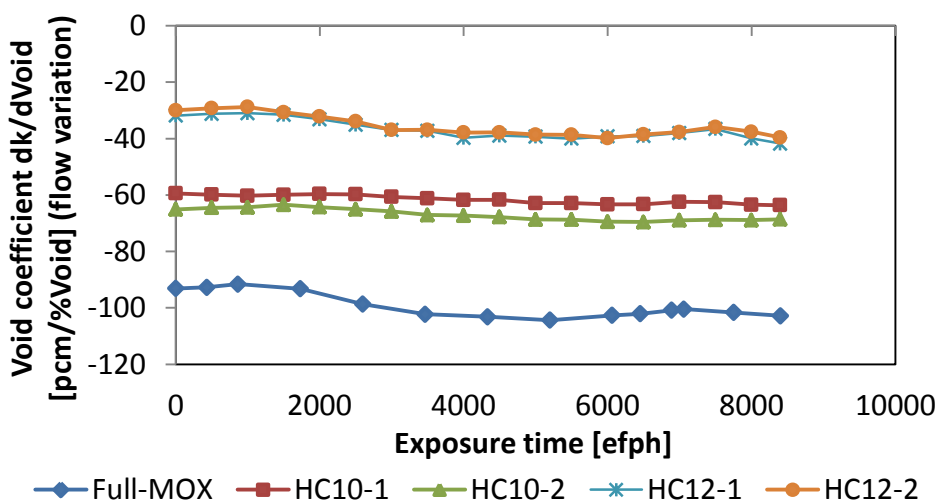
Fig. A.13: Coolant void reactivity coefficient determined by inlet flow rate variation during equilibrium cycle as function of exposure time.
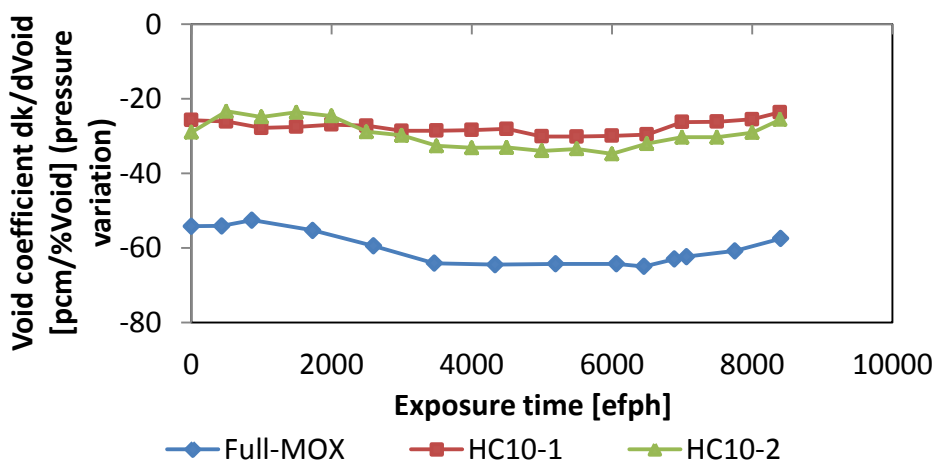
Fig. A.14: Coolant void reactivity coefficient determined by outlet pressure variation during equilibrium cycle as function of exposure time. See discussion in chapter 6.4.2 for results of cases HC12-1 and HC12-2.
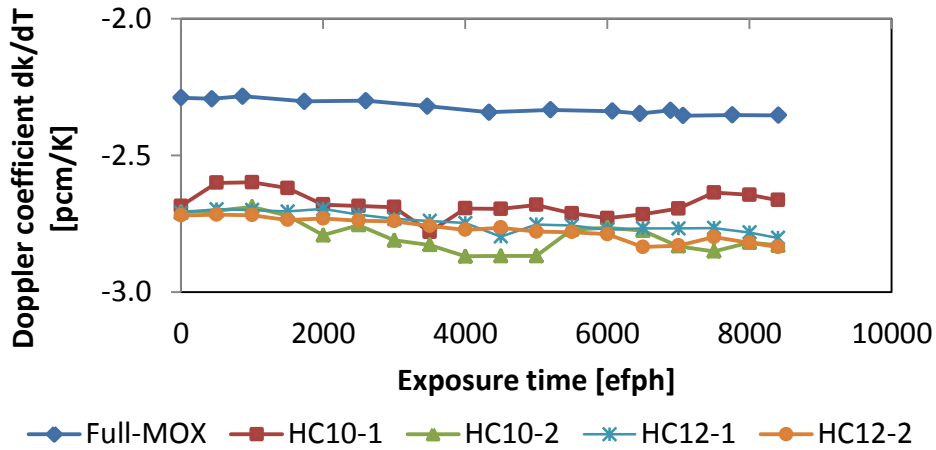
Fig. A.15: Doppler reactivity coefficient determined by uniform fuel temperature variation during equilibrium cycle as function of exposure time.
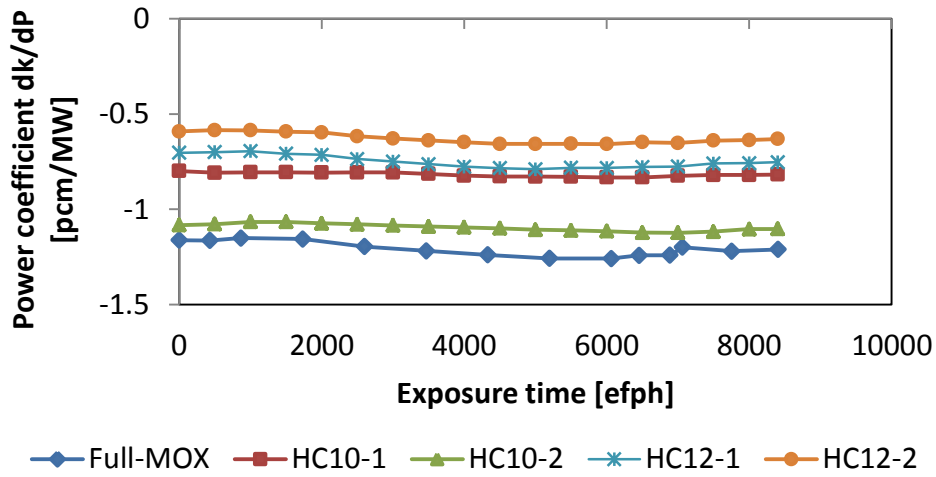
Fig. A.16: Power reactivity coefficient determined by power variation during equilibrium cycle as function of exposure time.
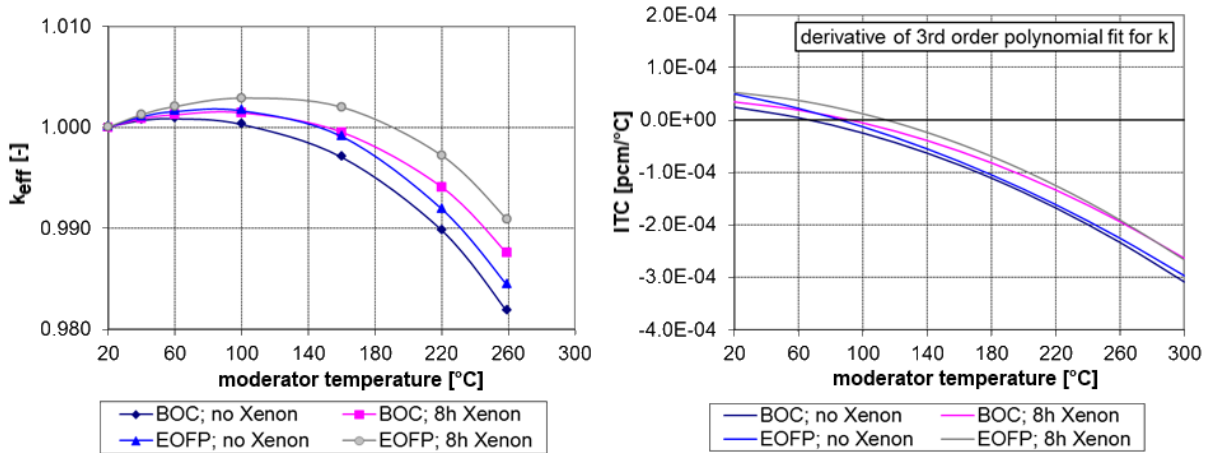
Fig. A.17: Isothermal temperature coefficient in core HC10-1.
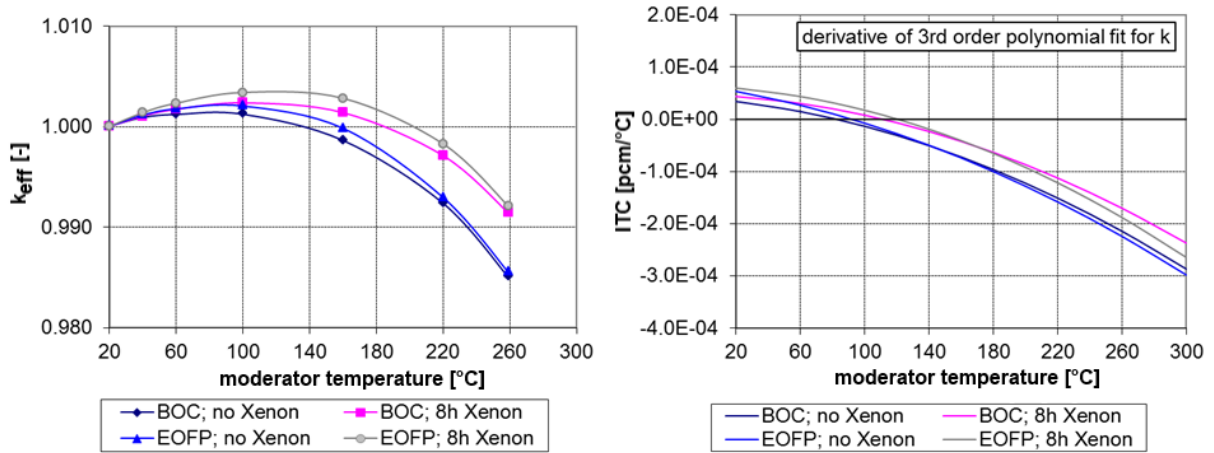
Fig. A.18: Isothermal temperature coefficient in core HC10-2.
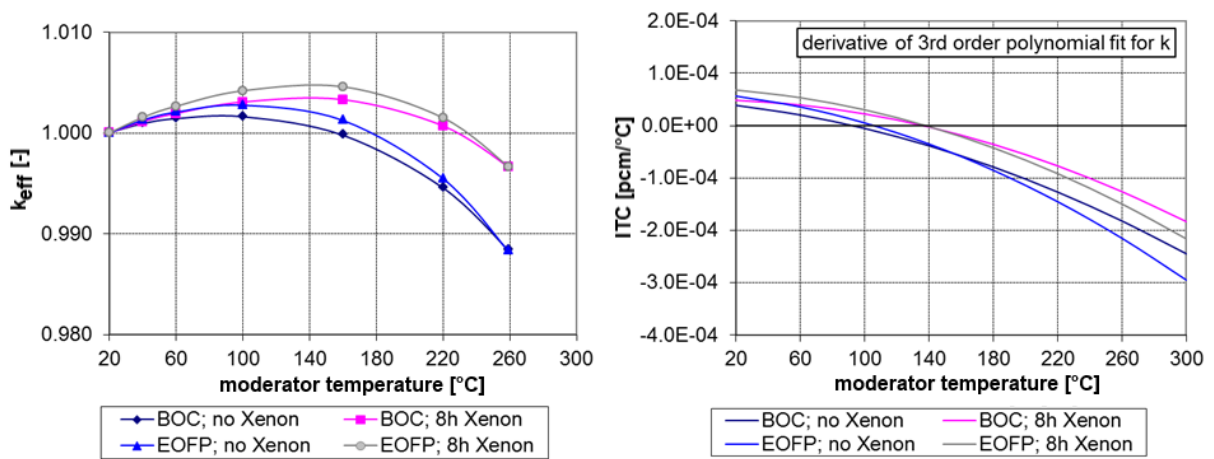
Fig. A.19: Isothermal temperature coefficient in core HC12-1.
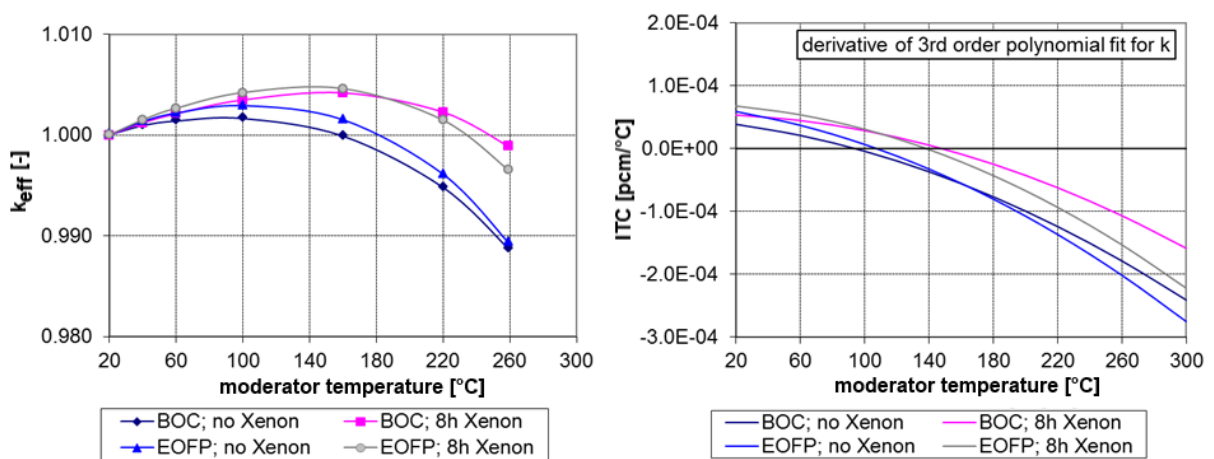
Fig. A.20: Isothermal temperature coefficient in core HC12-2.

Tab. A.6 Exact k$_{eff}$ results and corresponding reactivity components in terms of k$_{eff}$-differences (dk$_{eff}$) for comparison of the core k$_{eff}$ for different core states at begin of cycle.

k$_{eff}$	Full-MOX	HC10-1	HC10-2	HC12-1	HC12-2
HFP, equil. Xe, ARO	1.00267	1.00428	1.00145	1.00255	1.00360
HFP, equil. Xe, critical CR pattern	1.00005	1.00005	1.00004	1.00002	1.00003
HZP, Xe concentrations from HFP, ARO	1.07399	1.05189	1.04953	1.03302	1.03432
CZP, Xe concentrations from HFP, ARO	1.04836	1.04954	1.04493	1.01900	1.02004
CZP, no Xe, ARO	1.08068	1.07627	1.07074	1.05364	1.05486
CZP, no Xe, stuck-rod	0.97530	0.94679	0.93913	0.93970	0.93978
CZP , no Xe, ARI	0.95165	0.93256	0.92469	0.92349	0.92092
dk$_{eff}$	Full-MOX	HC10-1	HC10-2	HC12-1	HC12-2
CR reactivity bound to obtain critical conditions (HFP, equil. Xe)	-0.00262	-0.00423	-0.00141	-0.00253	-0.00357
HZP – HFP (Xe conc. from HFP, ARO)	0.07132	0.04761	0.04808	0.03047	0.03072
CZP – HZP (Xe conc. from HFP, ARO)	-0.02563	-0.00235	-0.00460	-0.01402	-0.01428
Xe conc. from HFP – No Xe (CZP, ARO)	-0.03232	-0.02673	-0.02581	-0.03464	-0.03482
CZP, no Xe – HFP, equil. Xe (ARO)	0.07801	0.07199	0.06929	0.05109	0.05126
Worth of all but the stuck CR (CZP, no Xe)	-0.10538	-0.12948	-0.13161	-0.11394	-0.11508
Stuck-rod worth (CZP, no Xe)	-0.02365	-0.01423	-0.01444	-0.01621	-0.01886

Tab. A.7 Overview of fuel utilization and fuel composition change in the different investigated core designs during one equilibrium cycle.

Cycle parameters		Full-MOX	HC10-1	HC10-2	HC12-1	HC12-2
Cycle burnup	MWd/kgHM	9.7	6.6	5.4	9.7	9.6
EOC FIR	-	0.867	0.951	0.958	0.936	0.936
Discharge Pu$_{qual}$ of batch 6	-	0.473	0.583	0.591	0.566	0.566

Core fuel composition at BOC

		Full-MOX	HC10-1	HC10-2	HC12-1	HC12-2
Av. Pu$_{fiss}$ enrichment	%	3.338	4.530	4.152	6.086	5.913
Pu$_{fiss}$ content	t	4.517	9.017	8.297	7.069	8.065
Pu$_{tot}$ content	t	7.902	14.544	13.302	11.556	13.184

Core fuel composition at EOC

		Full-MOX	HC10-1	HC10-2	HC12-1	HC12-2
Av. Pu$_{fiss}$ enrichment	%	2.925	4.342	4.003	5.759	5.596
Pu$_{fiss}$ content	t	3.916	8.578	7.952	6.616	7.550
Pu$_{tot}$ content	t	7.305	14.135	12.990	11.115	12.685

Change in core plutonium content between BOC and EOC

		Full-MOX	HC10-1	HC10-2	HC12-1	HC12-2
Pu$_{fiss}$	t	-0.601	-0.439	-0.346	-0.453	-0.515
Pu$_{tot}$	t	-0.597	-0.409	-0.312	-0.441	-0.499

Appendix B   Comparison of PARCS and MICROBURN-B2 for example low moderated BWR core

B.1   Modeled case

The case used for this comparison is an early stage of the HC10-1 core presented in the core design studies in chapter 6. In the model used here, the fuel contains no BPR at all and all excess reactivity at BOC is compensated with CR. The average fuel enrichment in fresh FA is 5 wt% Pu_{fiss}. The shuffling pattern and batch size are identical to core design HC10-1. The MICROBURN-B2 core model was transferred to PARCS as good as possible. Major modeling differences include:

- No bypass flow model in PARCS available. Active core flow predicted by MICROBURN-B2 was used as input for PARCS calculation
- Explicit reflector model (1 row radially and 1 axial layer at top and bottom) in PARCS without cross-section parameterization, since it is not available in PARCS (see code description in section 3.3.2)

As explained in section 3.3.2, the core averaged thermal-hydraulic conditions are used for cross-section look-up in the reflector nodes. This is an acceptable simplification for the modelling of PWRs, which are characterized by a rather homogeneous coolant density in the core (PARCS was originally developed for modelling PWR). In BWR, however, the coolant density changes significantly from bottom to top, due to void generation. Additionally, the density in a reflector node depends on the density of the neighboring fuel node. Accurate determination of local reflector cross-sections for BWR in PARCS would, therefore, require thermal-hydraulic calculation of the reflector bypass and additional parameterization of the cross-sections with e.g. the coolant density of the neighboring fuel node. Major code changes would be required to improve this issue, which is out of the scope of this work. As a compromise, a simplified methodology to model the reflector is chosen here. The reflector is modeled by separation in bottom, radial and top reflector. In each zone a single representative cross-section set is defined. In this way un-voided coolant can be considered in the reflector nodes at the core inlet and voided coolant in the reflector nodes at the core outlet. In the radial reflector, un-voided coolant with inlet condition is assumed. The adjacent fuel nodes are modelled with 40 % void content.

B.2   Selected results

The average cycle k_{eff} in PARCS compared to that predicted by MICROBURN-B2 is lower by approx. 0.4% in average as shown in Fig. B. (0.1 % at BOC and 0.8 % at EOC).
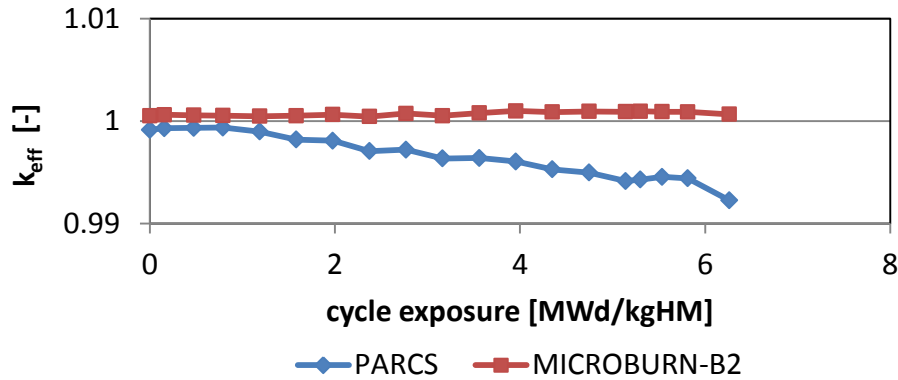
Fig. B.1: Equilibrium cycle effective multiplication factor k_{eff} as function of exposure.

This can be considered a good result for a code-to-code comparison considering the various differences which include:

- Different initial nuclear data, method and approximations used in lattice code (see Tab. 4.11)
    - o   different heterogeneous neutron flux leads to different nodal homogeneous material constants
    - o   differences in computed ADF between lattice codes leads to power profile deviations between core solvers
    - o   different yields for reactor poisons can easily influence the k_{eff} result by a few 100 pcm as can be seen from the poison worth shown in Fig. B.2
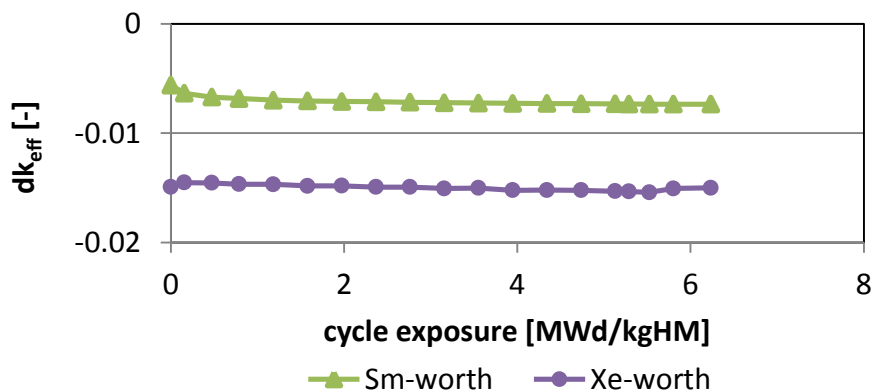
Fig. B.2: Poison reactivity defect dk_{eff} in PARCS calculation at HFP conditions as function of exposure.

- Different nodal methods used in core solver to solve the diffusion equation (ANEM / NEMMG),
- reflector model (analytic versus explicit),
- different TH models in core solvers leading to different local feedback.

In relation to the comparison done for CASMO-4 and TRITON presented in chapter 4.5, the downwards trend observed in Fig. B. is consistent.

The comparison of the power distribution and burnup profile is used here to compare the local prediction. Global results for PARCS compared to MICROBURN-B2 are the following:

- Radial power:
  - Higher BOC power at core center power (max +4.7%)
  - Lower EOC power at core center power (min -7.5%)
  - Large differences at reflector (up to +20% at EOC)
  - Strong gradients less pronounced in PARCS
  - Shift of sign of error from BOC to EOC
- Axial power:
  - Bottom peak less pronounced (whole cycle)
- Radial burnup:
  - Smaller deviation than for power
  - Power error cancels out over cycle

The relative local differences between PARCS (P) and MICROBURN-B2 (M) are determined as (P-M)/M and are given in per cent. As measure for the global error, the PWE and EWE are given (see equations (5.1) and (5.2)) In Fig. B.3 to Fig. B.6 the BOC and EOC power profile predicted by MICROBURN-B2 and the differences of PARCS to MICROBURN-B2 are shown. Largest radial power errors are found for BOC and EOC at positions of BOC CR insertion and next to the reflector. Local CR errors could result partially from deviations in predictions of history effects. In a PARCS benchmark against in-core measurements large differences for CR locations and the reflector region were observed [86]. Taking this experience into account, the power prediction seems adequate.

Since PARCS and MICROBURN-B2 use different methodologies to model the reflector, differences in this region are very likely. Improvements in ADF prediction by TRITON for PARCS could improve the results significantly as discussed in chapter 5. In addition, better reflector material constant parameterization in PARCS should be addressed in future code developments.

I:	J: 1	2	3	4	5	6	7	8	9	10	11	12	13	14	15
1	0.8	1.1	1.2	0.9	0.9	1.2	1.2	0.9	0.9	1.2	1.2	1.3	1.1	0.8	0.5
2	1.1	1.2	1.1	1.2	1.2	1.3	1.2	1.3	1.2	1.4	1.3	1.3	1.0	0.8	0.5
3	1.2	1.1	1.2	1.1	1.2	1.2	1.3	1.2	1.3	1.3	1.3	1.2	1.1	0.8	0.5
4	0.9	1.2	1.1	0.9	0.9	1.3	1.2	1.1	1.0	1.4	1.2	1.3	1.1	0.8	0.4
5	1.0	1.2	1.2	0.9	1.0	1.2	1.3	1.0	1.0	1.2	1.3	1.2	1.0	0.8	0.4
6	1.2	1.3	1.2	1.3	1.2	1.3	1.2	1.3	1.2	1.3	1.2	1.2	0.9	0.6	0.4
7	1.2	1.2	1.3	1.2	1.2	1.2	1.2	1.1	1.2	1.2	1.3	1.1	0.8	0.5	0.3
8	0.9	1.3	1.2	1.1	1.0	1.3	1.1	0.9	0.9	1.2	1.1	0.9	0.7	0.4	
9	0.9	1.2	1.3	1.0	1.0	1.2	1.2	0.9	0.8	1.0	1.1	0.8	0.5		
10	1.2	1.4	1.2	1.3	1.2	1.3	1.2	1.2	1.0	1.0	0.9	0.6	0.4		
11	1.4	1.3	1.3	1.2	1.3	1.2	1.2	1.1	1.0	0.9	0.7	0.5	0.3		
12	1.2	1.3	1.2	1.3	1.2	1.2	1.1	0.9	0.8	0.6	0.5	0.3			
13	1.1	1.0	1.1	1.0	1.0	0.9	0.8	0.6	0.5	0.4	0.3				
14	0.7	0.8	0.8	0.8	0.7	0.6	0.5	0.4							
15	0.4	0.4	0.4	0.4	0.4	0.4	0.3								

Fig. B.3: Radial bundle power profile at BOC predicted by MICROBURN-B2 and positions with partially inserted control rods.

:	J: 1	2	3	4	5	6	7	8	9	10	11	12	13	14	15
1	4.4	1.4	2.3	4.7	4.6	1.1	1.2	2.2	1.2	-1.8	-4.5	-1.3	-0.9	-0.7	2.1
2	3.4	2.2	2.4	2.3	2.5	0.7	0.4	0.7	0.7	-1.0	-0.9	-1.5	-0.5	-1.6	2.4
3	3.2	2.7	2.5	2.9	2.3	0.7	0.8	1.2	1.1	-0.2	-0.5	-0.6	-0.5	-0.4	3.0
4	4.1	2.1	2.6	3.5	2.9	0.8	1.2	1.9	2.1	-0.4	-0.6	-1.4	-0.9	0.0	4.6
5	3.1	1.8	1.8	2.6	2.6	0.8	1.1	2.3	2.1	-0.4	-0.7	-0.6	-1.0	-0.2	3.5
6	1.0	-0.1	-0.3	0.2	1.7	0.4	0.8	0.4	1.4	-0.2	-0.5	-1.5	-1.6	-2.0	2.6
7	0.2	-0.8	-1.4	-0.1	0.9	0.4	1.0	0.7	0.9	0.6	-0.8	-0.9	-2.2	-9.6	-0.8
8	2.9	-1.0	-1.2	1.0	1.6	0.8	1.6	3.2	3.4	0.2	-0.5	-1.9	-9.3	-0.2	
9	2.3	-0.8	-1.3	1.0	1.4	1.0	1.2	2.7	2.7	0.5	-0.9	-2.3	1.2		
10	-0.6	-1.2	-0.4	-1.5	-0.4	-0.5	0.6	-0.2	-0.8	-0.6	-0.7	-1.8	3.4		
11	-2.5	-1.4	-1.1	-2.8	-1.4	-0.9	-0.9	-0.3	-1.3	-0.7	-1.6	-8.9	1.7		
12	-4.7	-3.0	-1.6	-1.9	-1.2	-1.7	-0.9	-1.2	-0.3	-0.3	-7.8	5.4			
13	-5.4	-3.0	-2.1	-1.5	-1.3	-1.5	-2.1	-8.8	2.6	6.1	3.6				
14	-4.6	-4.6	-3.3	-1.8	-1.5	-2.2	-9.8	-0.3					PWE =		1.6
15	-1.9	-0.7	0.0	-0.1	1.3	0.7	-0.6						EWE =		3.5

Fig. B.4: Relative difference in radial bundle power profile between PARCS and MICROBURN-B2 at BOC in per cent.

The core center over-prediction of power at BOC becomes an under-prediction at EOC in PARCS. For the FA towards the core periphery the opposite trend can be observed. In addition, the adequate weighted error at BOC of PWE = 1.6 % and EWE = 3.5 % increases substantially at EOC (PWE = 3.4 % and EWE = 7.8 %).

I:	J: 1	2	3	4	5	6	7	8	9	10	11	12	13	14	15
1	1.3	1.3	1.4	1.3	1.4	1.3	1.4	1.3	1.3	1.2	1.1	1.1	0.9	0.6	0.3
2	1.3	1.4	1.3	1.5	1.4	1.4	1.3	1.4	1.3	1.3	1.1	1.1	0.8	0.6	0.4
3	1.4	1.3	1.4	1.4	1.4	1.3	1.4	1.3	1.3	1.2	1.2	1.0	0.9	0.6	0.3
4	1.3	1.5	1.4	1.4	1.4	1.4	1.4	1.4	1.3	1.3	1.1	1.1	0.9	0.6	0.3
5	1.4	1.4	1.4	1.4	1.4	1.3	1.4	1.3	1.3	1.2	1.1	1.0	0.8	0.6	0.3
6	1.4	1.4	1.3	1.4	1.3	1.4	1.3	1.3	1.2	1.2	1.0	1.0	0.7	0.5	0.3
7	1.3	1.3	1.4	1.3	1.4	1.3	1.3	1.2	1.2	1.1	1.1	0.9	0.7	0.4	0.2
8	1.3	1.4	1.3	1.4	1.3	1.3	1.2	1.2	1.1	1.1	1.0	0.8	0.5	0.3	
9	1.3	1.2	1.3	1.2	1.3	1.2	1.2	1.1	1.0	0.9	0.9	0.7	0.4		
10	1.2	1.3	1.2	1.3	1.2	1.2	1.1	1.1	0.9	0.9	0.8	0.5	0.3		
11	1.2	1.1	1.2	1.1	1.1	1.0	1.1	0.9	0.9	0.8	0.6	0.4	0.2		
12	1.0	1.1	1.0	1.1	1.0	1.0	0.9	0.7	0.7	0.5	0.4	0.3			
13	0.9	0.8	0.9	0.8	0.8	0.7	0.6	0.5	0.4	0.3	0.2				
14	0.6	0.6	0.6	0.6	0.6	0.5	0.4	0.3							
15	0.3	0.3	0.3	0.3	0.3	0.3	0.2								

Fig. B.5: Radial bundle power profile at EOC predicted by MICROBURN-B2 (no inserted control rods).

I:	J: 1	2	3	4	5	6	7	8	9	10	11	12	13	14	15
1	-3.1	-4.1	-3.9	-6.0	-5.2	-4.0	-3.4	-5.2	-4.6	-2.4	-2.4	2.1	4.3	6.9	13.2
2	-2.7	-2.8	-3.4	-3.3	-3.4	-3.3	-3.4	-2.3	-1.7	-0.7	0.8	2.6	4.7	6.2	13.4
3	-2.8	-3.0	-3.0	-3.4	-3.3	-3.6	-2.8	-2.2	-1.2	-0.4	1.3	3.0	4.9	7.2	13.8
4	-4.3	-3.0	-3.3	-5.3	-5.4	-3.2	-2.6	-3.7	-2.6	-0.1	1.3	3.0	4.8	7.9	15.5
5	-4.8	-3.3	-3.3	-5.4	-5.3	-3.2	-2.4	-3.2	-2.0	-0.1	1.7	3.5	5.1	8.0	15.3
6	-3.7	-3.4	-3.7	-3.2	-2.5	-2.1	-1.8	-1.2	0.0	1.3	2.3	3.7	5.2	7.5	14.9
7	-4.4	-4.1	-3.6	-2.9	-2.1	-1.9	-0.8	-0.8	0.5	1.9	3.1	4.3	5.2	0.4	12.8
8	-7.5	-3.7	-3.5	-3.0	-2.5	-0.6	0.0	0.1	0.5	2.6	3.6	4.2	-1.5	11.9	
9	-6.0	-3.2	-2.2	-2.3	-1.4	0.3	1.0	1.3	1.6	3.1	4.6	4.9	11.4		
10	-2.0	-1.0	-0.4	-0.5	0.3	1.3	2.1	2.4	2.3	4.4	5.6	7.0	14.8		
11	-0.2	0.4	1.0	-0.1	1.3	2.3	3.2	3.8	4.3	5.6	6.5	1.7	15.1		
12	-0.2	1.6	2.4	2.9	3.2	3.8	4.5	4.9	6.6	8.3	2.7	19.2			
13	1.3	3.1	3.9	4.5	5.0	5.4	5.5	-0.7	12.8	17.2	16.8				
14	4.3	4.4	5.4	6.7	7.1	7.4	0.8	11.8					PWE =		3.4
15	10.5	11.3	11.8	12.0	13.5	13.4	13.0						EWE =		7.8

Fig. B.6: Relative difference in radial bundle power profile between PARCS and MICROBURN-B2 at EOC in per cent.

This shift of the sign of the error for the local power form factor affects error cancelation for the burnup during the equilibrium cycle which can be seen by comparing of the EOC cycle burnup in Fig. B.7 and Fig. B.8. Most of the FA at the core periphery which will be discharged reveal a local deviation of the FA average burnup of less than 1 %.

I:	J: 1	2	3	4	5	6	7	8	9	10	11	12	13	14	15
1	26.6	29.6	16.5	30.2	19.7	27.5	16.0	22.4	27.7	23.0	35.3	14.0	14.3	31.2	35.0
2	27.5	8.5	31.3	8.3	22.7	8.4	35.3	8.1	21.7	7.9	21.6	7.2	32.1	19.9	34.1
3	16.1	30.8	16.2	28.2	16.1	31.8	15.8	23.9	14.3	31.3	14.9	20.6	13.1	24.9	35.4
4	33.4	8.4	29.0	21.9	23.0	8.4	23.8	8.1	28.3	8.1	35.3	7.2	19.9	19.2	33.1
5	15.6	23.5	15.8	23.1	15.7	32.5	15.1	30.5	16.1	24.0	14.9	19.7	14.1	19.4	34.8
6	22.1	8.5	31.3	8.5	32.5	8.6	24.6	8.5	27.1	8.1	33.9	6.8	33.3	34.4	34.0
7	23.9	31.6	16.4	24.3	15.5	27.8	16.4	34.8	15.9	27.0	7.4	12.5	25.8	32.0	35.9
8	28.5	8.1	30.9	8.4	32.3	8.5	34.2	16.2	27.2	7.6	15.3	21.2	35.1	36.3	
9	20.2	31.6	8.4	29.2	16.4	27.5	15.8	26.4	23.1	32.9	6.3	24.8	34.6		
10	27.1	8.0	33.2	8.2	23.5	8.1	26.6	7.5	34.0	6.4	13.8	35.3	36.2		
11	7.7	21.4	14.4	37.3	15.0	34.4	7.3	19.0	6.3	13.8	33.2	34.6	34.9		
12	36.0	7.2	20.6	7.2	19.8	6.7	12.5	28.0	21.0	31.4	30.8	35.1			
13	14.1	32.5	13.1	19.7	14.0	32.4	26.6	34.5	35.2	34.6	34.8				
14	34.5	20.0	31.6	19.3	27.7	34.7	34.2	37.7							
15	35.7	33.6	34.9	37.6	34.3	36.7	33.1								

Fig. B.7: Radial bundle mass-weighted exposure in MWd/kgHM at EOC predicted by MICROBURN-B2.

	1	2	3	4	5	6	7	8	9	10	11	12	13	14	15
1	-0.2	-1.4	-1.2	-1.3	-0.4	-0.9	-1.0	-1.1	0.1	-0.8	-1.3	0.8	0.2	0.4	0.0
2	0.4	-0.9	-0.7	-0.8	-0.1	-1.1	-0.9	0.0	0.2	-0.1	0.3	1.0	0.1	-0.6	-0.1
3	-0.4	-0.8	-0.3	-0.1	-0.5	-1.8	-0.6	-0.9	0.0	-0.7	0.4	0.0	1.1	0.4	0.4
4	-0.1	-0.7	-0.3	-1.0	-0.8	-1.1	-0.8	-2.0	-0.9	-0.4	-0.1	0.8	-1.4	1.0	0.2
5	-1.3	-0.6	-0.6	-0.8	-1.6	-0.5	-0.5	-1.2	-1.7	-1.9	0.2	0.4	-0.4	0.2	-0.3
6	-0.4	-1.4	-1.0	-1.4	0.1	-1.2	-1.2	-1.3	0.0	-0.1	0.3	0.6	-0.7	-1.0	-0.4
7	-1.7	-1.8	-2.3	-1.8	-0.4	-0.8	-1.3	-1.6	-0.5	0.3	0.3	0.6	-0.4	-0.8	-0.1
8	-0.9	-1.4	-1.3	-2.9	-1.6	-1.1	-0.3	-1.5	-1.5	-0.1	-0.5	-0.5	-1.6	0.5	
9	-0.2	-1.7	-1.7	-0.5	-1.9	0.4	-0.4	0.4	-0.8	-0.2	0.4	-0.2	-1.3		
10	-1.1	-0.2	-0.4	-1.4	-0.6	-0.5	-0.1	-0.5	-0.2	0.2	-0.5	-1.4	0.3		
11	-0.3	-0.2	0.3	-1.4	-0.6	0.3	0.2	0.5	0.0	-0.3	-0.4	-2.1	-0.4		
12	-1.5	-0.2	-0.1	0.3	0.8	0.4	0.5	0.0	-0.7	-0.2	-0.5	0.2			
13	-2.6	-0.9	0.2	0.9	-0.2	0.4	-0.3	-1.4	-1.0	1.0	0.0				
14	-1.1	-1.4	-0.7	0.0	-0.5	-0.5	-1.2	-0.6					PWE =		0.7
15	0.1	0.7	0.4	-0.9	0.5	-1.2	0.0						EWE =		1.2

Fig. B.8: Relative difference in radial bundle exposure profile between PARCS and MICROBURN-B2 at EOC in per cent.

Last but not least the axial power shape predicted by both codes was assessed in Fig. B.9. The general shape is satisfactory but PARCS predicts less pronounced bottom power peak as MICROBURN-B2. This results most likely from different control rod effects in the model (CRs are inserted from the bottom). Similar observations have been reported in [86] for PARCS comparison against measurements.

	BOC	EOC
PWE	6.9%	6.9%
EWE	27.2%	28.3%
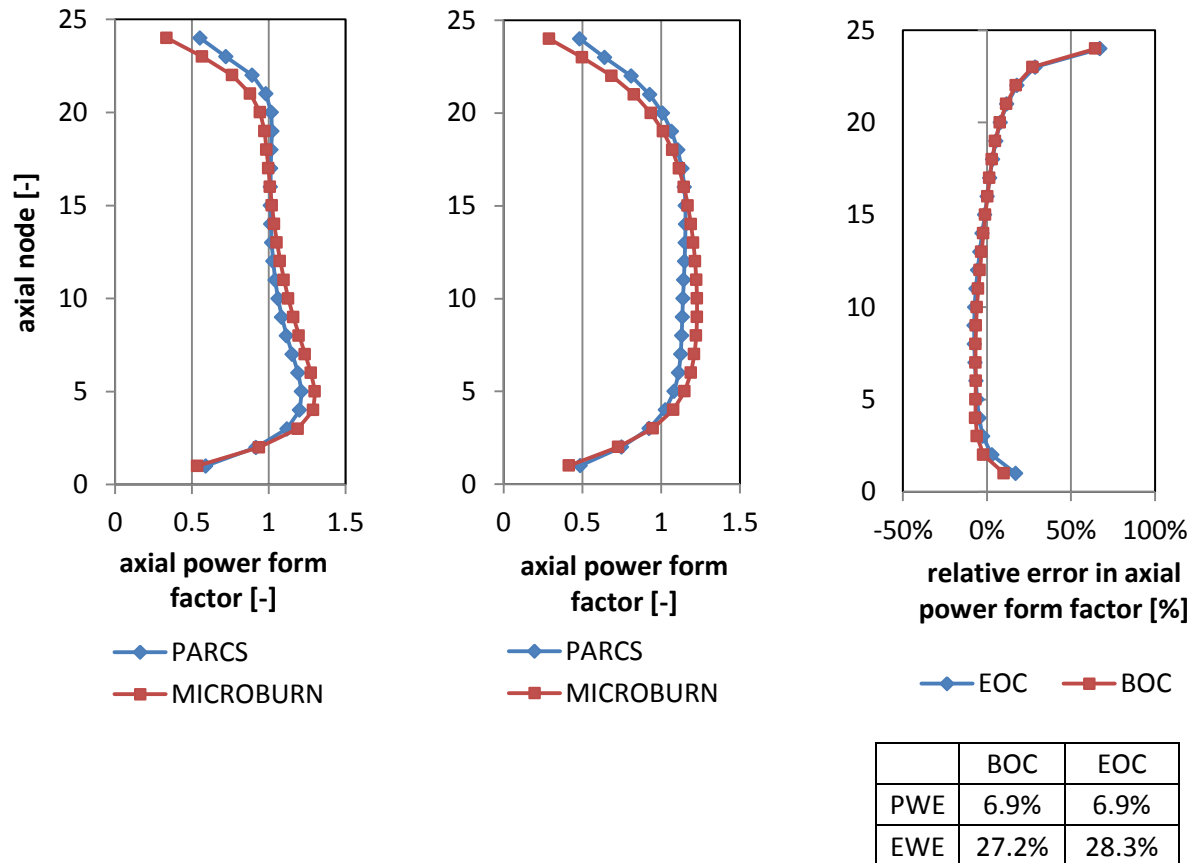
Fig. B.9: Axial power profile at BOC(left) and EOC (middle) as predicted by MICROBURN-B2 and PARCS and relative difference between the code predictions (right).

References

[1]   S. Wissel, O. Mayer-Spohn, U. Fahl and A. Voß, "CO2-Emissionen der nuklearen Stromerzeugung," Universität Stuttgart, Institut für Energiewirtschaft und Rationelle Energieanwendung, 2007.

[2]   H. Hondo, "Life cycle GHG emission analysis of power generation systems: Japanese case," Energy, vol. 30, pp. 2042-2056, 2005.

[3]   M. Lenzen, "Life cycle energy and greenhouse gas emissions of nuclear energy: A review," Energy Conversion and Management, vol. 49, p. 2178–2199, 2008.

[4]   "Key World Energy Statistics," [Online]. Available: https://www.iea.org/publications/freepublications/publication/kwes.pdf.

[5]   W. Oldekop, H.-D. Berger and Z. Wilfried, "General Features of Advanced Pressurized Water Reactors with Improved Fuel Utilization," Nuclear Technology, vol. 59, pp. 212-227, 1982.

[6]   "NUGENIA ROADMAP 2013," [Online]. Available: http://nugenia.org/docs/NUGENIA_roadmap.pdf.

[7]   "SNETP Position Paper on the European Commission's Communication for a policy framework for climate and energy in the period from 2020 to 2030," [Online]. Available: http://www.snetp.eu/www/snetp/images/snetp_position_paper_on_ec_2030_policy_framework_final.pdf.

[8]   "SNETP - Strategic Research and Innovation Agenda (SRIA)," [Online]. Available: http://www.snetp.eu/www/snetp/images/stories/Docs-SRA2012/sria2013_web.pdf.

[9]   M. Lamm, "Entwicklung von Kernkraftwerken und Brennstoffkreislaufkonzepten mit hoher Konversionsrate – Ein Konzeptüberblick," in Jahrestagung Kerntechnik, 2011.

[10]   H. Märkl and H. Moldaschl, "Development of a high conversion reactor in Swiss-German cooperation," Kerntechnik, vol. 57, no. 1, pp. 7-13, 1992.

[11]   H. Bairiot, P. Blanpain, D. Farrant, T. Ohtani, V. Onoufriev, D. Porsch and R. Stratton, "Status and Advances in MOX Fuel Technology," IAEA, Technical reports series No. 415, 2003.

[12]   G. Bender, M. Rost and W. U. Timm, "Design studies for full-MOX BWR cores," in Proceedings of PHYSOR 2010, 2010.

[13]   W. Timm and G. Bender, "Design Studies for full-MOX BWR Cores," Internal report A1C-1337609-0, AREVA NP GmbH, Erlangen, 2010.

[14]   "EU Stresstest National Report of Germany - Implementation of the EU Stress Tests in Germany," Tech. rep., Federal Ministry for the Environment, Nature Conservation and Nuclear Safety, 2011.

[15]   "EU Stresstest National Report of Germany - Implementation of the EU Stress Tests in Germany -
        Annex 1," Tech. rep., Federal Ministry for the Environment, Nature Conservation and Nuclear Safety,
        2011.

[16]   "Gundremmingen nuclear-power station," Kernkraftwerk Gundremmingen GmbH, [Online]. Available:
        http://www.kkw-gundremmingen.de/download/Gundremmingen_nuclear_power_station.pdf.

[17]   E. Rebhan, Energiehandbuch: Gewinnung, Wandlung und Nutzung von Energie, Springer-Verlag, 2002.

[18]   "Fuel design data," Nuclear Engineering International, p. 45, September 2013.

[19]   M. C. Edlund, "High Conversion Ratio Plutonium Recycle in Pressurized Water Reactors," Annals of
        Nuclear Energy, vol. 2, pp. 801-807, 1975.

[20]   Y. Ronen, Ed., High Converting Water Reactors, Boca Raton, Florida: CRC Press, 1990.

[21]   C. H. M. Broeders, "Neutronic investigations of an equilibrium core for a tight-lattice light water
        reactor," Kerntechnik, vol. 57, no. 1, pp. 23-30, 1992.

[22]   H.-D. Berger, H. Finnemann, M. Schatz, G. J. Schlosser, K. Thieme and M. Wagner, "Core design studies
        for a tight lattice pressurized water reactor with improved fuel utilization," Kerntechnik, vol. 57, no. 1, pp.
        31-36, 1992.

[23]   R. Brogli, H. Moldasch and I. Rummel, "Results of the verification period 1985-1990 of the German-Swiss
        high converting reactor PWR-C1," Nuclear Engineering and Design, vol. 147, pp. 1-16, 1993.

[24]   Y. Ishiguro and K. Okumura, "Pancake Core High Conversion Light Water Reactor Concept," Nuclear
        Technology, vol. 84, pp. 331-343, 1988.

[25]   F. Damian, S. Douce, A. Bergeron, B. G. and, F. Moutin and D. Pialla, "Improvement Of The Conversion
        Ratio In PWR," in Proceedings of PHYSOR 2010, 2010.

[26]   D. Baldova and E. Fridman, "High Conversion Th-U233 fuel assembly for current generation of PWRs,"
        in Proceedings of PHYSOR 2012, 2012.

[27]   V. G. Rodrigues, "Untersuchungen zum hochkonvertierenden Siedewasserreaktor," Ph.D. dissertation,
        Universität Hannover, 1983.

[28]   R. Takeda et al., "A Conceptual Core Design of a Plutonium Generation Boiling Water Reactor," in
        Technical aspects of high converter reactors, Nuremberg, 1992.

[29]   R. Takeda et al., "Plutonium Generation Boiling Water Reactor Concept," in Proceedings of PHYSOR'90,
        Marseille, 1990.

[30]   K. Yamada, M. Aoyama, K. Haikawa, K. Sakurada, L. E. Fenner and T. Anegawa, "Core and Dynamic
        Characteristic Design for ABWR-II," in 7th International Conference on Nuclear Engineering ICONE,
        Tokyo, Japan, 1999.

[31] *J. Yamashita, A. Nishimura, T. Mochida and O. Yokomizo, "A new boiling water reactor core concept for a next-generation light water reactor,"* Nuclear Technology, *vol. 96, no. 1, pp. 11-19, 1991.*

[32] *J. Yamashita and T. Mochida, "Development of a high-conversion boiling water reactor,"* Nuclear Technology, *vol. 96, no. 1, pp. 20-28, 1991.*

[33] *T. Kondo, T. Mochida and J. Yamashita, "Technology development issues for high-conversion BWRs using island-type MOX fuel,"* Nuclear Technology, *vol. 145, pp. 257-265, 2004.*

[34] *T. Yokoyama, R. Yoshioka, Y. Tsuboi, Y. Sakashita and S. Matsuyama, "Study on Fast Spectrum BWR Core with Breeding Characteristics," in* Proceedings of the Workshop on Advanced Reactors with Innovative Fuels, *1999.*

[35] *Y. Sakashita, T. Yokoyama and Y. Tsuboi, "Core Characteristics Of Breeding BWR For BARS (BWR With Advanced Recycle System)," in* 7th International Conference on Nuclear Engineering ICONE, *Tokyo, Japan, 1999.*

[36] *T. Iwamura, S. Uchikawa, T. Okubo, T. Kugo, H. Akie, Y. Nakano and T. Nakatsuka, "Concept of innovative water reactor for flexible fuel cycle (FLWR),"* Nuclear Engineering and Design, *vol. 236, pp. 1599-1605, 2006.*

[37] *B. Feng and F. Ganda, "Reducing the Void Coefficient of Reactivity in High Conversion Water Reactors," in* Proceedings of ICAPP 2013, *2013.*

[38] *T. Hino, M. Ohtsuka, R. Takeda, J. Miwa, Y. Ishii and K. Moriya, "Core Designs of RBWR (Resource-renewable BWR) for Recycling and Transmutation of Transuranium Elements - an Overview," in* Proceedings of ICAPP 2014, *2014.*

[39] *A. Hall, T. Downar, A. Ward, M. Jarrett, A. Wysocki, Y. Xu and K. Shirvan, "Advanced Methods Development for Equilibrium Cycle Calculations of the RBWR," in* Proceedings of ICAPP 2014, *2014.*

[40] *P. M. Gorman, G. Zhang, J. E. Seifried, C. R. Varela, J. L. Vujic and E. Greenspan, "The fuel-self-sustaining RBWR-Th core concept and parametric studies," in* Proceedings of ICAPP 2014, *2014.*

[41] *B. A. Lindley, S. S. Drera, J. F. Kelly, S. F. Ashley and G. T. Parks, "An open-cycle RBWR concept utilizing LEU-Th seed-blanket fuel," in* Proceedings of ICAPP 2013, *2013.*

[42] *Y. Shaposhnik, E. Shwageraus and E. Elias, "Effect of Axial Void Distribution on Performance of High Conversion BWRs," in* Proceedings of NUTHOS-9, *2012.*

[43] *A. M. Gomez-Torres, V. H. Sánchez-Espinoza, K. Ivanov and R. Macian-Juan, "DYNSUB: A high fidelity coupled code system for the evaluation of local safety parameters – Part I: Development, implementation and verification,"* Annals of Nuclear Energy, *vol. 48, pp. 108-122, October 2012.*

[44] *A. M. Gomez-Torres, V. H. Sánchez-Espinoza, K. Ivanov and R. Macian-Juan, "DYNSUB: A high fidelity coupled code system for the evaluation of local safety parameters – Part II: Comparison of different*

temporal schemes," Annals of Nuclear Energy, *vol. 48, pp. 123-129, October 2012.*

[45] A. Ivanov, V. Sánchez, R. Stieglitz and K. Ivanov, *"High fidelity simulation of conventional and innovative LWR with the coupled Monte-Carlo thermal-hydraulic system MCNP-SUBCHANFLOW,"* Nuclear Engineering and Design, *vol. 262, pp. 264-275, 2013.*

[46] M. Calleja, V. Sánchez, J. Jimenez, U. Imke, R. Stieglitz and R. Macián, *"Coupling of COBAYA3/SUBCHANFLOW inside the NURESIM platform and validation using selected benchmarks,"* Annals of Nuclear Energy, *vol. 71, pp. 145-158, 2014.*

[47] A. Hébert, Applied Reactor Physics, J. Yelon, Ed., Presses Internationale Polytechnique, 2009.

[48] W. M. Stacey, Nuclear Reactor Physics, John Wiley & Sons, Inc., 2001.

[49] J. J. Duderstadt and L. J. Hamilton, Nuclear Reactor Analysis, John Wiley & Sons, Inc., 1976.

[50] P. Reuss, Neutron Physics, EDP Sciences, 2008.

[51] Y. Azmy and E. Sartori, Nuclear Computational Science - A Century in Review, Springer, 2010.

[52] D. G. Cacuci, Ed., Handbook of nuclear engineering, New York: Springer, 2010.

[53] T. Kozlowski, *"Spatial Homogenization Methods for Pin-By-Pin Neutron Transport Calculations," Ph.D. dissertation, Purdue University, 2005.*

[54] S. Dürigen, *"Neutron Transport in Hexagonal Reactor Cores Modeled by Trigonal-Geometry Diffusion and Simplified P3 Nodal Methods," Ph.D. dissertation, Karlsruhe Institute of Technology (KIT), 2013.*

[55] B. R. Moore, H. Zhang and S. Congdon, *"Comparison of Methods for BWR Prediction Accuracy As Applied to a Small BWR/4," in* Mathematics and Computation, Reactor Physics and Environmental Analysis in Nuclear Applications*, Madrid, 1999.*

[56] A. Smolinska, *"Developing A Basis For Predicting And Assessing Trends In Core Tracking In The Boiling Water Reactor Commercial Power Industry," Master thesis, University of Florida, 2004.*

[57] M.-Y. Hsiao, J. K. Wheeler and C. d. l. Hoz, *"Application of CASMO-4/MICROBURN-B2 Methodology to Mixed Cores with Westinghouse Optima2 Fuel,"* Nuclear Science and Engineering, *vol. 167, pp. 230-241, 2011.*

[58] Janis - Java-based Nuclear Data Information System (Version 3.4) [program], Le Seine St-Germain, 12, Boulevard des Iles, 92130 Issy-les-Moulineaux, May 2012.

[59] Ö. Bernander, *"Boiling Water Reactors: Start-up Dynamics and Stability," in* The 1999 Frédéric Joliot/Otto Hahn Summer School*, Karlsruhe, Germany, 1999.*

[60] Scale: A Comprehensive Modeling and Simulation Suite for Nuclear Safety Analysis and Design, Version 6.1, Available from Radiation Safety Information Computational Center at Oak Ridge National Laboratory as CCC-785, ORNL/TM-2005/39, June 2011.

[61] *M. J. Driscoll, T. J. Downar and E. E. Pilat, The linear reactivity model for nuclear fuel management, La Grange Park, Ill., USA: American Nuclear Society, 1990.*

[62] *N. E. Todreas and M. S. Kazimi, Nuclear systems, 2 ed., vol. 1: Thermal hydraulic fundamentals, Taylor & Francis, 1993.*

[63] *R. T. Lahey and F. J. Moody, The thermal-hydraulics of a boiling water nuclear reactor, 2 ed., La Grange Park, III.: American Nuclear Soc., 1993.*

[64] *J. J. Carbajo, G. L. Yoder, S. G. Popov and V. K. Ivanov, "A review of the thermophysical properties of MOX and UO2 fuels,"* Journal of Nuclear Materials, *vol. 299, no. 3, pp. 181-198, 2001.*

[65] *P. Emonot, A. Souyri, J. Gandrille and F. Barré, "CATHARE 3: A new system code for thermal-hydraulic in the context of the NEPTUNE project," in* NURETH-13, *Kanazawa City, Ishikawa Prefecture, Japan, September 27-October 2, 2009.*

[66] *M. Glück, "Validation of the sub-channel code F-COBRA-TF - Part I. Recalculation of single-phase and two-phase pressure loss measurements,"* Nuclear Engineering and Design, *vol. 238, pp. 2308 - 2316, 2008.*

[67] *H. Oertel, Ed., Prandtl–Essentials of Fluid Mechanics, Springer, 2010.*

[68] *B. Pershagen, Light Water Reactor Safety, Nykoping, Sweden: Pergamon Press, 1989.*

[69] *"Physics of Plutonium Recycling - Volume VII - BWR MOX Benchmark Specification and Results," OECD Publication, 2003.*

[70] *"MOX Fuel Cycle Technologies for Medium and Long Term Deployment," Conference Proceedings, IAEA, Vienna, 1999.*

[71] *"Management of Recyclable Fissile and Fertile Materials," NEA No. 6107, OECD, 2007.*

[72] *T. Lefvert, "Improving fuel economy by optimized in-core fuel management,"* Kerntechnik, *vol. 52, no. 4, pp. 228-233, 1988.*

[73] *M. Edenius, K. Ekberg, B. H. Forssén and D. Knott, "CASMO-4 User's Manual," 1995.*

[74] *Z. Zhong, T. Downar and M. DeHart, "Benchmarking the U.S. NRC Neutronics Codes NEWT and PARCS with the VENUS-2 MOX Critical Experiments," in* Nuclear Mathematical and Computational Sciences: A Century in Review, *Gatlinburg, Tennessee, 2003.*

[75] *W. J. Marshall and B. T. Rearden, "Criticality Safety Validation of SCALE 6.1," ORNL/TM-2011/450 Revised, Oak Ridge National Laboratory, 2013.*

[76] *B. J. Ade, "SCALE/TRITON Primer: A Primer for Light Water Reactor Lattice Physics Calculations," NUREG/CR-7041, prepared for the U.S. Nuclear Regulatory Commission by Oak Ridge National Laboratory, Oak Ridge, Tenn., 2012.*

[77]   *"MICROBURN-B2 Steady State BWR Core Physics Methods," Manual, EMF-1833(P), AREVA NP Inc., 2010.*

[78]   *T. Downar, Y. Xu and V. Seker, "PARCS v3.0 U.S. NRC Core Neutronics Simulator - Theory Manual," Ann Arbor, MI 48109, 2012.*

[79]   *T. Downar, Y. Xu and V. Seker, "PARCS v3.0 U.S. NRC Core Neutronics Simulator - User Manual," Ann Arbor, MI 48109, 2012.*

[80]   *A. Ward, Y. Xu and T. Downar, "GenPMAXS - v6.1.1 - Code for Generating the PARCS Cross Section Interface File PMAXS," 2013.*

[81]   *C. Beckert and R. Koch, "Reactor cell calculations with the codes HELIOS, MCNP and TRANSFAY: comparison of the results," Annual Report 2004 – Wissenschaftlich-Technische Berichte: FZR 155, May, 2005.*

[82]   *J. Leppänen, R. Mattila and M. Pusa, "Validation of the Serpent-ARES code sequence using the MIT BEAVRS benchmark – Initial core at HZP conditions,"* Annals of Nuclear Energy, *vol. 69, pp. 212 - 225, 2014.*

[83]   *"TRACE V5.0 THEORY MANUAL, Field Equations, Solution Methods, and Physical Model," U. S. Nuclear Regulatory Commission, Washington, DC 20555-0001.*

[84]   *V. H. Sánchez-Espinoza, W. Hering, A. Knoll and R. Böer, "Analysis of the OECD/NEA PWR Main Steam Line Break (MSLB) Benchmark Exercise 3 with the Coupled Code System RELAP5/PANBOX," FZKA 6518, Forschungszentrum Karlsruhe GmbH, Karlsruhe, 2002.*

[85]   *B. Collins, L. Li, D. Wang, S. Stimpson, D. Jabaay, A. Ward, Y. Xu and T. Downar, "PATHS: A Steady State Two-Phase Thermal Hydraulic Solver for PARCS Depletion," in* NURETH-14, *Toronto, Ontario, Canada, 2011.*

[86]   *C. Demaziére, M. Stálek and P. Vinal, "Comparison of the U.S. NRC PARCS Core Neutronics Simulator Against In-Core Detector Measurements for LWR Applications," International Agreement Report, Division of Nuclear Engineering, Chalmers University of Technology, SE-41296 Gothenburg, 2011.*

[87]   *U. Imke, "Input Instructions for SUBCHANFLOW 2.4," Karlsruhe, 2013.*

[88]   *A. Berkhan, "Qualifizierung des Thermohydraulik-Unterkanalcodes SUBCHANFLOW für die Anwendung auf Leichtwasserreaktoren," Diploma Thesis, KIT, INR, Karlsruhe, 2011.*

[89]   *U. Imke, V. Sánchez and R. Gomez, "SUBCHANFLOW: An empirical knowledge based subchannel code," in* Jahrestagung Kerntechnik, *Berlin Germany, 2010.*

[90]   *U. Imke and V. H. Sánchez, "Validation of the Subchannel Code SUBCHANFLOW Using the NUPEC PWR Tests (PSBT),"* Science and Technology of Nuclear Installations, *vol. 2012, no. Article ID 465059, p. 12, 2012.*

[91] W. Jaeger, J. P. Manes, U. Imke, J. J. Escalante and V. H. Sánchez-Espinoza, "Validation and comparison of two-phase flow modeling capabilities of CFD, sub channel and system codes by means of post-test calculations of BFBT transient tests," Nuclear Engineering and Design, *vol. 263, pp. 313-326, 2013.*

[92] V. Sánchez, U. Imke, A. Ivanov and R. Gomez, "SUBCHANFLOW: A Thermal-Hydraulic Sub-Channel Program to Analyse Fuel Rod Bundles and Reactor Cores," Cancún, Q.R., México, 2010.

[93] A. Gomez, W. Jäger, V. Sánchez and U. Imke, "On the Influence of Shape Factors for CHF Predictions with the Sub Channel Code SUBCHANFLOW during a Rod Ejection," in NUTHOS-9, Kaohsiung, Taiwan, 2012.

[94] M. T. Schlenker and V. H. Sánchez-Espinoza, "Increasing the Fuel Utilization in Gen-II BWR with Reduced-Moderation Square Lattice Fuel Assemblies," in Proceedings of ICAPP 2014, 2014.

[95] M. T. Schlenker, "Status report on PhD work," Institute for Neutron Physics and Reactor Technology, Karlsruhe Institute of Technology, 2013.

[96] A. Lejosne, "Monte Carlo Investigations for a Boiling Water Reactor Fuel Assembly," Internship report, Institute for Neutron Physics and Reactor Technology, Karlsruhe Institute of Technology, 2013.

[97] T. Kozlowski and T. Downar, "PWR MOX/UO2 Core Transient Benchmark," NEA No. 6048, OECD, 2007.

[98] B. D. Ivanov, "Methodology For Embedded Transport Core Calculation," Ph.D. dissertation, Pennsylvania State University, 2007.

[99] B. Neykov, F. Aydogan, L. Hochreiter, K. Ivanov, H. Utsuno, K. Fumio, E. Sartori and M. Martin, "NUPEC BWR Full-size Fine-mesh Bundle Test (BFBT) Benchmark, Volume I: Specifications," OECD/NEA, Paris, France, 2005.

[100] S. M. Goldberg and R. Rosner, Nuclear Reactors: Generation to Generation, American Academy of Arts and Sciences, 2011.